TAMPEREEN TEKNILLINEN YLIOPISTO
TAMPERE UNIVERSITY OF TECHNOLOGY

AMIR FARUGHIAN

MODELING AND SIMULATION OF BESS-UPGRADED POWER TRANSMISSION SYSTEMS FOR FREQUENCY CONTROL

Master of Science thesis

Examiner: Prof. Enrique Acha
Examiner and topic approved by the Faculty Council of the Faculty of Computing and Electrical Engineering
on 3rd September 2014

ABSTRACT

Amir Farughian: Modeling and Simulation of BESS-Upgraded Power Transmission Systems for Frequency Control
Tampere University of Technology
Master of Science Thesis, 98 pages, 2 Appendix pages
January 2015
Master's Degree Programme in Electrical Energy Engineering
Major: Smart Grids
Examiner: Professor Enrique Acha

Keywords: Batteries, Frequency Stabilization, Energy Storage, BESS, PSCAD, PowerWorld, DC/DC converter, Power Transmission Systems

This thesis reports on the evaluation of the impact of a battery energy storage system (BESS) on the voltage and frequency stability of a power transmission system.

With the increased penetration of renewable energy sources, particularly wind power, into the power system network new challenges regarding the two major concerns in the transportation and distribution of electrical energy, i.e. power quality and system stability, are being experienced. One way to reduce these concerns is the application of MW-level Battery Energy Storage Systems (BESSs). Despite a long-standing interest in the BESS technology, its application in the transmission system had not been seriously considered until relatively recently.

Since the main focus for this study is frequency stability, a comprehensive discussion on frequency control, including primary and secondary frequency controls is included. This provides the opening for the evaluation of the impact of the BESS on system frequency. In addition, this thesis outlines several BESS installations from early 1980s to today's state of the art technology.

The thesis conducts research using modeling and simulation in PSCAD and PowerWorld environments to carry out a comprehensive assessment of the impact of the BESS technology to ameliorate the frequency excursions that follow a power load increase in a high-voltage transmission system and providing effective voltage support.

In brief, the findings of this thesis indicate the positive influence of the BESS on the power transmission system stability.

PREFACE

This thesis is submitted in partial fulfilment of the requirement for a Master's Degree at the department of Electrical Energy Engineering at Tampere University of Technology.

Writing this thesis has been challenging but in the process of writing I have learned a lot. I am grateful for the learning opportunity.

Foremost, I would like to express my sincere gratitude to my advisor Professor Enrique Acha for his continuous support, hard questions and insightful comments. His immense knowledge, indispensable guidance and constructive feedback helped me in all the time of research and writing of this thesis.

I also would like to thank TUT for providing the support and equipment I have needed to produce and complete my thesis.

In conclusion, I recognize that this research would not have been possible without the financial support of Professor Pertti Järventausta for funding my research.

Tampere, 16.1.2015

Amir Farughian

CONTENTS

LIST OF SYMBOLS AND ABBREVIATIONS

AC	Alternating Current
AGC	Automatic Generation Control
BESS	Battery Energy Storage System
BMS	Battery Management System
CAES	Compressed-Air Energy Storage
CCM	Continuous Current Mode
CSM	Copper-Stretch-Metal
DC	Direct Current
GPD	Gross Domestic Product
HVDC	High Voltage Direct Current
Li-ion	Lithium-ion
LFC	Load Frequency Control
LOS	level of smoothing
NaS	Sodium-Sulfur
PCS	Power Conversion System
PWM	Pulse Width Modulation
SC	Synchronous Condenser
σ	Quality of Frequency Control
SMES	Superconducting Magnetic Energy Storage
SOC	State of Charge
SOH	State of Health
STATCOM	Static Synchronous Compensator
VSC	Voltage Source Converter

A	Ampère (unit of current)
$ctrl$	Converter controller output signal
δ	Duty cycle of the switch
e	Error in the frequency
k_i	Integral gain of converter controller
k_p	Proportional gain of converter controller
q	Duty cycle (only in PSCAD model)
T_m	Mechanical torque
V	Volts (unit of voltage)
V_c	Converter output voltage (only in PSCAD model)
ω	Machine speed (rad/s)
ω_{ref}	Reference angular frequency (rad/s)

1. INTRODUCTION

Demand for electric power continues to increase unabated. A relationship exists between a country's electricity consumption and its wealth. The wealthier the people are, the more electricity they consume. Usually the Gross Domestic Product (GDP) per capita is used to express the wealth level of a country. By definition, GPD is the monetary value of goods and services produced within a country. GDP per capita is the GDP divided by the number of people of the country. The US dollar is generally used as the common monetary unit when comparing GDPs of different countries. However, the buying power of the US dollar varies relatively from country to country. For this reason, the GDP is sometimes expressed in the local purchasing power of the US dollar and called GPD (PPP) (gross domestic product at purchasing power parity). Arguably, the GDP (PPP) per capita is a better indicator of standard of living than the GDP per capita. Figure 1.1 indicates the electricity use per person versus the GDP (PPP) per capita for a number of countries in 2008.

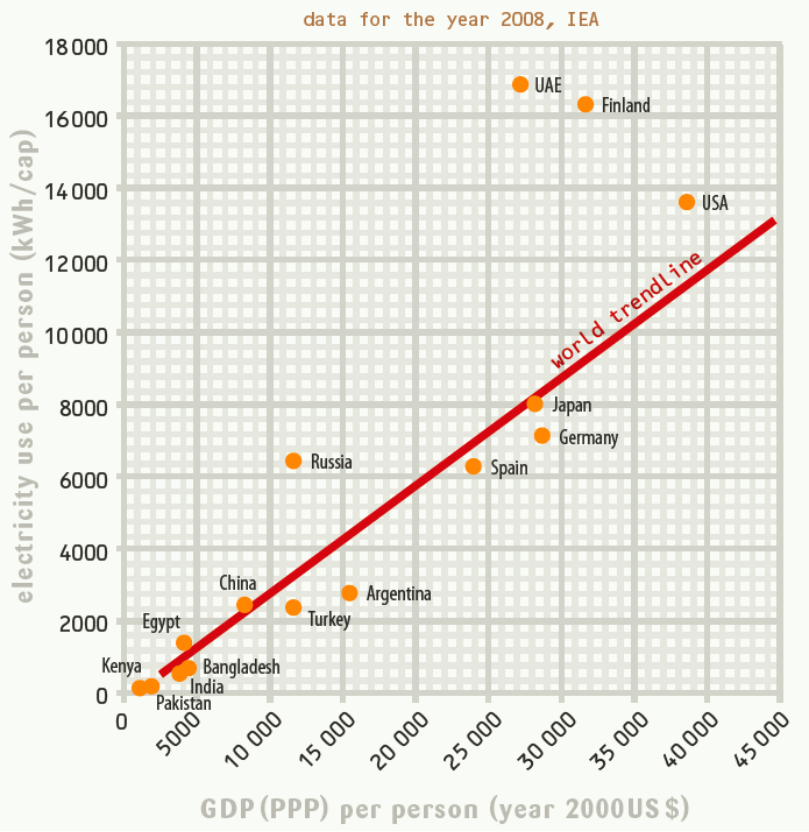

Figure 1.1 *Electricity use in relationship with GDP (PPP) [1].*

1.1 Electricity Demand Pattern

The electricity demand pattern differs from country to country. That is one of the reasons why different countries have different generation portfolios. Demand for electrical energy also depends on the time of the day, day of the week and the season. For example, demand for electricity usually is at its lowest level after midnight because of reduced human activity. In the morning, the demand for electric energy increases drastically; shops open, appliances are switched on and factories increase their electricity consumption. That causes the so-called morning ramp-up. In hot countries, the major consumer of electricity is air conditioning. In such areas, demand for electricity peaks after noon when the solar radiation reaches its highest point.

Finland is a country with high living standards based on industrial activity. It is situated in the Fennoscandian region of Northern Europe. Because of its cold climate, large industrial activity and high wealth level, Finland has an average annual electricity consumption of 15.7 MWh/capita. After Norway with 23.2 MWh/capita, Finland has the highest annual electricity consumption in the world (data IEA, year 2011) [2].

1.2 Matching Electricity Supply and Demand

An electric power supply operator is responsible for continuously matching electricity demand and electricity supply. The matching is needed because as soon as the electricity demand exceeds the power delivered by the prime-movers driving the generators, the difference will result in energy being drawn from the rotating masses of the generators. Therefore, the generators' rotational speed drops and as a result of this, the frequency drops. A change in frequency may affect sensitive devices such as electric clocks and special types of illumination equipment. In addition, if the imbalance between demand and supply becomes significant and long-term, the whole system may collapse. The stability of the frequency is by itself an indicator for balance between electricity generation and demand. The behavior of a synchronous generator following an imbalance in the system will be discussed in more details in Chapter 3. The nominal value of the frequency varies between countries. Nowadays, most electrical power is generated at either 50 or 60 Hz. In practice, the frequency varies slightly around the nominal value.

In addition, the voltage at the point of use must be maintained within a permissible range. The generator output voltage can be accurately controlled by adjusting its magnetic field. Transformers in distribution systems can also control their output voltage in proportion to demand but they cannot adjust the system frequency.

1.3 Storage of Electricity

The strategic importance of energy storage cannot be over emphasized. By storing electrical energy, valleys and peaks in demand would be smoothed out and the excess of electricity production could be stored for later use when demand is at its peak. It would be very attractive if electrical energy could be cheaply and easily stored in large quantities. Electricity can only be stored directly as electric charges in the so-called capacitors. Unfortunately, there are three major drawbacks with capacitor storage: (i) the storage capacity of even the most advanced capacitors is limited to 0.3 Wh/kg, although laboratory experiments indicate that reaching 5Wh/kg might be possible; (ii) capacitors cost at present more than 5000 euros per kWh of stored energy [1]; (iii) no insulator is perfect and the charge stored in capacitors leaks away in roughly one day. Hence, capacitors can be used to cover only short periods of power shortage - they are only suitable for short-term energy storage.

1.4 Storage Technologies

Nevertheless, there are other energy storage technologies available, namely,

(i) supercapacitors;

(ii) advanced batteries such as sodium-sulfur; redox-flo; lithium ion; zinc-bromine;

(iii) electromechanical flywheels;

(iv) pumped-hydro energy storage;

(v) superconducting magnetic energy storage (SMES);

(vi) compressed-air energy storage (CAES).

Figure 1.2 shows some of these energy storage technologies. CAES and pumped-hydro technologies have long response times i.e. long lead time to come on line from standby or spinning-reserve status. Thus, they are not considered suitable for power-quality applications that require rapid responses and will not be discussed further in this thesis.

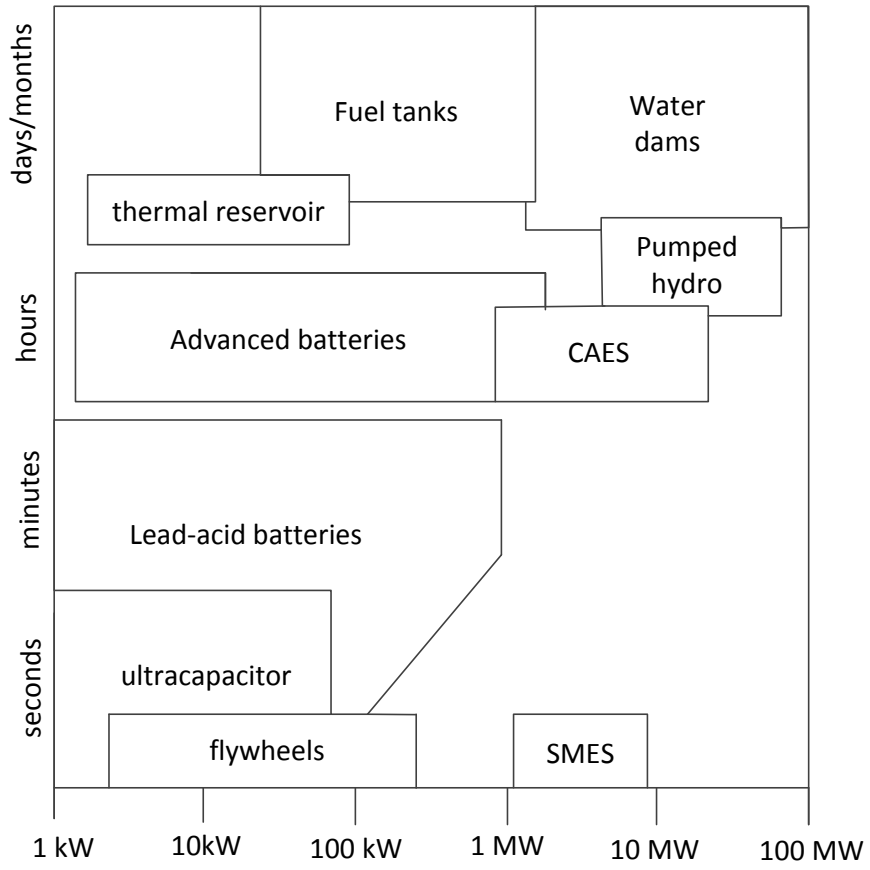

Figure 1.2 *Energy management, power quality and ride-through storage applications [3].*

Lead-acid batteries

Chemical energy storage devices (batteries) are among the leading energy storage technologies today. The fundamental difference between batteries and capacitors is that capacitors store energy directly as charges, whereas in batteries energy is stored in chemical reactants capable of generating charges.

Lead-acid batteries are the best well-developed type in the category of kW-level energy storage devices. Today, the major battery systems operate with rechargeable lead acid and the primary manganese dioxide-zinc batteries [3]. The lead-acid cell has a negative electrode of finely divided elemental lead, and a positive electrode of powdered lead dioxide in an aqueous electrolyte [4].

Lead–acid batteries are usually rated at 25°C. In this temperature they operate best. Exposure to low ambient temperatures leads to performance decline and exposure to high ambient temperatures results in shortened life [5]. Batteries supply DC when charging and receive DC when discharging. Therefore, when they are used in AC systems, conversion in both directions is mandatory.

Lithium-ion batteries

Lithium-ion batteries are gaining a dominant position in the rechargeable battery market. The primary reason is the high energy density that these batteries have. In other words, a lithium-ion cell with a specific size and weight is able to supply substantially more energy than competing technologies of the same size or weight [6]. Lithium has a low atomic number and a high electrode potential and that enables Lithium-ion batteries to provide high-energy density compared to, for instance, lead and zinc-based batteries [3].

Supercapacitors

In conventional capacitors, energy is stored in the electric charges between two conducting plates separated by a dielectric material. The quantity of the stored energy is obtained as follows:

$$W = \frac{CV^2}{2} \tag{1.1}$$

where W, C and V are the stored energy, the capacitance and the voltage across the capacitor, respectively. The capacitance is proportional to the area of the plates and the inverse distance between the plates,

$$C = \frac{KA}{d} \tag{1.2}$$

where K, A and d are the electric constant of the dielectric material, the area of the charged plates and the distance between the charged plates, respectively. However, supercapacitors differ from conventional capacitors. They store energy at the interface between the ionic electrolyte and the electrode which is typically carbon. The high surface area of the carbon materials (up to 2000 m^2 g^{-1}) and the small electrode separation (in the order of a few angstroms) enable supercapacitors to exhibit high energy and power density with an unlimited charge–discharge cycle life [7].

Flywheels

Flywheels store energy as rotational energy. The rotor (flywheel) is accelerated to a very high speed by an integrated motor. To minimize friction losses, the rotor is placed in a vacuum chamber and magnetic bearings are used. When energy is extracted from the system, the rotor speed reduces according to the principle of energy conversion and when energy is added to the system the rotor speed increases. The flywheel system has

a high round trip energy efficiency — 85 to 90% compared to 70 to 75% of the electrochemical battery [8].

Flywheels as energy storage systems are still under development. They could be suitable in frequency regulation and spinning reserve applications. They have the advantage of having unlimited number of charging/discharging cycles. However, their current capacity is not sufficient to be used in large-scale electricity supply applications [9].

Battery Energy Storage System (BESS)

From the FACTS point of view, the combination of a VSC with a DC power source results in significant improvements over the traditional STATCOM. When a DC power source such as a battery pack is integrated with a STATCOM, the arrangement is termed BESS. Figure 1.3 illustrates the BESS schematically; it comprises a battery pack with its controller and a power conditioning system.

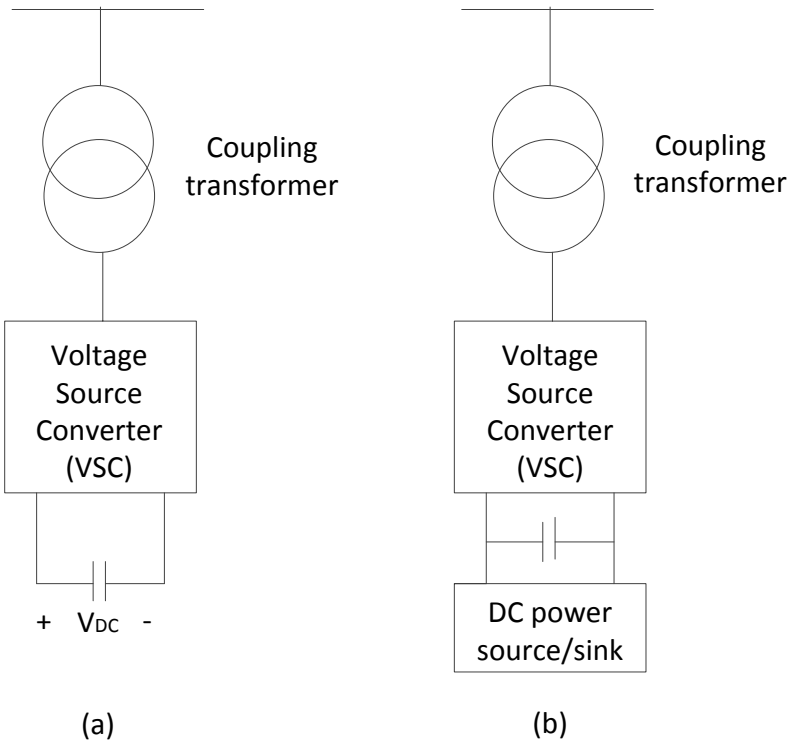

Figure 1.3 *(a) STATCOM connected to a power system point; (b) Battery Energy Storage System [10].*

The control and power-conditioning system (C-PCS) interfaces the battery pack to the load system (utility or end user) and regulates the battery charge/discharge operating mode, charging rate, etc. The C-PCS cost is significant and it can be greater than 25% of the overall energy storage system [11]. The C- PCS includes power converters,

control circuits, filters and the transformer. The transformer, among other functions, is charged with isolating the DC and AC systems.

For more information about this technology the following references [12] - [14] are recommended. It is common to refer to DC to AC converters as inverters, DC to DC converters as choppers and AC to DC converters as rectifiers. Also, AC to AC converters are referred to as power controllers if the conversion is at the same frequency and if the conversion is at different frequencies, they are referred to as cyclo-converters [13]. Frequently, power electronic systems combine multiple conversion processes and are simply referred to as converters or power-conditioning systems.

Figure 1.4 shows the basic concept of a converter. By alternately opening and closing the switches N and P, a single-phase, alternating, square-wave voltage can be impressed across the load by the battery. Notice that the voltage waveform contains harmonics which normally would need to be removed by filtering and control.

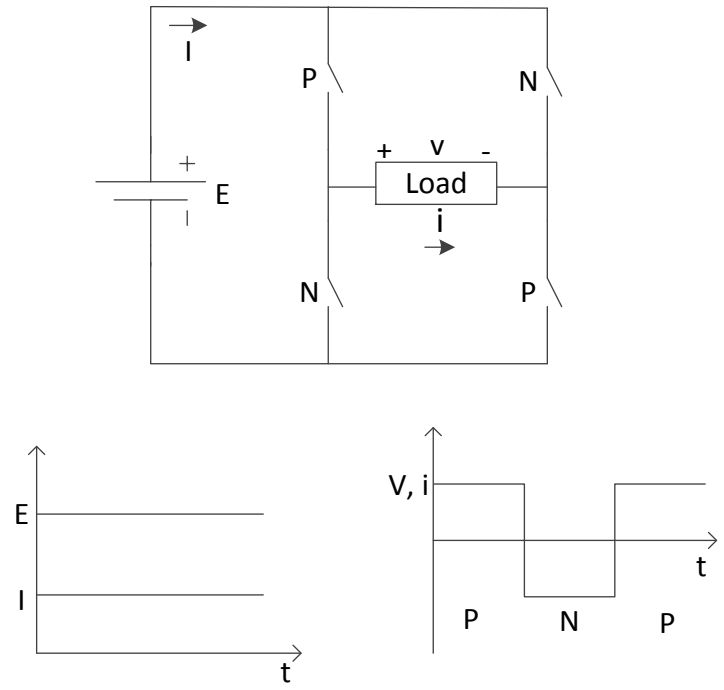

Figure 1.4 *Schematic diagram of basic converter concept [15].*

In most utility applications, the battery interfaces a three-phase transmission or distribution point of common coupling (PCC) via a three-phase converter. Figure 1.5 presents the basic circuit diagram of a three-phase inverter. The three outputs a, b and c, provide three-phase power to a PCC via a three-phase coupling transformer. Figure 1.5 also shows the switching sequence and idealized transformer excitation waveforms. Note that each time-frame represents 60 electrical degrees. As the waveforms suggest, the output of this inverter approximates a sinusoidal voltage. By placing diodes or

switches in parallel with each of the six switches, the battery will be able to either supply or absorb VARs.

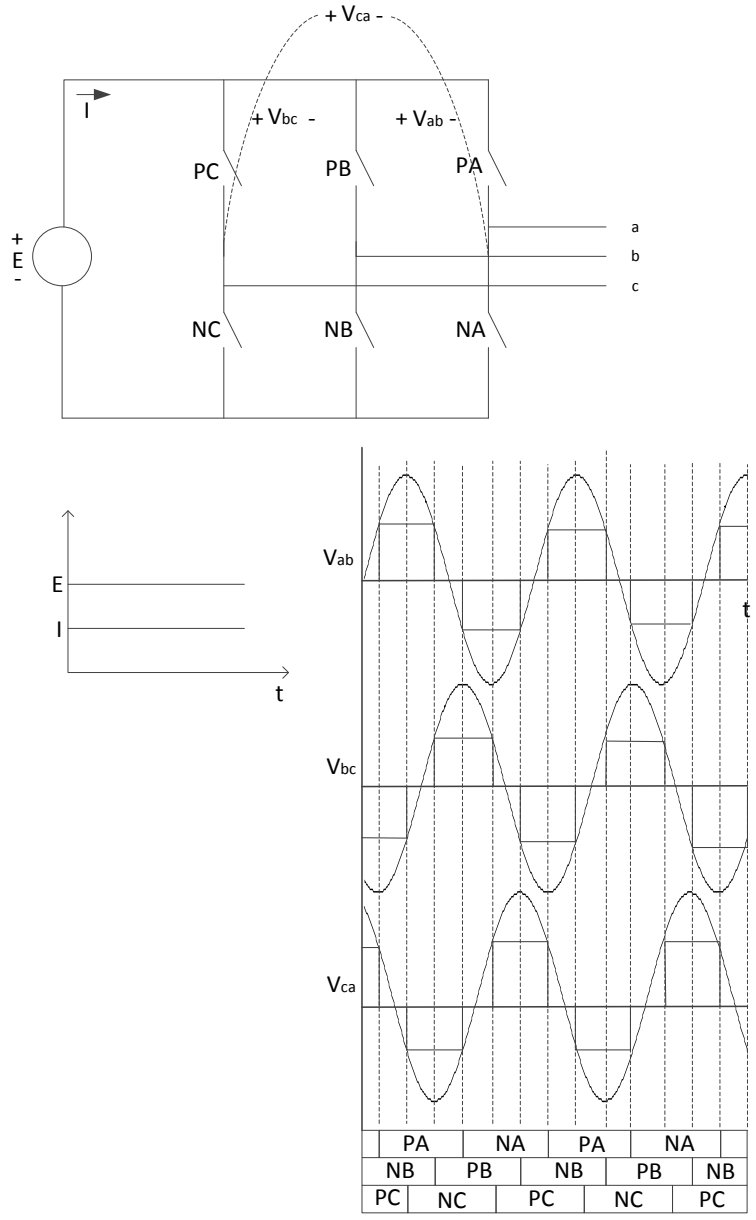

Figure 1.5 *Schematic diagram of basic three-phase converter [15].*

The inverter presented in Figure 1.5, is a six-pulse inverter, which means that every 60 electrical degrees the excitation pattern at the nodes a, b and c will change. The full cycle is completed every 360 electrical degrees. Converters with higher number of pulses, e.g., 12 or 48 pulse converters, may be realized by adding more switches and transformers. The higher the number of pulses, the higher the number of lower harmonics that will be eliminated, resulting in improved output sinusoidal waveforms. With the advent of faster switches such as MOSFETs and IGBTs, pulse width modulation (PWM) converters became an option. One of the advantages of PWM is that

they have the capacity to produce only high frequency harmonics, which are easier to filter out than lower frequencies.

The other major component of the BESS is the battery pack. Currently, different types of batteries are commercially available and some more advantages are being developed. The most popular are: (i) lead acid; (ii) Lithium ion; (iii) Sodium Sulphur (NaS); (iv) Metal air.

1.5 The Challenge

With the increased penetration of renewable energy sources, particularly wind and solar power, into the power system network new challenges concerning the reliability and satisfactory operation of power systems are being experienced. The primary energy resources such as the wind and the solar radiation can vary a great deal and, to a greater or lesser extent, this will result in electrical power with high variability being injected into the power grid, a phenomena which is undesirable from the operation point of view of the network. One way to address such problems is the application of MW-level application of Battery Energy Storage Systems (BESSs). Despite a long-standing interest in the BESS technology, its application in the transmission system had not been seriously considered until relatively recently. The onset of a new generation of BESS using Li-ion batteries and state of the art power electronics converter topologies and control techniques has changed the landscape and now transmission systems operators are increasingly receptive to this application. There are encouraging reports published [16], [17] on operational experiences gained the adoption this new technology in at least two actual installations. There has been studies on the application of the BESS technology to frequency control in power transmission systems using modelling and simulation in the Simulink environment, which has thrown favorably results in support of the use of this technology in this application. This has provided the motivation for conducting further research using modelling and simulation in the PSCAD and PowerWorld environments to gain deeper understanding of the BESS technology at the system level and to evaluate its potential in addressing the frequency excursions and providing effective voltage support. This work reports the findings of the research.

1.6 Frequency Control in Electrical Power Systems

In an electrical power network, the total generated power ought to match the power consumed by the load and the transmission losses. If the load exceeds the power delivered by the machines driving the generators, the difference will result in energy being drawn from the rotating mass, the so-called inertia, of the generators. This leads to the generators' rotational speed drops i.e. the frequency drops. Similarly, if the generation is more than the load, the system frequency will increase. In order to restore the frequency to the initial value, control actions on the generators' output must be

taken. Based on the mechanism and speed of the action, the frequency control is divided into three categories:

- Inertial and primary frequency control
- Secondary frequency control / load frequency control (LFC) / automatic generation control (AGC)
- Tertiary frequency control

Generating units have energy stored in their rotating mass. Immediately after an imbalance occurs between generation and demand, this inertia acts as a buffer and limits the rate of change in frequency. This energy stored in the inertia gives time for the generating units to adjust their output in order to restore the balance. This natural response of the generating units, where no control is provided, is called inertial response. The inertial response is followed by primary frequency control. Primary frequency control is achieved through the speed governor mechanism. After sensing the frequency error, an automatic droop control loop in the governor acts to adjust the mechanical power on the prime mover in order to adjust the generator output. Sometimes, the inertial response is considered to be part of the primary frequency control [18] and it is also clear that they co-exist for a period of time.

Following the primary frequency control, there will still be a steady-state error in the frequency. To correct this error, the governor set points are changed and the frequency is restored to the reference value. This is called "secondary frequency control". Secondary control is slower than primary control. It is in a time frame of minutes [19]. A detailed analytical discussion of primary and secondary control is presented in Chapter 3.

Following the primary and the secondary frequency control actions, a tertiary control might be carried out. Primary and secondary frequency controls are fast and automatic compared to tertiary control. The purpose of tertiary frequency control in power grids is to restore primary and secondary reserves and make large-scale generation adjustments, if needed. Tertiary control is a manual control. It comes into play as a last resort if both primary and secondary frequency controls fail to function properly [20].

A typical frequency response following a sudden increase in the load is illustrated in Figure 1.6. The inertial response that results from a load increase is followed by the primary frequency control for up to about 20 – 30 seconds. Beyond that, the secondary control is activated to restore the frequency back to its pre-disturbance value, after a time of about 5-10 minutes.

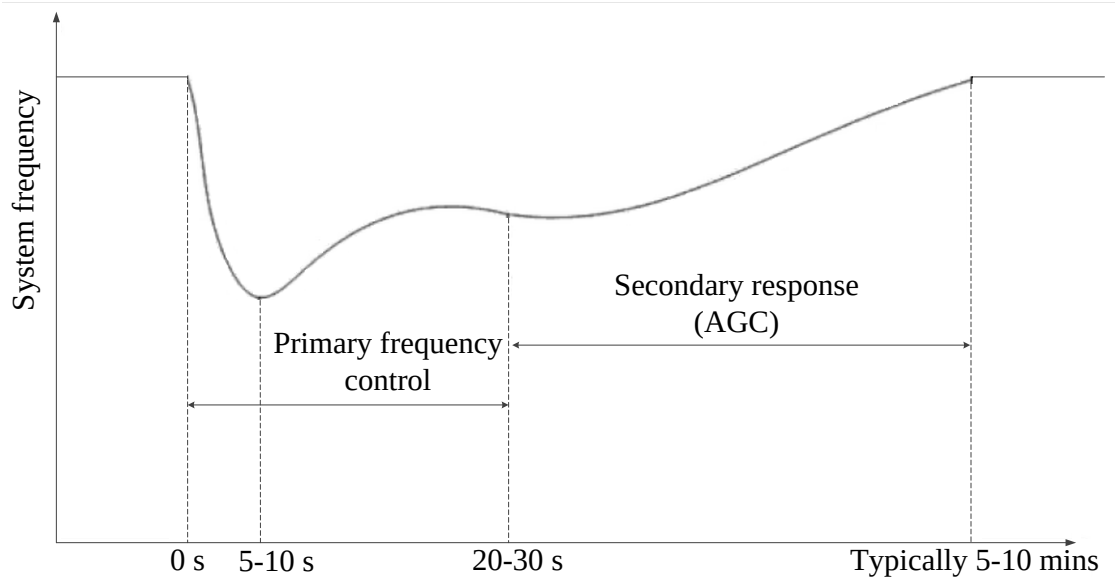

Figure 1.6 *Inertial response, primary and secondary frequency control [18].*

1.7 Research Objectives

The main objectives of the research presented in this thesis are listed below:

- To investigate the effectiveness or otherwise of a modern BESS to yield effective frequency support in high-voltage AC transmission systems subjected to step changes in power load.

- To carry out a fundamental study of the power electronics structure and control methods used by a modern BESS so as to enable its suitable representation in the industry-standard software package PSCAD and its seamlessly combination with the model of an equivalent high-voltage AC transmission system.

- To gain first-hand experience of the modeling flexibility or otherwise of the recently released battery model by the PSCAD developers. In particular, to benchmark the computing times involved in the simulation studies of power systems frequency stability using this software – its computing intensive intrinsic nature is always a worry when combining very-high-frequency switching equipment and utility-size power grids.

- To assess the suitability of an alternative modeling and simulation tool, namely, the transient stability option within PowerWorld, which ought to perform faster calculations but at the expense of incurring rather gross simplifications in the representation of the BESS.

- To carry out a comprehensive comparison of the results furnished by the PSCAD and PowerWorld simulation packages and to provide recommendations for the use or otherwise of these packages for the purpose of conducting frequency stability studies of BESS-upgraded power systems.

1.8 Outline of the Thesis

The thesis comprises seven chapters. The BESS technology for power systems applications is presented in Chapter 2. The first part of Chapter 3 describes the synchronous generators response to imbalances of demand and supply. The second part of Chapter 3 addresses key aspect of frequency control theory. Chapter 4 discusses the BESS representation carried out within PSCAD and presents the simulation results for the case when the BESS is applied to provide frequency support in a high-voltage transmission system comprising four equivalent hydro-generators. Chapter 5 discusses the BESS model and simulation results in PowerWorld for the case when the BESS model available in PowerWorld is applied to provide frequency support in a high-voltage transmission system comprising four equivalent turbo-alternators. A comparison of simulation results furnished by PSCAD and PowerWorld is presented in Chapter 6. This thesis concludes with Chapter 7 where the main conclusions are drawn together with future lines of research in this timely topic of frequency control in electrical power systems.

2. BESS TECHNOLOGY FOR POWER SYSTEMS APPLICATIONS

This chapter discusses the BESS technology for power systems applications. A succinct review of the previous work conducted on this subject is presented first. Since the battery is the cornerstone of the BESS, a brief discussion of some of chemistries that go into the batteries of the kind suitable for utility-scale applications, is provided. The operating principles of the DC/DC converter and the DC/AC converter are discussed; they provide the backdrop for the simulations carried out in Chapter 4. The chapter concludes with some examples of utility – scale BESS facilities installed since 1980.

2.1 Literature Review

Over the years, a wide range of applications have been proposed for battery energy technology. In [21] the advantages of using battery energy technology in power quality and reliability of power systems are discussed. The main focus is on voltage depressions and power interruptions. Ref. [22] discusses the application of the BESS in damping inter-area oscillation. The paper also discusses different strategies to determine the best location for placing the BESS for damping inter-area oscillations. The paper concludes that the best location for placing the BESS depends on different control strategies applied to control the active and reactive power of the BESS.

Ref. [23] discusses the impact of the BESS on frequency regulation improvement. The paper concluded that the BESS is capable of providing great improvement in the system dynamic even under random load disturbance. A monetary analysis of the BESS for load leveling and peak shaving applications are described in [24]. It is claimed that prior to this work an explicit monetary value analysis of the BESS applications have been not considered. The paper suggests that the utilities are more likely to ask for primary control power in the future. The paper also claims that neglecting the commercial side of the BESS has led to over-sized devices and, hence, non-profitable. Three years later, a method for optimal sizing of the BESS in an isolated power system is presented in [25].

Although not mentioned explicitly, the work prior to 2010 presented the first generation technology i.e. the battery technology was mostly of Lead-acid type and the power inverter was a six (or twelve-pulse) bridge using conventional thyristors and phase control, i.e., Graetz bridge.

Before long, the Graetz bridge started to be replaced by the Voltage Source Converter (VSC) using GTO valves and PWM control. Ref [26] presents an improved BESS model in which the SOC of the battery and the actual PWM control of the VSC have been considered. Another application of the BESS in power systems i.e. smoothing power fluctuations from a wind farm is discussed in [27]. The three parameters influencing the level of smoothing (LOS) are battery storage capacity (C), maximum charge/discharge power of the battery (P) and the smoothing time constant (T). The paper proposes a criterion to identify the LOS of the output power of a wind power system. This is followed by a method, based on such a criteria, to find the optimal parameter combination of C, P and T.

Several investigations have been carried out to study and quantify the impact of BESS on the power system operation and economics. "BESS operational models" are used for assessing the operational benefits of BESS in response to power system disturbances at appropriate time scale. "BESS economic models", concerned with the economics/optimal sizing, model the BESS from cost perspective. Completely different BESS models are used for these two types of studies.

BESS models used for economic analysis:

To evaluate the benefits of the BESS for utility and demand applications several studies have been carried out.

(i) Utility side application: Ref. [28] provides a description of the method used for the determination of BESS installation site and capacity for load leveling application in a distribution system in Korea. By calculating the improvement in load factor at each main transformer in the distribution substation the BESS installation site and capacity is determined.

(ii) Demand side application: Ref. [29] describes that in order to determine the optimal BESS size and optimal contract capacities for time of use (TOU) rate customers at Taiwan Power Company advanced multi-pass dynamic programming was modified.

BESS models for power system studies:

The operational models of BESS may be classified based on the power system study time scale. So far the investigations have been mainly focused on evaluating the effect of BESS on (i) reliability and (ii) stability of the power system.

i) BESS-power system reliability analysis: [30] provides the focus on finding a method for evaluating the reliability of generating systems operating in parallel with energy storage facilities. To provide a better insight to power system planners the "wellbeing technique - incorporating deterministic technique into a probabilistic evaluation" is suggested.

ii) BESS-power system stability analysis: in order to quantify the technical benefits of BESS for regulating frequency in an isolated power system, Ref. [31] provides the example of the calculation of frequency variance for a measured load disturbance of an isolated system with and without BESS in Israel.

2.1 Battery Technology

In batteries, chemical energy is converted into electrical energy and vice versa. Batteries are made of stacked cells and the desired voltage and current levels can be obtained by connecting the cells in series and parallel. Batteries combinations are often rated in terms of their energy and power capacity. Some other important features of batteries are:

- Lifespan (usually given in terms of the number of cycles)
- Efficiency
- Self-discharge
- Depth of discharge
- Energy density
- Operating temperature

Battery technology has undergone significant development in recent times. There are different types of batteries for different applications. Some of the batteries which are more suitable for power system (utility-scale) applications are briefly discussed below and the characteristics of major state-of-the-art batteries are summarized in Table 2.1.

1. Lead-acid:

Each cell of a lead-acid battery comprises a negative electrode of lead (Pb), a positive electrode of lead dioxide (PbO_2) and a separator that electrically keep the electrodes apart. The electrodes and the separator are flooded in dilute sulfuric acid (H_2SO_4) electrolyte [32].

2. Lithium-ion:

The negative electrode in Lithium–ion batteries is made of lithium metal oxide ($LiCoO_2$, $LiMO_2$, etc.) and the positive electrode is made of graphitic carbon. The battery electrolyte is comprised of lithium salts dissolved in organic carbonates. The open circuit cell voltage is 4 V.

3. Nickel–Cadmium:

Nickel–cadmium batteries consist of nickel hydroxyl-oxide as the cathode and metallic cadmium as the anode. The electrolyte is made of a concentrated solution of potassium hydroxide containing lithium hydroxide. The open circuit voltage is 1.3 V.

4. Nickel–Metal Hydride:

Nickel-metal hydride batteries are similar to nickel-cadmium batteries in terms of their characteristics. The major difference is the cathode. Instead of Cadmium, the cathode is made of hydrogen absorbed in a metal hydride. The metal hydride in the cathode is oxidized to form a metal alloy and nickel hydroxyl-oxide in the anode is reduced to nickel hydroxide when the battery is discharged. The process is reversed when the battery is charged. The open circuit cell voltage is 1.2 V.

5. Sodium–Sulfur :

The positive electrode in Sodium–Sulfur (NaS) batteries is liquid Sulfur and the negative electrode is liquid Sodium. A solid beta-alumina ceramic electrolyte separates the electrodes. These batteries operate at a relatively high temperature of about 300 ◦C.

6. Flow Electrochemical Batteries:

A simplified block diagram of a flow battery is shown in Figure 2.1. The flow battery consists of a reactor (electrochemical cell), two tanks (reservoirs) and two pumps. The reactor is comprised of two electrodes separated by an ion-selective membrane. The pumps circulate the electrolytes through the reactor. The chemical energy is converted to electricity when the two electrolytes circulate through the reactor.

The energy density of the battery depends on the size of the tanks and the amount of electrolytes. However, the power density is determined by the rates of the electrodes' reactions.

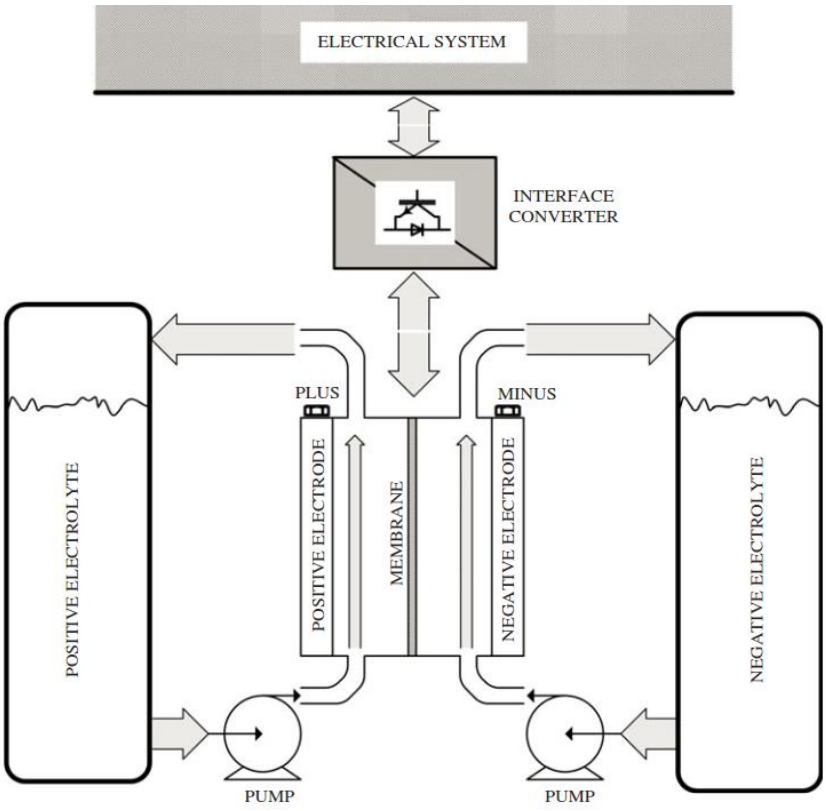

Figure 2.1 *Simplified block diagram of a flow electrochemical battery energy storage system [32].*

Lead-acid batteries are the oldest and the most mature technology amongst the batteries mentioned above. They have been used in many (a vast range of) power applications. In the 1980s, the available BESS technology was Lead-acid batteries. This technology may be considered as the first generation BESS technology. The 30 MW BESS in the Israel power systems is a good case in point. The objective of that BESS was frequency regulation. The electrochemical reaction at the negative electrode is generally expressed as

$$PbO_2 + H_2SO4 + 2H^+ + 2e^- \underset{charge}{\overset{discharge}{\rightleftharpoons}} PbSO_4 + 2H_2O \quad (2.1)$$

and at the negative electrode as

$$Pb + H_2SO_4 \underset{charge}{\overset{discharge}{\rightleftharpoons}} PbSO_4 + 2H^+ + 2e^- \quad (2.2)$$

The overall reaction is

$$PbO2 + Pb + 2H2SO4 \underset{charge}{\overset{discharge}{\rightleftharpoons}} 2PbSO4 + 2H2O \quad (2.3)$$

From early 2000 Lead-acid batteries were being displaced in favor of batteries with higher energy density, longer life cycle and lower maintenance requirements such as, Nickel-Cadmium (efficiency = η = 60-70%; energy density ρ = 35-60 W-h/kg), Sodium-Sulfur (η = 86-89%; ρ = 50-200 W-h/kg) and Vanadium-Redox Flow (VRF) (η = 80%; ρ = 10-20 W-h/kg).

The Li-ion, NaS and NiCd batteries are promising technologies for high power density battery applications. Of these, the Lithium-ion batteries have greater potential for future development. Lithium-ion batteries were produced and brought into the mass market by Sony Co. in 1991. Despite of their high initial cost (2.17 $/W-h), they soon gained popularity due to their high-energy density (88 W-h/kg), good performance and lack of memory effects. However two main drawbacks are the high cost and detrimental effect that deep discharging has on their lifetime Recently Lithium–ion and lithium polymer batteries have been used in portable applications and broad applications in the automotive industry are being identified.

The major advantages of Nickel-Cadmium batteries are their long life cycle, rapid charge capability, long-term storage capability and wide operating temperature range. High initial cost, low cell voltage and the environmental hazard of cadmium are major disadvantages of Nickel-Cadmium batteries. On the other hand, Nickel-metal hydride batteries provide similar advantages as nickel-cadmium batteries with the added benefit of being considered environmentally friendly since no toxic material such as cadmium is used. High initial cost and memory effect are major disadvantages of Nickel-metal hydride batteries

NiCd and Lead-acid are capable of providing excellent pulsed power, however they contain toxic heavy metals and are severely affected by self-discharge. Sodium–Sulfur (NaS) batteries are used in transportation and power smoothing applications. Although the NaS battery is much smaller than NiCd, the high operating temperature (300 C) is a concern.

The flow batteries are suitable for applications in which long duration storages are required owing to their non-self-discharge capability. The major drawback is their high (capital and running) costs.

An assortment of battery technologies along with their applications and some of their characteristics are represented in Table 2.2.

Table 2.1 *Summary of state-of-the-art electrochemical batteries [32].*

	Energy density (Wh/kg)	Power density (Wh/kg)	Life time (cycle)	Operating temperature (°C)
Lead-acid	20 - 35	25	200 - 2000	15 - 25
Lithium-ion	100 - 200	360	500 - 2000	-40 to 60
Lithium-polymer	200	250 - 1000	>1200	-40 to 60
Nickel-cadmium	40 - 60	140 - 180	500 - 2000	-20 to 60
Nickle-metal hybrid	60 - 80	220	<3000	-20 to 60
Sodium-sulfur	120	120	2000	

Table 2.2 *Battery technologies – commercial units used in electric utilities [33].*

Battery type	Largest capacity	Location & application
Lead acid (flooded type)	10 MW/40 MWh	California-Chino Load Leveling
Lead acid (valve regulated)	300 kW/580 KWh	Turn key system Load Leveling
Nickel Cadmium (NiCd)	27 MW/6.75 MWh	GVEA Alaska Control power supply Var compensation
Sodium Sulphur (NaS)	9.6 MW/64 MWh	Tokyo Japan Load Leveling
Vanadium redox (VRB)	1.5 MW/1.5 MWh	Japan Voltage sag Peak load shaving
Zinc Bromine	1 MW/4 MWh	Kyushu EPC
Regenerative fuel cell	15 MW/120 MWh	Innogy's Little Barford station UK

2.2 BESS Ancillary Systems

2.2.1 DC/DC converter

The DC/DC converter is responsible for controlling the active power flow exchange between the battery and the grid. The power flow control is achieved by setting the average DC output voltage at the appropriate value.

The basic circuit of a DC/DC boost converter together with its current and voltage waveforms is shown in Figure 2.2. These correspond to the case when the converter operates in the continuous current mode (CCM), i.e., the inductor current never drops to zero. When the switch is on, the diode D is off and the inductor current increases. When the switch is off, the energy stored in the inductor is released to the output RC circuit via the diode.

According to Figure 2.2b and using Faraday's law for the inductor

$$V_s\,\delta\,T = (V_O - V_S)(1-\delta)T \tag{2.4}$$

where δ is the duty cycle of the switch (the time the switch is on) and T is the time period. From equation (2.4), the DC voltage transfer function is obtained:

$$M_V \equiv \frac{V_O}{V_S} = \frac{1}{1-\delta} \tag{2.5}$$

The output voltage, as the converter name suggests, is always greater than the input voltage ($0 < \delta < 1$).

As it can be seen from Figure 2.2b, the current supplied to the output RC circuit is discontinuous. Therefore, a large filter capacitor is required to limit the output voltage ripple. When the diode D is off, the filter capacitor must supply the output DC current to the load. The minimum value of the filter capacitance C_{min} that results in the voltage ripple V_r is given by

$$C_{min} = \frac{\delta V_O}{V_r R f} \tag{2.6}$$

where f is the switching frequency.

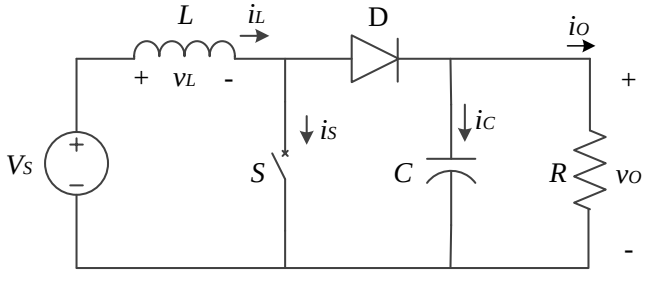

(a)

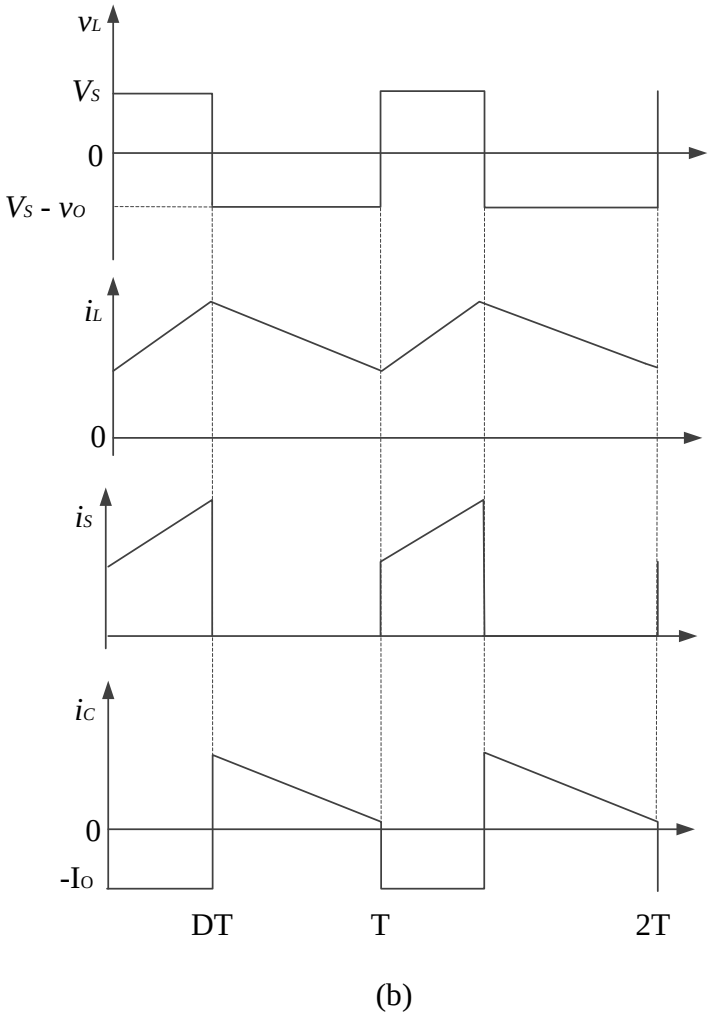

(b)

Figure 2.2 *Boost converter: (a) circuit diagram; (b) waveforms [34].*

2.2.2 DC/AC Converter

Power exchanges between the BESS and the power grid takes place through a DC/AC converter. The DC/AC converter or voltage source converter (VSC), also known to power engineers as STATCOM, is classified as a member of the FACTS family of equipment. It has several advantages such as the capacity to compensate either the lack or excess of reactive power, a wide voltage and reactive power regulating range, a fast speed of response, high control ability and a small footprint. The VSC injects or draws reactive power in order to regulate the voltage magnitude at the bus at which the VSC is connected to. In this work the VSC is used to convert the DC voltage and current generated by the battery pack and modulated by the DC/DC converter, into AC voltages and currents. In the following sections, the operating principles of the VSC are explained.

2.2.3 VSC Operating Principles

A VSC bears a great deal to the Synchronous Condenser (SC) from the operational vantage. Figure 2.3 shows the equivalent circuit of a SC Comprising an AC voltage source (E) behind a transient reactance, with its magnitude being controlled by tuning the field current. It follows that by adjusting the magnitude E, the reactive current generated by the SC can be varied. When $E = V$, the reactive current output is almost zero. For the case when $E > V$, it operates as an equivalent capacitor whereas when $E < V$ it acts as an equivalent inductor. Assuming a lossless SC, the internal voltage angle φ is zero and reactive current (I_r) is obtained as,

$$I_r = \frac{E - V}{X'} \tag{2.7}$$

A VSC may be represented by the same equivalent circuit.

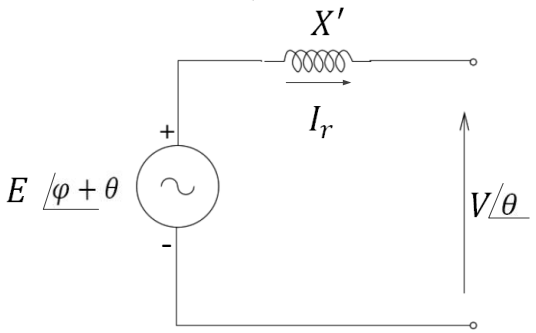

Figure 2.3 *A synchronous condenser [35].*

Figure 2.4 shows the schematic diagram of a single phase STATCOM. Notice that V_{PN} is the output voltage. The voltage V_{dc} remains constant if an energy source e.g. a battery, is provided on the DC bus. The switches T_1 and T_2 operate in a cycle in a coordinated fashion such that when T_1 is on T_2 is off and vice-versa. The use of the diodes enables the current to flow in the reverse direction. When T_1 conducts:

$V_{PN} = \frac{V_{dc}}{2}$.

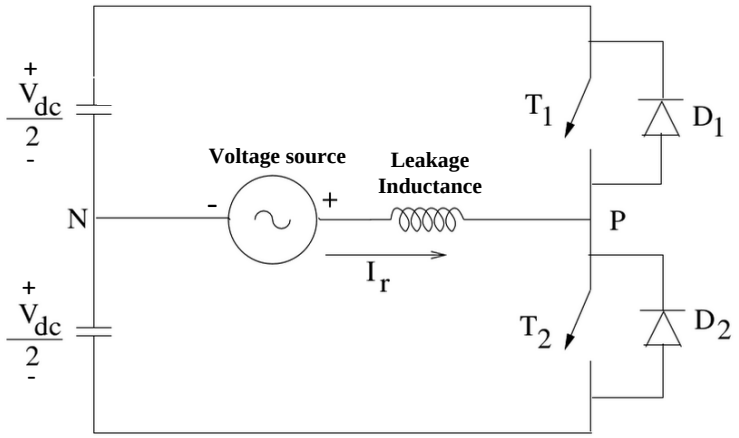

Figure 2.4 *A single phase STATCOM [35].*

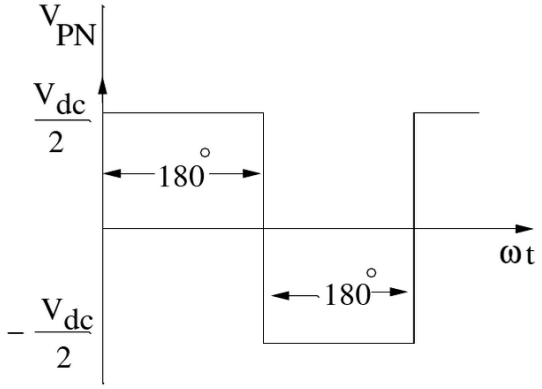

Figure 2.5 *Waveform of v_{PN} [35].*

When T_2 conducts:

$$V_{PN} = -\frac{V_{dc}}{2}$$

Figure 2.5 shows the voltage waveform across PN. The switches $T_1$and T_2 are synchronized with the AC voltage which has a sinusoidal waveform of frequency ω. The RMS value of the fundamental component of V_{PN}:

$$E_1 = \frac{\sqrt{2}}{\pi}\int_0^{\pi}\frac{V_{dc}}{2}\sin(\omega t)\,\mathrm{d}(\omega t) = \frac{\sqrt{2}}{\pi}\,V_{dc} \qquad (2.8)$$

For the case when T_1 is on (T_2 is off) and $E_1 < V$, I_r is inductive, i.e., the current (I_r) is negative and flows through the switch T_1. After 90° , the current flowing through the switch T_1 becomes zero and then increases above zero. In this case the diode D_1starts conducting. A similar description applies when T_2 is on and T_1 is off.

It is useful at this stage to contrast the basic operation of a SC and a VSC, while the AC voltage at the output of a SC is generated by rotation of the DC field winding on the rotor at synchronous speed, in a VSC the synchronized operation of the switches gives rise to the AC output voltage. In a VSC the DC capacitors are charged from the AC circuit and a source of DC energy supply is not required, as long as only reactive current is all that is required from the VSC. The DC field of the SC is also fed from the AC output voltage via a rectifying circuit and sliprings. However, unlike a SC, the output voltage of a STATCOM may contain harmonics and filtering equipment is required. Nevertheless, a STATCOM has some key advantages over a SC, namely faster speed of response, no contribution to short circuit current, absence of moving parts which leads to easier maintenance. Above all, it enables the incorporation of a DC power source. The steady state control characteristic of a STATCOM is illustrated in Figure 2.6 with the assumption of no losses and supplying/drawing a purely reactive current ($I_{STATCOM}$).

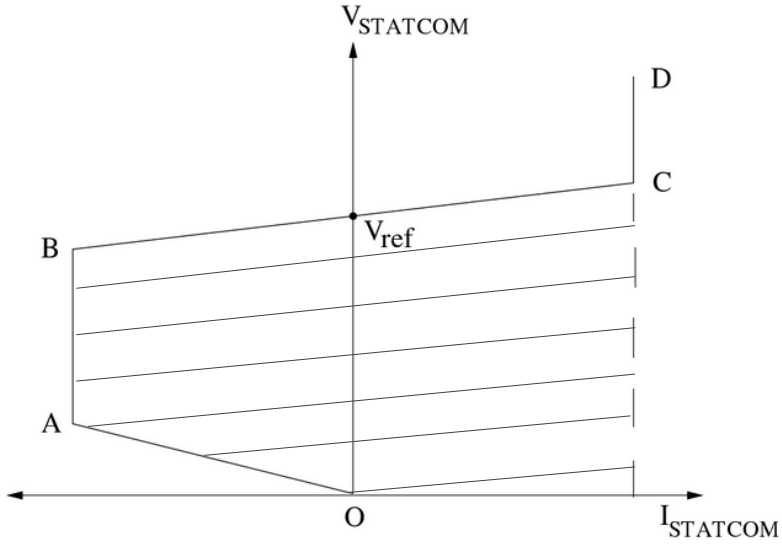

Figure 2.6 *STATCOM control characteristic [35].*

2.2.4 Three-Phase Six-Pulse STATCOM

The STATCOM used in this work is a six-pulse, three-phase STATCOM. The circuit diagram is shown in Figure 2.7. It consists of six switches (or valves) made up of IGBTs with antiparallel diodes. Its principle of operation is based on the assumption that each switch conducts once in a cycle and for 180°. As shown in Figure 2.7, switches are numbered according to the sequence they are fired. The two valves connected in series in the same leg conduct in a complementary manner. To prevent short-circuits only one of the switches (valves) is on at any given time. The following two simplifying assumptions are made in the operation of the six-pulse STATCOM.

1- The DC side voltage is constant if a rather large (infinite size) capacitor is used.
2- Losses are negligibly small

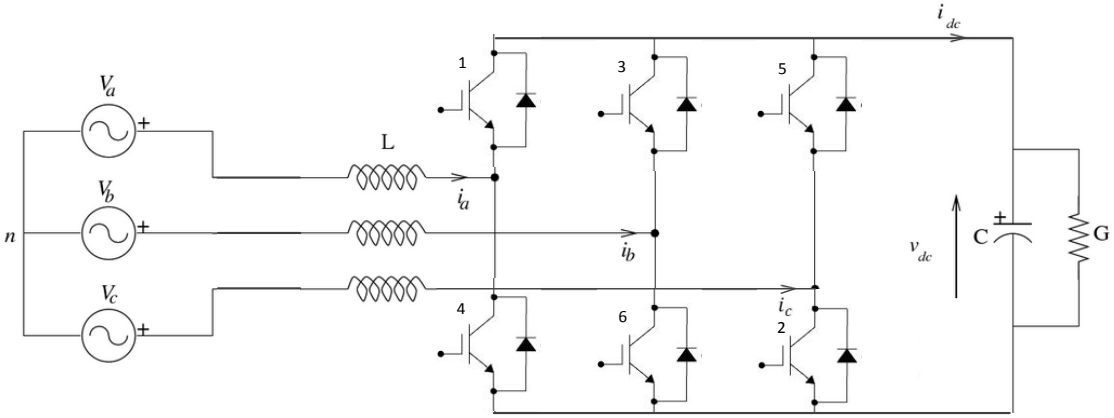

Figure 2.7 *A six pulse VSC diagram [35].*

The voltage waveform E_{aN} is shown in Figure 2.8. E_{bN} and E_{cN} have similar waveforms except that they are phase shifted by 120° (E_{bN} lags E_{aN} by 120° and E_{cN} lags E_{bN} by 120°). E_{an}, E_{bn} and E_{cn} are measured with respect to the source neutral and obtained using the following equations:

$$E_{an} = E_{aN} + V_{Nn} \tag{2.9}$$

$$E_{bn} = E_{bN} + V_{Nn} \tag{2.10}$$

$$E_{cn} = E_{cN} + V_{Nn} \tag{2.11}$$

Assuming a symmetric circuit and balanced operation:

$$E_{an} + E_{bn} + E_{cn} = 0 \tag{2.12}$$

Hence,

$$V_{Nn} = -\frac{E_{aN} + E_{bN} + E_{cN}}{3} \tag{2.13}$$

and

$$E_{an} = 2\frac{E a_{aN}}{3} - \frac{E_{bN}}{3} - \frac{E_{cN}}{3} \tag{2.14}$$

$$E_{bn} = 2\frac{E_{bN}}{3} - \frac{E_{cN}}{3} - \frac{E_{aN}}{3} \tag{2.15}$$

$$E_{cn} = 2\frac{E_{cN}}{3} - \frac{E_{aN}}{3} - \frac{E_{bN}}{3} \tag{2.16}$$

The fundamental frequency component of E_{an} is obtained as follows:

$$E_{a1} = \frac{4}{\pi\sqrt{2}} \int_0^{\pi/2} E_{an} \sin \omega t \, d\omega t = \frac{\sqrt{2}}{\pi} V_{dc} = 0.45 \, V_{dc} \tag{2.17}$$

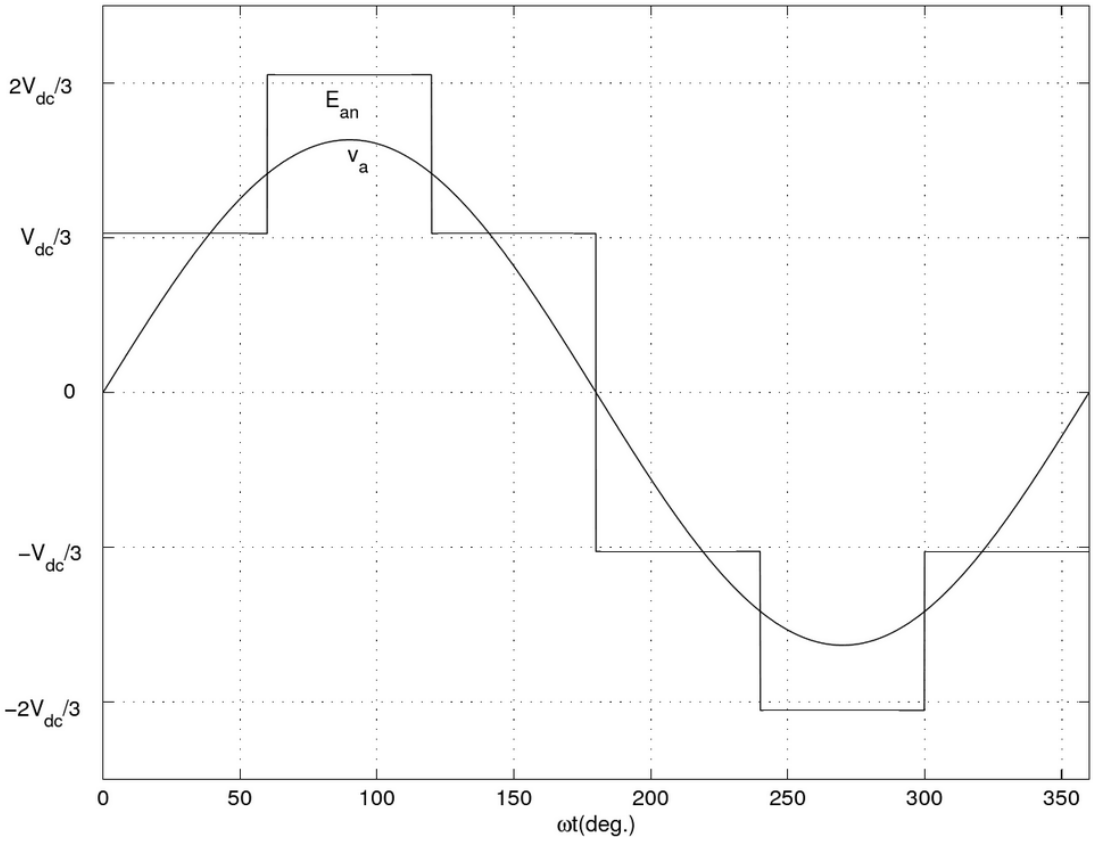

Figure 2.8 *Waveform of v_a along with E_{an} [35].*

The voltage waveform E_{an} contains a fundamental frequency component and harmonic components which calculated from the following equation:

$$E_{ah} = \frac{E_{a1}}{h} = \frac{0.45 V_{dc}}{h}$$

$$h = 6k \pm 1, \quad k = 1, 2, 3 \tag{2.18}$$

The RMS value of the fundamental component of the reactive current (I_r) and harmonic current (RMS) are given by equations (2.19) and (2.20).

$$I_r = \frac{V - 0.45 \, V_{dc}}{\omega L} \tag{2.19}$$

$$I_h = \frac{0.45 \, V_{dc}}{\omega L h^2} \tag{2.20}$$

2.3 BESS Power Electronics

In the context of the BESS, two principle power electronic-based systems are at work:

1. Power conversion system (PCS)
2. Battery management system (BMS).

The PCS controls the flow of power between the battery storage, and the load. The BMS is required to monitor the status of the batteries, facilitate in balancing battery cells during charge/discharge and communicate information to the PCS. The PCS may be connected directly to the utility, the load, the energy storage or even a renewable source. In this work the focus will be on the grid-connected parallel configuration i.e. the BESS is connected in parallel with the utility to the load as shown Figure 2.9.

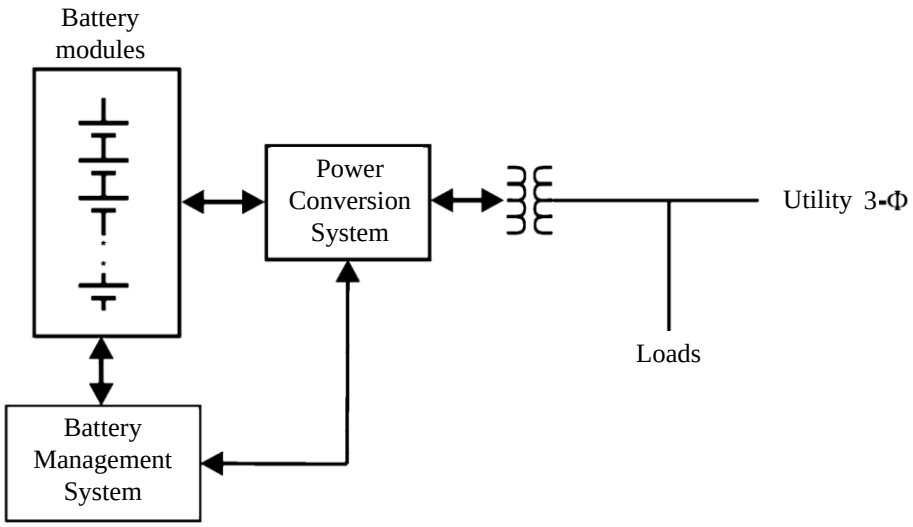

Figure 2.9 *Basic representation of the grid-connected parallel configuration [36].*

2.3.1 Power Conversion Systems (PCSs)

Prior to the evolution of modern power electronics, power converters were typically rotary machines [37]. By contrast, modern converters depend on fast, high-power semiconductor switches.

In most fielded systems (750 kVA and below) the PCS uses insulated-gate bipolar transistors (IGBTs). These devices are both gated on and gated off (hard switched) and often switched at several kHz. At 10 MVA and above, PCSs typically use Silicon-Controlled Rectifiers (SCRs) and gate turn-off thyristors (GTOs) which are only gated on or off and normally the switching is in the range of hundreds of Hz [36]. While uncertainties remain for the range from 750 kVA to 1MVA, 1GBTs are used in most systems. In the range of 1 to10 MVA, there are few fielded systems [36].

2.3.2 Battery Management Systems

The BMS monitors the measurements of cell temperature, voltage, and current. The BMS estimates the battery state-of-charge (SOC) or state-of-health (SOH) based on these measurements and information such as the battery age and the number of charge/discharge cycles. In addition, the BMS may protect the battery by disconnecting it from the power conversion system (PCS) in bad events such as over voltage, under-voltage, over temperature and over-current. It may also be equipped with a thermal management or active cooling system [38].

2.4 Battery Energy Storage System (BESS)

Up to around 1980s, the battery energy systems were considered as a useful resource for a single application-load leveling. According to the classical load-leveling or peak-shaving application, BESS would be charged at night time when the electric grid is lightly loaded and discharged when the electric grid needed energy to serve the peak loads i.e. during late afternoon and early evening hours.

This single-application concept was revisited in late 1980s when researches at Electric Power Research Institute (EPRI) and Sandia National Laboratories began suggesting that multiple functions could be performed in both the transmission and distribution sides of the electric grid by BESS.

A case in point is the 17 MW Berliner Kraft- und Licht (BEWAG) battery system in Germany, which provided spinning reserve and frequency regulation. It was installed in 1986 and was the largest Lead-acid BESS in the world at that time [36]. It functioned for nine years until the end of the battery's service life. The battery consisted of 7080 cells, each with a capacity of 1000 Ah. The cells used copper-stretch-metal (CSM) technology. For detailed discussion of CSM technology Ref. [39] is recommended.

The BEWAG system was followed by the 20-MW Puerto Rico Electric Power Authority (PREPA) BESS. PREPA BESS was commissioned in 1996 and, as BEWAG, provided spinning reserve and frequency regulation for Puerto Rico's island grid. The PREPA consisted of 6000 flooded cells, each with a capacity of 1280 Ah. The power-conditioning system consisted of two paralleled converters rated at 10 MVA and had 6-pulse GTO bridges (18 pulses).

A relatively modest size BESS is the 1.3 MW Metlakatla system located in the island community of Metlakatla, Alaska. It was initially intended to mitigate the significant voltage and frequency fluctuations caused by intermittent motor loads at the local lumber mill. Soon after, it was used to supply spinning reserve. The Metlakatla system was renovated in 2008 and currently uses lead-acid batteries in a valve-regulated cell design [40].

Another BESS with low capacity is the 2-MW PQ2000. It is the first model of a modular, transportable BESS. It was specifically intended to provide up to 2 MVA for 30 seconds or less where power quality is imperative for continued operation. This system continuously monitors the grid voltage. When a disturbance is detected, switches in the PQ2000 replace the grid power with the power supplied by the BESS. The switching speed is relatively fast (of one cycle in this case), which is essential for this type of application [36].

The 46-MW BESS that was commissioned by Golden Valley Electric Association (GVEA) in Fairbanks, Alaska, in 2003 represents a high capacity BESS on the other end of the size spectrum. The system uses rechargeable nickel–cadmium cells and an ABB converter [36]. The cells are positioned in four parallel strings, with a nominal voltage of ±2,500 VDC and a storage capacity of 3,680 Ah. The GVEA system is specifically used for the following purposes:

1. Voltage support under steady state and emergency situations
2. Black start, in case the connection between Fairbanks and Anchorage goes down and Fairbanks becomes an island
3. Automatic scheduling
4. Transmission line stabilizing
5. Automatic generation control
6. Automatic scheduling
7. scheduled load increases

Chile [41] and California [42] are two good examples of quite recently installed battery energy storage facilities. The facility in Northern Chile integrates a 20 MW of advanced battery energy storage with a 544 MW thermal plant. The main objective of this BESS has been to increase the capacity of the plant while maintaining reliability and operational flexibility. This BESS includes one million advanced Lithium-ion battery cells, making up ten 2 MW battery containers and five 4 MW power control containers. In California, the primary function of the BESS application has been to maintain the critical process loads during outages resulting from external disturbances to the plant. This BESS is capable of supplying critical loads of up to 2.5 MW for one hour (one hour is the required time to safely shutdown the plan). The secondary function of this system is to extend the spinning reserve of the plant.

An overview of the latest BESS projects indicate that slightly more than forty nine percent of Spain’s electricity is produced by renewable energy sources such as wind and solar power [43]. This said to be non-firm generation and it is raising concerns among power systems operators because wind drops and clouding would leave the system very exposed. Toshiba and the Spanish electricity provider Fenosa have joined forces [44] to

install a pilot at the Alcada de Henares distribution substations, near Madrid, to test its latest transportable lithium-ion Battery Energy Storage System (BESS).

The initial pilot will be followed by many more demonstration projects at various sites. The pilot programme aims to assess the transportable BESS's capability in supporting the electricity supply at key areas under seasonal or temporary high electricity demands. Additional attributes of the BESS technology is its effectiveness to regulate the inherent power and voltage fluctuations brought about by variable renewable energy resource. The pilot of the transportable BESS is rated at 500 kW output and 776 kWh.

Another storage technology project relates to Alstom's commercial project, MaxSine^{TM} eStorage, to be deployed at Nice Grid, as part of one of the largest smart grid demonstration projects in France. The project brings together 27 partners from 12 EU countries. The aim is to create a local microgrid integrating the MaxSine^{TM} eStorage connected to a point of common coupling with 200 PV installations [45].

2.5 Summary

The battery is the cornerstone of the BESS. The battery technology has undergone very significant developments in recent years. Some of the battery types suitable for power systems applications were presented and some of their advantages and disadvantages were discussed. The Lead-acid battery is the oldest and the best well-developed technology, hence, there is very little room for improving further this type of battery technology. This contrasts with the Li-ion option which continues to gain commercial ground in power systems applications.

The operating principles of DC/DC converter and the DC/AC converter were discussed. This has provided the background for the simulation studies carried out in Chapter 4. Also, some examples of utility-scale BESS facilities in current operation were discussed.

3. FREQUENCY CONTROL THEORY

This chapter is dedicated to load frequency control in power systems. The importance of frequency stability and control will be discussed first followed by a brief description of the requirements and criteria on control performance. Since the generator is the main element which determines the frequency in a power system, it is reasonable to dedicate a section to briefly describe the frequency control loops and governing systems in the generating units. Two main control stages i.e. primary frequency control and secondary frequency control will then be explained in detail. A short discussion on the quality of frequency control will conclude this chapter.

3.1 Frequency Stability Importance

An electrical power system must deliver stable electricity to customers. Voltage and system frequency are the main variables to guarantee the system stability. In this chapter the focus will be only on the frequency stability. The frequency of a power system is dependent on real power balance. An imbalance between the electrical power consumed in the system and the mechanical power delivered by the turbines brings about a frequency perturbation throughout the system. Hence, system frequency can be considered as a useful index to indicate system generation and load balance [46].

One of the most recent proposed definitions of *power system stability* is [47] “the ability of an electric power system, for a given initial operating condition, to regain a state of operating equilibrium after being subjected to a physical disturbance, with most system variables bounded so that practically the entire system remains intact”.

Consequently, *Frequency instability* is defined as the inability of a power system to maintain the frequency within the operating permissible limits. Poor coordination of control and protection equipment can be the causes of frequency instability [48].

Frequency control is becoming more important as power grids grow in size and networks with greater complexity and changing structure develop. From an economic perspective, the growing demand for efficient and reliable power systems has caught the attention of electricity producers striving to maintain system frequency within permissible limits, as much as possible.

In the early days of power systems, very basic controls were used. In most cases, system control was performed manually. It is also worth mentioning that the first systems

commonly had ample stability margins, so very often the presence of controls was unnecessary to guarantee the stability in most operating conditions. Gradually the systems grew in size and the loading increased. Consequently, higher demands for quality of supply i.e. the voltage profile and the frequency, were required. Automatic controllers and regulators emerged to fulfil those new requirements. The frequency of the system cannot be maintained within desired limits without control. The variation of the load is the main reason for frequency and voltage control. The power system control has also the ability to enhance the economic performance of the power system. In summary, there are three important reasons for power systems control, namely,

• Quality

• Security

• Economy

The first controllers introduced in power grids, were local controllers i.e. both the controller input and the quantity controlled were at the same location. For instance, the voltage control and primary frequency control of synchronous generators were performed by local controllers. As the systems grew in size and tie-lines connecting different subsystems developed, local controllers could no longer provide a reliable and economical operation of the system. Several local controllers had to be synchronized and made to work together and data from different local controllers had to be transferred to a main control center and in return, they received global control actions. Accordingly, a hierarchical control structure had to be established [49].

3.2 Requirements and criteria on Control Performance in Europe

Requirements and responsibilities on control performance of systems are set by a coordinating organization. Only European systems are discussed below as an example. The "Union for the Co-ordination of Transmission of Electricity" (UCTE) is the association of transmission system operators in Europe responsible for a reliable market base by efficient and reliable electric power highways [50].

It has the responsibility to coordinate the operation of transmission system operators of 22 European countries. “Through the networks of the UCTE, about 450 million consumers are supplied with electric energy – annual electricity consumption totals approximately 2300 TWh in this region” [50]. Information regarding standards, requirements, principles and regulations in transmission system operators is available in the UCTE operation handbook. The handbook addresses the issue of performing load frequency control by the participating countries. It contains five chapters concerning frequency control, namely,

A. Primary control

B. Secondary control

C. Tertiary control

D. Time control

E. Measures for emergency conditions

As an example, criteria and requirements in primary frequency control are very briefly presented here.

3.2.1 Criteria

Nominal frequency: The set-point frequency f_0 defines the target value of the system frequency for system operation. The nominal frequency in synchronous areas is 50 Hz.

Frequency deviations: Different criteria are considered to differentiate the value of deviation:

1. *Calling up of Primary Control:* Primary control is activated only if frequency deviation exceeds ±20 mHz.

3. *Minimum Instantaneous Frequency:* Instantaneous frequency should not drop below 49.2 Hz (that corresponds to -800 mHz as maximum permissible deviation from the nominal value).

4. *Load-Shedding Frequency Criterion:* Load-shedding starts when the frequency of a system is 49.0 Hz (or below). The detailed step-plans for load-shedding determine additional frequency criteria for further measures.

5. *Maximum Instantaneous Frequency*: "The instantaneous frequency must not exceed 50.8 Hz in response to a loss of load or interruption of power exchanges equal to or less than the reference incident" [51].

Deployment Times of Primary Control Reserve: "The time for starting the action of primary control is a few seconds starting from the incident, the deployment time for 50 % or less of the total primary control reserve is at most 15 seconds and from 50 % to 100 % the maximum deployment time rises linearly to 30 seconds" [51].

3.2.2 Requirements

Accuracy of Frequency Measurements: For the primary control purpose, the accuracy of local frequency measurements used in the primary controllers has to be better than 10 mHz.

Insensitivity of Controllers: The insensitivity range of primary controllers is not allowed to exceed ±10 mHz. Where there are dead bands in specific controllers, they have to be offset within the CONTROL AREA / BLOCK concerned.

Voltage control policy is also specified in the Operation Handbook. Similar to frequency control, voltage control can also be divided into primary, secondary, and tertiary voltage control. In general, the voltages of the 380/400 kV network have to be maintained within the range 380–420 kV [50]. Further discussion over the voltage control is out of the scope of this work.

3.3 Governing Systems and Frequency Control Loops

As mentioned earlier, in a power grid load is constantly changing. If the load-generation balance is not maintained, a deviation in frequency will occur. Primary frequency control is the first step towards restoring the frequency to the reference value. Supplementary controls (secondary and tertiary controls) will be activated subsequently for more precise control.

The primary frequency control is achieved through the governing system of the generators. Thus it is reasonable to look into the governing systems and control loops in the generating units. Sections 3.3.1 to 3.3.3 describe the governing system. Section 3.3.4 explains the frequency control loop in a single generating unit. Simple low-order linearized models for the turbine and governor are presented in section 3.4.

3.3.1 The Governing System

Electrical energy is produced by synchronous generators driven by prime movers, usually turbines or diesel engines. The turbine can be a steam turbine, a gas turbine or a hydro turbine equipped with a governor.

The governor receives a signal representing the shaft speed of the generator (≡ system frequency) and compares this with the set-point (50 Hz), also receives a set-point for power output. The governor adjusts a throttle valve in the steam supply to the turbine in order to regulate the shaft speed and power output. The governor is situated at the power station.

The governor uses feedback of speed and power output and compares these with the desired “set point” values. Figure 3.1 shows the ideal governor characteristics.

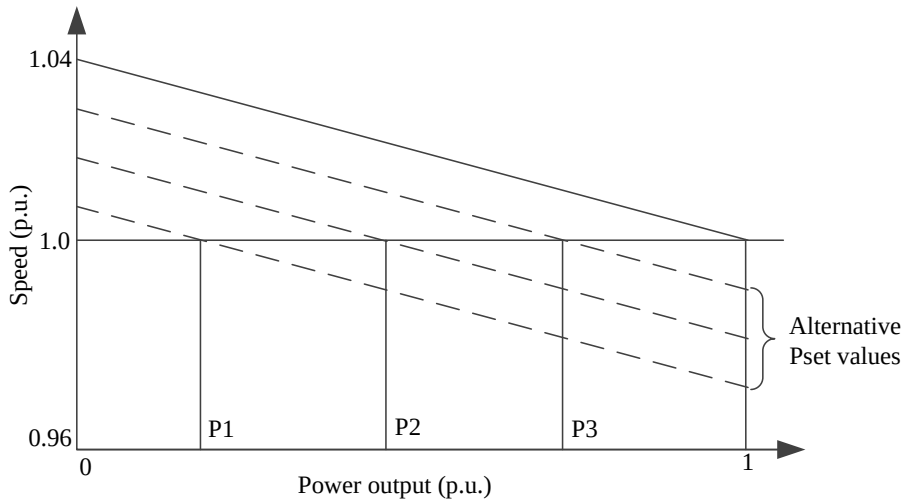

Figure 3.1 *Ideal governor characteristics.*

Governors are usually set up to give the full range of power output (0 to 1 p.u.) for a frequency or speed change of 0.04 p.u. This is referred to as 4% "droop"

$$Governor\ Droop = \frac{change\ in\ speed\ (p.u.)}{change\ in\ output\ (p.u.)} * 100 \quad per\ cent$$

3.3.2 Load Sharing Between Generators via Governor Action

Suppose that two synchronous generators operate in parallel and supply a total load of MW_T. The capacities of the machines are MW_1 and MW_2 and both have 4% droop as shown in the power-speed characteristic of Figure 3.1. Calculate the load taken by each machine according to governor action.

Solution:

Let x power be supplied from the MW_1 generator and α be the drop in speed from no-load speed.

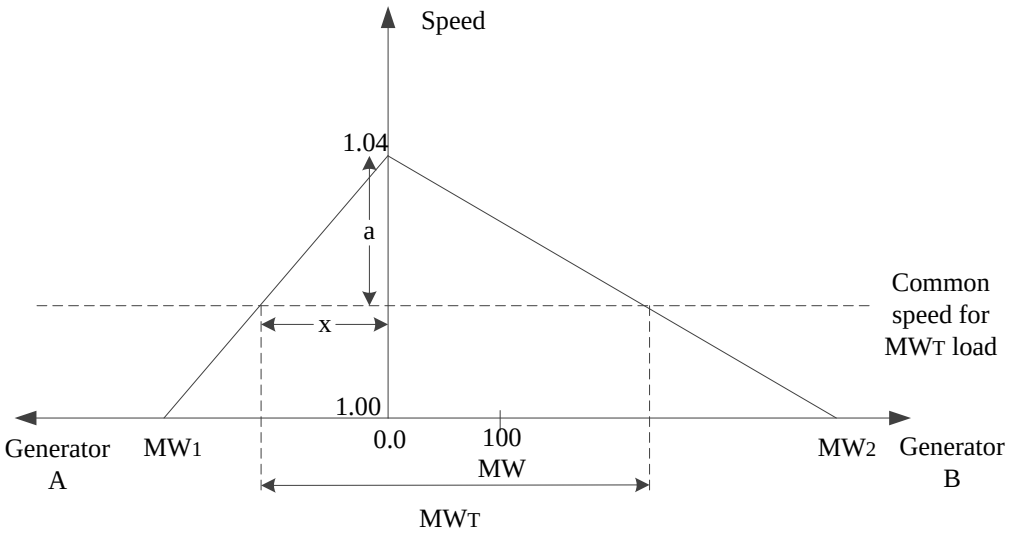

From the above figure:

$$\frac{4}{MW_1} = \frac{\alpha}{x}$$

and for the MW_2 machine

$$\frac{4}{MW_2} = \frac{\alpha}{MW_T - x}$$

Therefore

$$x = \frac{MW_1}{MW_1 + MW_2}$$

For instance when MW_1 = 100 MW, MW_2 = 22 MW and MW_T = 200 MW, x = 66.6 MW. Therefore, the loading on the 200 MW machine is 133.3 MW.

Note that when the generator droops are equal, the generators share the total load in proportion to their capacities (or ratings). Hence it is desirable for the droop settings of all generators to be equal.

3.3.3 Dynamic Response of Governor

Since there are time delays and time lags in the movement of the valve and the steam turbine response, the governor does not give an instantaneous response.

Suppose a generator is subject to a step reduction in demand (Figure 3.2):

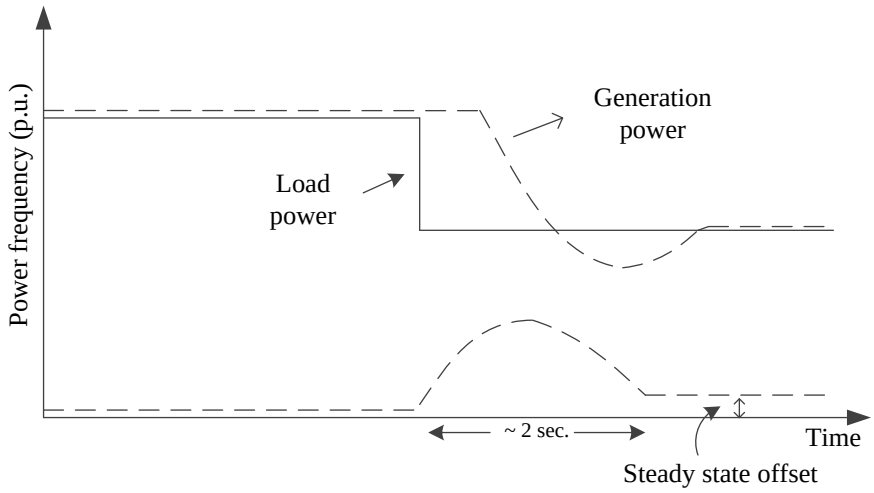

Figure 3.2 *Generator response to a step reduction in demand.*

Notice that because the generator is a "proportional" controller (i.e. it is a simple constant gain) a steady state offset frequency error is required to allow the generated power to settle at a lower level, at which it balances the load.

3.3.4 Control Loops

Figure 3.3 shows the schematic block diagram of a synchronous generator along with its frequency control loops. The frequency deviations are sensed by the *speed governor* through primary and supplementary control loops. The hy*draulic amplifier* provides mechanical force to position the gate (valve) in order to control the water (or steam) flow, and the function of the *speed changer* motor is to provide a steady-state power output setting for the turbine [46].

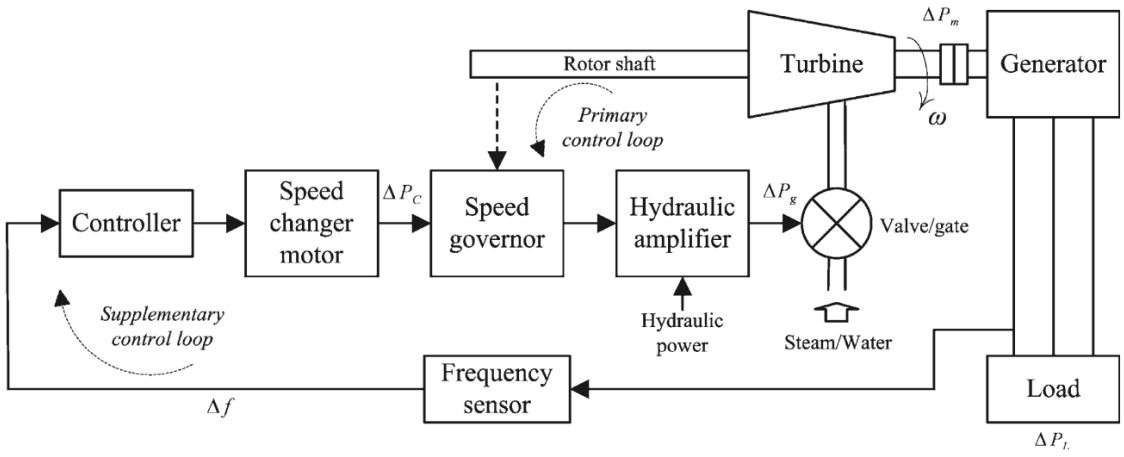

Figure 3.3 *The block diagram of a synchronous generator with its basic frequency control loops [46].*

Each generating unit has its own governing system which controls the rotor speed by adjusting the output power of the generator. All generating units contribute to the overall change in generation, regardless of the location of the load change in the grid, through their speed governing system. However, this primary control action is not sufficient to restore the frequency to the reference value and supplementary control loops are required.

3.4 Frequency Response Modelling

Although power systems have a highly non-linear and time-varying nature, for the purpose of frequency control synthesis and analysis, a simple low-order linearized model is used. For the block diagram presented in Figure 3.3 of one generating plant, the following simplified frequency response is used.

$$\Delta P_m(t) - \Delta P_L(t) = 2H\frac{d\Delta f(t)}{dt} + D\Delta f(t) \tag{3.1}$$

Equation (3.1) expresses the relationship between the incremental mismatch power ($\Delta P_m - \Delta P_L$) and the frequency deviation (Δf). Δf, Δp_m and ΔP_L are the frequency deviation, mechanical power change and the load change. H is the inertia constant and *D* is the load damping coefficient.

Using the Laplace transform, (3.1) will be written as:

$$\Delta P_m(s) - \Delta P_L(s) = 2Hs\Delta f(s) + D\Delta f(s) \tag{3.2}$$

Equation (3.2) can be represented in a block diagram as shown in Figure 3.4. Consequently, using this generator–load model (equation (3.2) and Figure 3.4), the described block diagram of the closed-loop synchronous generator (Figure 3.3) can be reduced as shown in Figure 3.5.

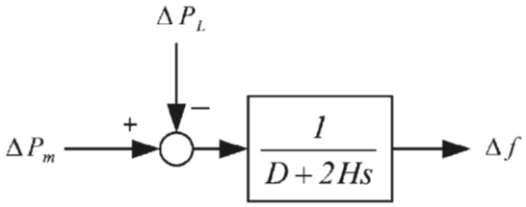

Figure 3.4 *Generator load model [46].*

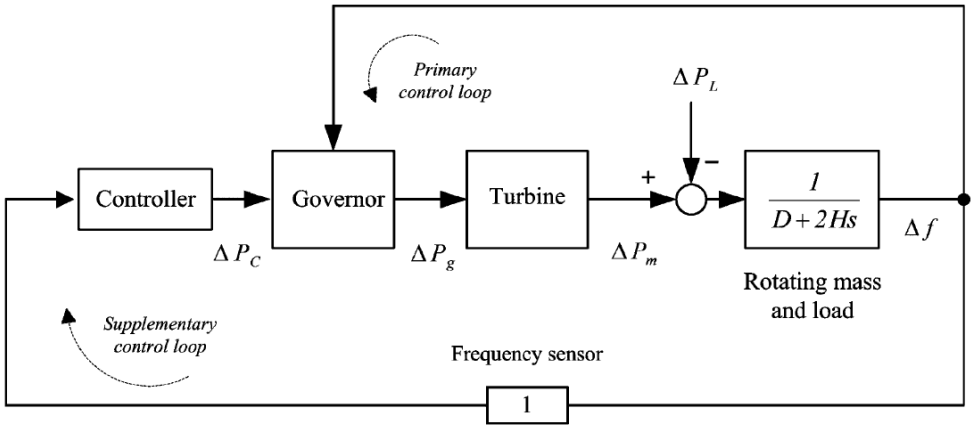

Figure 3.5 *Reduced block diagram of Figure 3.3 [46].*

In power system frequency analysis and control design several low order models for representation of turbine and generator dynamics have been proposed [52]. As an example, steam and hydraulic turbine models are presented here. Figures 3.6 – 3.8 illustrate the block diagrams of the speed governor and the turbine for steam and hydraulic governor units appropriate for load frequency control analysis. R (and R_h) is the speed-droop characteristic and T_g, T_t, T_r, T_{tr}, T_{gh} and T_{th} are generator–turbine time constants. A combination of the block diagrams in Figures. 3.5 and 3.6 is shown Figure 3.9 which is the block diagram of a non-reheat steam generator unit with its frequency control loops. Further discussion of turbine and governor models is out of the scope of this section.

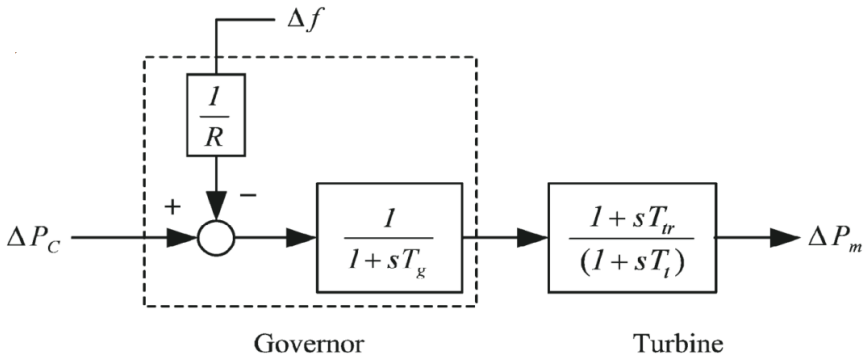

Figure 3.6 *Block diagram of turbine–governor; non-reheat steam unit [46].*

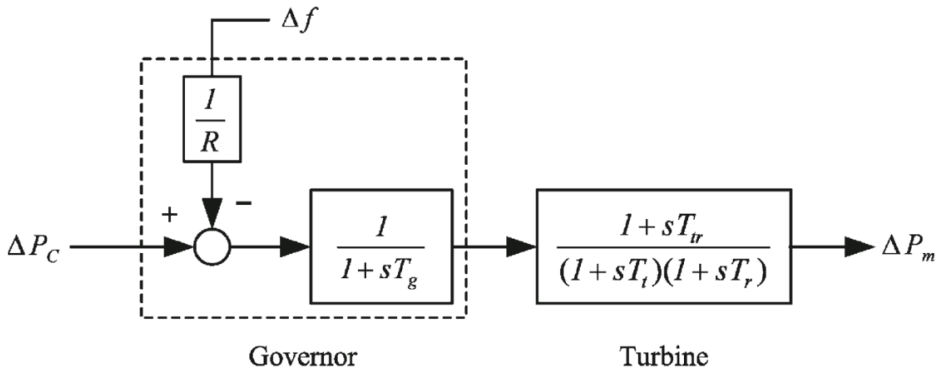

Figure 3.7 *Block diagram of turbine–governor; reheat steam unit [46].*

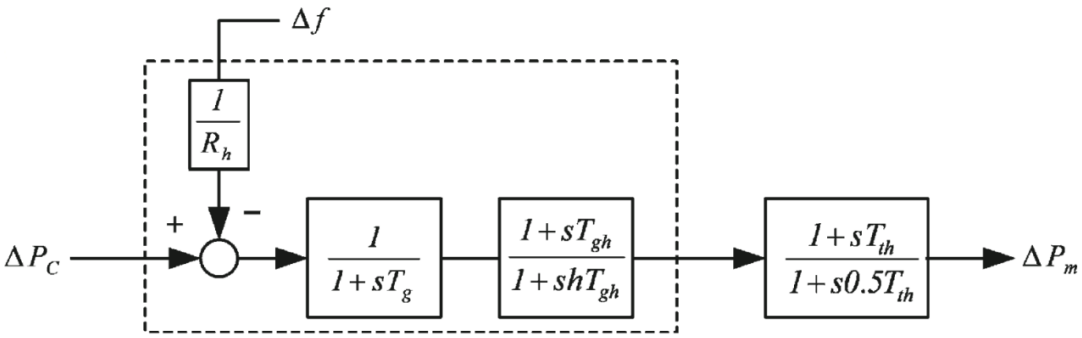

Figure 3.8 *Block diagram of turbine–governor; hydraulic unit [46].*

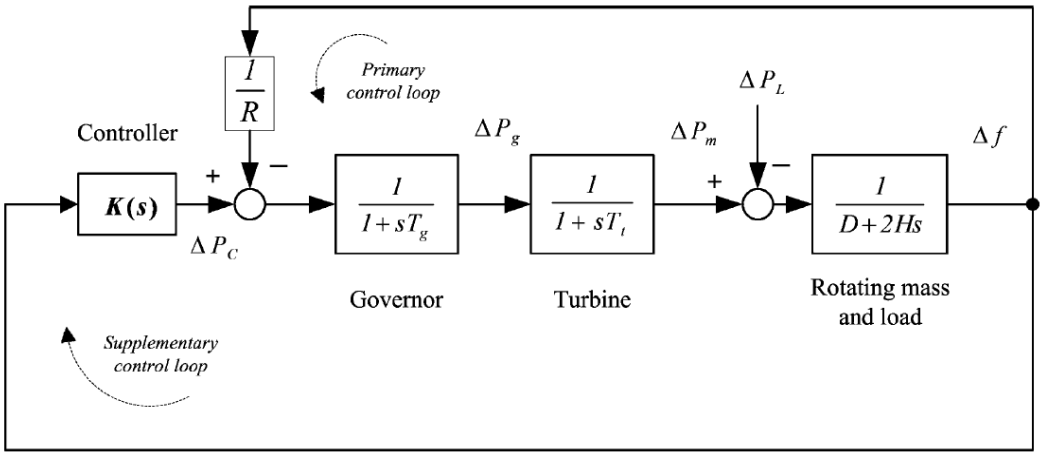

Figure 3.9 *Governor model with frequency control loops for a non-reheat steam generator unit [46].*

3.5 Power System Control

Power system control is needed in order to:

- maintain the balance between generation and load plus losses

- maintain constant frequency and voltage.

- maintain network security

- operate the system at minimum operating cost

We will consider control over the timescale from 1 second to 1 day. Control is achieved by the following subsystems:

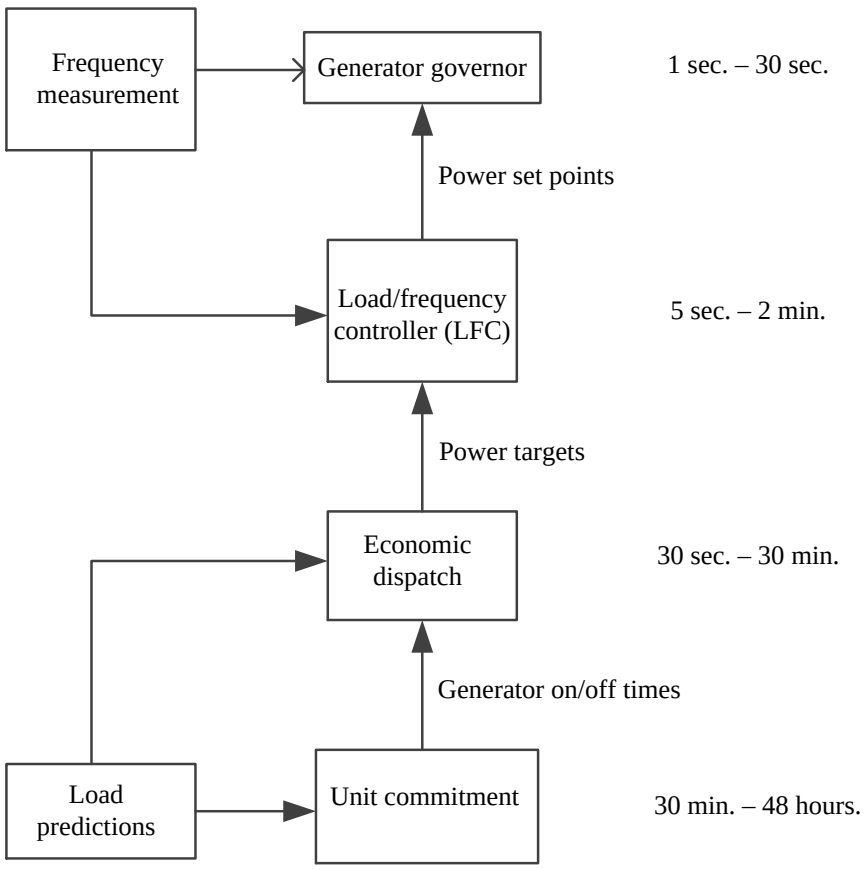

Load Frequency Controller: this is a software package running on an area control or central control computer and linked to the power stations via data communications. It adjusts the power output set points of all the generators to try and achieve steady 50 Hz operation and to maintain tie-line flows at their scheduled values.

Economic Dispatch: software which adjusts target power values over a 30 min. period which are then passed on to the LFC. The objective is to minimize the overall fuel cost of operation while satisfying various constrains and limitations.

Unit Commitment: software which optimizes the schedule of bringing the generators on to the system and off again following the daily cycle of demand.

Load Prediction: software which predicts the demand for electricity over the next 24 hours- 1 week.

3.6 Primary and Secondary Frequency Control

This section presents two frequency control stages i.e. primary and secondary frequency controls. The main focus will be on the primary frequency control due to its relevance to this project presented in the next chapters. The time of simulations carried out is shorter than one minute (as mentioned earlier, secondary frequency control is within 5 to 10 minutes). Before presenting the primary and secondary control, the "generation characteristic" needs to be briefly discussed. Generation characteristic determines the ability of a power system to compensate for an active power imbalance at the cost of a deviation in frequency [53].

3.6.1 Generation characteristic

The rotational speed of generators in the power system is proportional to the system frequency:

$$\frac{\Delta f}{f_n} = \frac{\Delta \omega}{\omega_n} \tag{3.3}$$

In steady-state, from equation (3.3), it is possible to formulate an equation that expresses the power-frequency characteristic of a single generating unit:

$$\frac{\Delta f}{f_n} = -\frac{\rho_i \Delta P_{mi}}{P_{ni}}, \qquad \frac{\Delta P_{mi}}{P_{ni}} = -\frac{K_i \Delta f}{f_n} \tag{3.4}$$

where Δp_{mi} is the change in mechanical power of the ith generating unit; P_{ni} is the nominal power of the ith generating unit; and ρ_i is the droop of the ith generating unit defined as follows:

$$\rho = \frac{\Delta f^*}{\Delta P^*} = \frac{\frac{f_{smin} - f_{smax}}{f_0}}{\frac{P_{max} - P_{min}}{P_0}} \tag{3.5}$$

where Δf^* is the relative frequency deviation; f_{smin} , f_{smax} are the frequencies corresponding to minimum unit and maximum load, respectively. P_{min} , P_{max} are powers under minimum unit and maximum loading conditions; and P_0 is the unit reference power (rated power) [19].

For a power system consisting of N_G generators, in steady state, all the generating units operate synchronously at the system frequency. Based on equation (3.4) the total power change in the system can be obtained as the sum of changes in all generators, as follows:

$$\Delta P_T = \sum_{i=1}^{N_G} \Delta P_{mi} = -\Delta f \sum_{i=1}^{N_G} \frac{K_i P_{ni}}{f_n} \tag{3.6}$$

where ΔP_T is the overall change in the total generated power. Figure 3.10 shows how the equivalent speed-droop (generation) charactristic can be formed by adding the individual generating units' speed-droop (generation) characteristic based on equation (3.6).

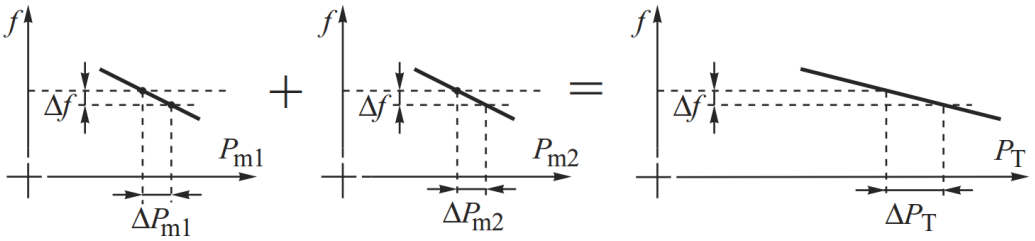

Figure 3.10 *Equivalent generation characteristic of all the units as the sum of the speed-droop characteristic of the individual generating units [53].*

For a power system consisting of a large number of generating units, the equivalent generation characteristic is close to a horizontal line resulting in a little frequency deviation even in the case of a relatively large power change.

In obtaining the equivalent generation characteristic in Figure 3.10, it was assumed that the speed-droop characteristics of all the generating units are linear over the full range of frequency variations. In practice there is an upper limit for power i.e. when the operation point is at the upper limit of the power, a further change in frequency will not

result in more output power. This is illustrated in Figure 3.11 for a single generating unit. This will change the equivalent generation characteristic as shown in Figure 3.12.

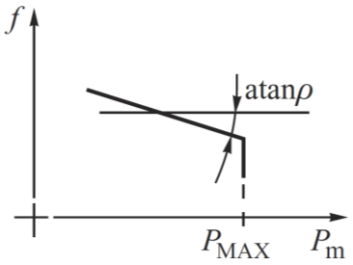

Figure 3.11 *Speed-droop characteristic of a generating unit with a power upper limit [53].*

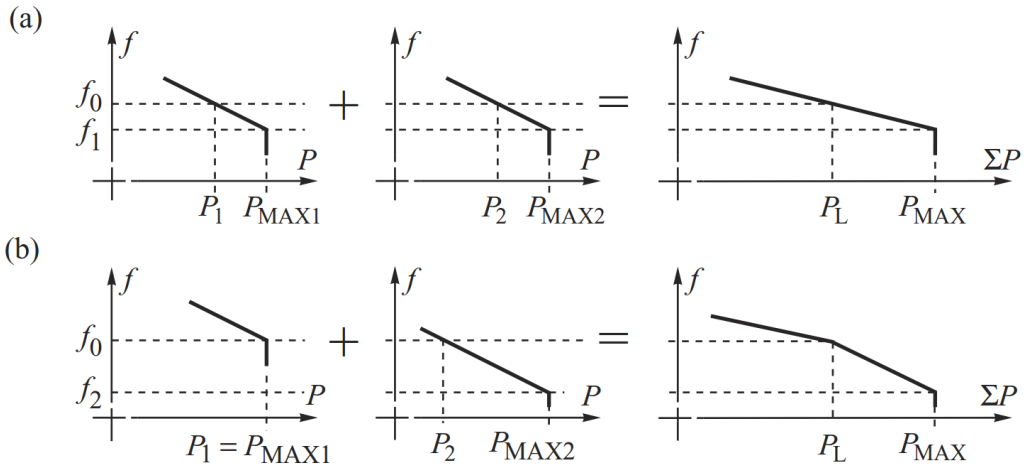

Figure 3.12 *Impact of the presence of an upper limit power [53].*

Nevertheless, in an actual power system the generation characteristic is nonlinear. It consists of many short sections and at some point it becomes a vertical line owing to the output power upper limits described earlier. For small variations in power and frequency, it is convenient to approximate the characteristic in the vicinity of an operational point by a linear representation with a local droop value. The total generation may be assumed to be equal to the total load P_L, i.e.,

$$\sum_{i=1}^{N_G} P_{mi} = P_L \tag{3.7}$$

where N_G is the number of generating units. Dividing equation (3.6) by P_L gives

$$\frac{\Delta P_T}{P_L} = -K_T \frac{\Delta f}{f_n} \quad \text{or} \quad \frac{\Delta f}{f_n} = \rho_T \frac{\Delta P_T}{P_L}, \tag{3.8}$$

where

$$K_T = \frac{\sum_{i=1}^{N_G} K_i P_{ni}}{P_L}, \quad \rho_T = \frac{1}{K_T}. \tag{3.9}$$

3.6.2 Primary Control

Constant system frequency is attained when the total generation and the total system demand (including losses) are equal. Such a case corresponds to the generation characteristic approximated by equation (3.8). However, the system loads are also frequency dependent and an equation similar to (3.8) expresses such a non-linear-dependency, in linearized form:

$$\frac{\Delta P_L}{P_L} = K_L \frac{\Delta f}{f_n} \tag{3.10}$$

where K_L is the *frequency sensitivity coefficient of the power demand.* Empirical studies indicate that the generation characteristic is much more frequency dependent than the load characteristic. Typically K_L is in the range of 0.5 to 3 whereas K_T is about 20. Note that K_T and K_L have opposite sign implying an increase in frequency leads to a drop in generation and a rise in load.

Figure 3.13 shows the generation characteristic (equation (3.8)) together with the load characteristic (equation (3.10)) in the (P, f) plane. The intersection of the load and generation characteristics is the system equilibrium point. Following an increase in the total demand ΔP_{demand}, a new equilibrium point is reached, as indicated in Figure 3.13. The increase in the demand is compensated in two ways. Firstly, by an increase in the generation by ΔP_T and secondly, by a decrease in the demand by ΔP_L. The new operating point is at a new frequency f_2 lower than the old frequency f_1. It should be noted that in practice $\Delta P_T > \Delta P_L$.

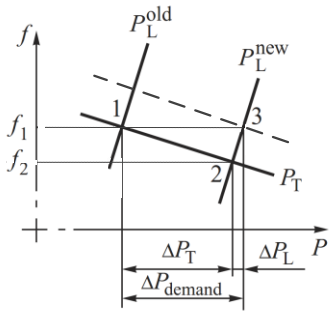

Figure 3.13 *Equilibrium points when a disturbance occurs [53].*

As deduced from Figure 3.13, the frequency response of the system can be presented as follows:

$$\Delta P_{demand} = \Delta P_T - \Delta P_L = -(K_T + K_L)P_L \frac{\Delta f}{f_n} = -K_f P_L \frac{\Delta f}{fn}. \quad (3.11)$$

Clearly, when there is an increase in demand the primary control is activated only if there are still generating units which are not yet operating in their full-load mode.

In Figure 3.13 the decrease in the demand by ΔP_L is due to the frequency dependency of the load and the increase in generation by ΔP_T is caused by the turbine governors. The action of the turbine governors in response to frequency changes while the reference values of regulators are maintained, is referred to as *primary frequency* control [53]. The main characteristic of primary frequency control is its relatively fast response, whose action time is less than 30 seconds following a load-generation imbalance.

3.6.3 Secondary Control

In addition to the primary frequency control, a large synchronous generator may be equipped with a secondary frequency control loop. When the frequency variations exceed a pre-defined value, the turbine-governor (speed governing) control will take action in order to change the power input to the prime mover. The rotor acceleration finally reaches zero and the frequency reaches a new state nearer to the reference value. This action is referred to earlier as primary frequency control. Following the primary frequency control, there still is a steady-state error in the frequency. To overcome such an error, supplementary actions may be taken i.e. the governor set points are changed and the frequency is restored to its initial value [19]. To remove the error and return the frequency to the initial desired value, the generation characteristic has to be shifted upwards to the position drawn by the dashed line in Figure 3.13. In order to do so, the P_{ref} setting requires changing in the governing system. By making the same change in the P_{ref} setting of more individual governors the overall generation characteristic of the system moves upwards. Finally the restoration of the rated frequency is obtained but now at the required increased value of power demand. Such a control action applied to the governing systems of the individual turbines is referred to as *secondary frequency control* or *load frequency control (LFC)* or *automatic generation control (AGC).* The objectives of the LFC are:

- to maintain tie-line power flows at the scheduled levels

- to maintain system frequency at 50 Hz

- to maintain synchronous time = clock time

- to control the individual generator power outputs to the target levels (provided by economic dispatch)

By way of example consider a two area systems (Figure 3.14):

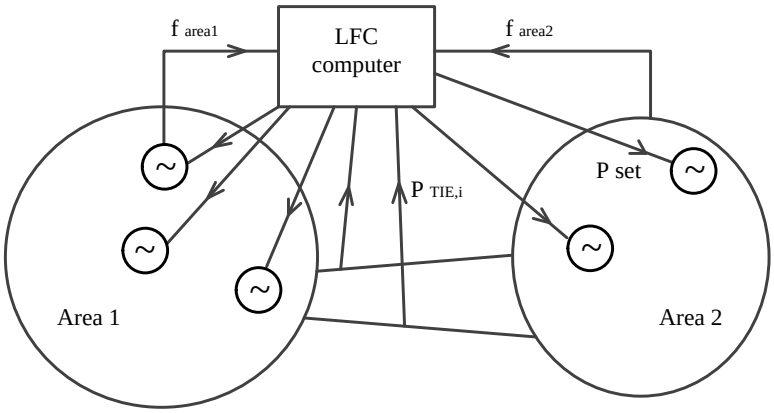

Figure 3.14 *LFC for a two-area system.*

The inputs to the LFC software are:

- f_{area1}: frequency of area 1

- f_{area2}: frequency of area 2

- P_{TIEi} : power flow on tie-line i

The LFC attempts to minimize the following functions:

$$\alpha \,.\sum_{i=1}^{NT}(P_{TIEi} - P_{TIEi}^{SCH})^2 \,.dt$$

$$+\beta \,.\sum_{i=1}^{NA}(f_{areai} - 50)^2 \,.dt$$

$$+\gamma \,.\int_0^{\infty}\sum_{i=1}^{NA}(f_{area1} - 50)^2 \,.dt$$

where $\alpha, \beta \; and \; \gamma$ are weighting coefficients
NT = number of tie-lines
P_{TIEi}^{SCH} = scheduled flow on tie-line i
NA = number of areas.

Notice that functions are squared in order to penalize $+ve$ and $-ve$ errors between desired and actual values. The integral is introduced in order to penalize any deviation

between synchronous time and actual time. The integral of frequency represents synchronous time and if the integral of time is needed to zero then electric clocks will show the correct time.

The above function can be evaluated for a particular area, rather than calculated for all the areas, and is referred to as the Area Control Error (ACE).

The generator outputs in that area are then adjusted according to

$$\Delta P_{gen} = K_1\, ACE + K_2 \int_0^{\infty} (ACE)dt \tag{3.12}$$

where ΔP_{gen} = Total change in power output for all generators in the area

$K_1 =$ Total change in power output for all generators in the area

$K_2 =$ Proportional Gain

$K_2 =$ Integral Gain

This is an example for proportional plus integral feedback. Usually a separate control algorithm is used for each area, and each area has its own control computer.

For a typical disturbance on a two area system where, for instance, additional load occurs in Area 1, the LFC would respond response as follows:

i. Frequency falls in both areas and the phase angle changes across tie-lines drawing in more power from area 2.
ii. The LFC in area 1 and area 2 responds to the frequency error and tie-line error by loading additional generation in area1 and possibly some additional generation support from area 2 this depending on the relative values of α and β.

The total generation change for the area ΔP_{gen} is subdivided among the generators according to *participation factors.*

$$\Delta P_{gen} = \frac{PF_1\, P_{gen1} + PF_2\, P_{gen2} + \cdots + PF_N\, P_{genN}}{\sum_{i=1}^{N} PFi} \tag{3.13}$$

$$0 \leq PF_i \leq 1$$

$$N = number\ of\ generators\ in\ the\ area.$$

The values of the participation factors PF_i may be determined using economic dispatch results:

$$PF_i \propto PE_{geni}^{T+\Delta T} - PE_{geni}^{T} \tag{3.14}$$

where $PE_{geni}^{T+\Delta T}$ = Economic output of generator i at time $T + \Delta T$

PE_{geni}^{T} = Economic output of generator i at time T

Expressing (3.14) in a normalized form,

$$PF_i = \frac{PE_{geni}^{T+\Delta T} - PE_{geni}^{T}}{\sum_{i=1}^{N}(PE_{geni}^{T+\Delta T} - PE_{geni}^{T})} \tag{3.15}$$

The objective is for each generator to move from its most economic output at time T to its most economical output at time $T + \Delta T$. If this movement is obtained by the LFC responding to frequency errors then the above PF_i will achieve the desired movement for each generator.

3.7 Quality of Frequency Control

The quality of frequency control can be evaluated under two different scenarios:

1. Quality of frequency control during the normal operation of the system.

3. Quality of frequency control during large deviations of frequency following major disturbances such as the unplanned outage of a generating unit.

For the first scenario, the frequency quality control is assessed by determining the standard deviation:

$$\sigma = \sqrt{\frac{1}{n}\sum_{i=1}^{n}(f - f_{ref})^2} \quad , \tag{3.16}$$

where n is the number of measurements.

In order to assess frequency control quality for the second scenario, a method called "trumpet method" is employed [19]. Figure 3.15 shows the frequency deviation of a system following the outage of a large generating unit (thick line) where the reference frequency is 50.01 Hz and a frequency error Δf_0 exists before the disturbance. The frequency sharply declines to f_2 due to the disturbance and gradually is restored to the reference value by frequency control. The two exponential curves (dashed lines) referred to as the trumpet characteristic and defined as:

$$H(t) = \begin{cases} f_{ref} \pm A\, e^{-\frac{t}{T}} & t \leq 900\ s \\ \pm 20\ mHz & t \geq 900\ s, \end{cases} \tag{3.17}$$

where the values of these parameters are system dependent and obtained on experience. If the frequency is maintained within the trumpet characteristic following a disturbance, the frequency control is deemed to be satisfactory.

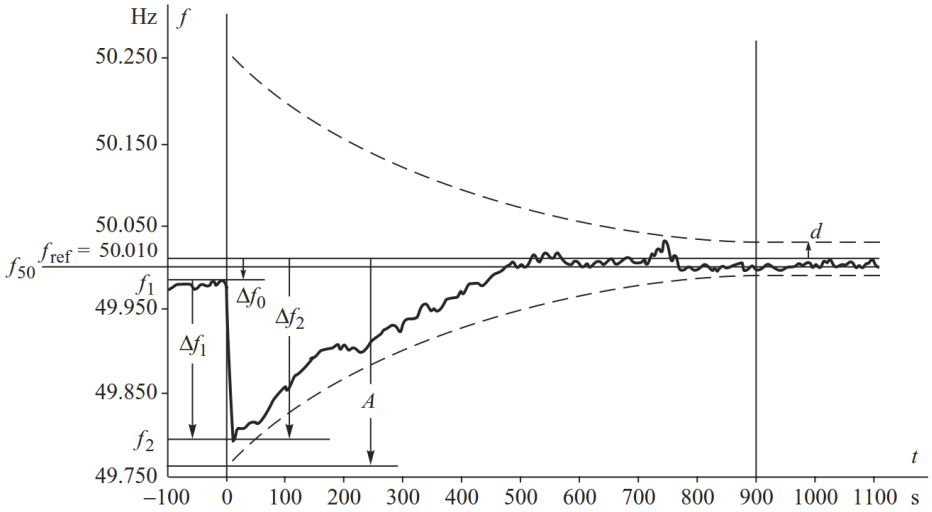

Figure 3.15 *Quality assessment of frequency control using the trumpet characteristic [19].*

3.8 Frequency Operating Standards

A frequency variation following any short-term power imbalance is initially offset by the kinetic energy stored in the generating unit's rotating parts. In case of a large generation loss, the frequency may drop rapidly and without an adequate system response frequency deviation might exceed the working range of the plant. Abnormal frequency excursions may have high negative impact on the efficiency, reliability and operation of a power grid. Substantial frequency excursion may harm equipment and overload transmission lines. These substantial frequency deviations may cause the system collapse.

Table *3.1 Frequency operating ranges and control actions [46].*

Frequency deviation range	Condition	Control action
Δf_1	No contingency or load event	Normal operating
Δf_2	Generation/load or network event	LFC operating
Δf_3	Separation event	Emergency operating
Δf_4	Multiple contingency event	Emergency operating

Depending on the amplitude of the frequency excursions, supplementary controls, natural governor reaction and emergency controls may all be necessary to preserve power system frequency. Therefore, characterizing the frequency deviations experienced in a power system may bring about substantial benefits. One possible approach may be based on the frequency excursion ranges and the corresponding control actions as indicated in Table 3.1, where Δf_1, Δf_2, Δf_3 and Δf_4 are frequency excursion ranges. Under normal system operation, the frequency is maintained close to the reference value (nominal frequency) by keeping the balance between generation and load. In Table 3.1, Δf_1 represents excursions in the frequency range which can be attenuated by primary control. For larger excursions, say (Δf_2), supplementary controls should be activated, with the value of Δf_2 corresponding to the accessible amount of operating reserved power in the grid.

The frequency control system purpose is to eliminate frequency deviations which are relatively small and occur slowly. In cases of large active power imbalances in the grid resulting in rapid frequency changes that occur during a fault condition, the LFC system fails to operate properly. For such large frequency deviations, say $\Delta f_3$and Δf_4, the emergency control and protection schemes have to be activated to restore the system frequency.

These measures vary from grid to grid. For instance in Australia, for the mainland regions, Δf_1, Δf_2, Δf_3 and Δf_4 are defined as 0.3Hz, 1Hz, 2Hz and 5Hz, respectively [54]. In all Grid Codes, the acceptable frequency excursion for normal operation is small (about 1%). Larger excursions trigger protection devices to trip either generators or load (i.e. load shedding) in order to restore power balance.

3.9 Summary

System frequency is one of the main variables to guarantee the system operational integrity. A load – generation imbalance causes a deviation in the system frequency and the primary frequency control is the first step towards restoring the frequency to its nominal value. The primary frequency control is achieved through the governing system of the generators. Based on the frequency error and a set point for the power output, the governor adjusts a throttle valve in the steam supply of the turbine in order to regulate the rotor speed.

Following the primary frequency control, there will still be a steady-state error will remain. To correct this error, the governor set points are adjusted to restore the frequency to the reference value. This is called *secondary frequency control* or *load frequency control (LFC)*. After the primary and secondary frequency controls, the tertiary control, which is a manual control, might be performed. In order to assess the quality of frequency control, a method called *trumpet method* may be employed.

4. MODELING AND SIMULATION USING PSCAD

This chapter addresses the applicability of a BESS in a high-voltage transmission system to provide frequency support. The modeling and simulations are carried out using the PSCAD simulation environment. The high-voltage transmission system used as the test system is known as the "two-area, four-machine system of Kundur" [55].

Since the generators are key parts of the simulation, it is reasonable to discuss generator modelling in PSCAD, first. A hydro-generator model available within the PSCAD library conforms well to the task in hand and fits on well with the test transmission systems [55], and it is used in the simulations carried out in this chapter. The complete BESS model is then described. The simulations results show that the BESS does improve power system frequency stability and that its impact is largely dependent on the BESS's rating.

4.1 PSCAD

PSCAD/EMTDC^{TM}, an industry standard simulation tool for studying the transient behavior of electrical power networks, is a powerful tool for the evaluation of the impact of new power technologies in the power network. It contains a comprehensive library of models which support a wide range of AC and DC power plant components and controls and facilitates the speedy and precise modeling of FACTS, custom power and HVDC systems. A user-friendly graphical interface facilitates all aspects of the simulation, including circuit assembly, run-time control, result analysis and reporting, all this within one single integrated environment.

PSCAD/EMTDC's complex algorithms and methods are transparent to the user, giving the freedom to focus on the analysis rather than the mathematical modeling. The user has the option of either using its own user-defined models or chose from the large base of built in components available in PSCAD/EMTDC.

4.2 Generator Modelling in PSCAD

Currently there are four fully developed generator models available in PSCAD-EMTDC: A *Synchronous Machine*, a *Squirrel Cage Induction Machine*, a *Wound-Rotor Induction Machine* and a *DC Machine*. Using generalized machine theory, all these models are programmed in state variable form.

The synchronous machine model in PSCAD has representation of saturation only in the d-axis since it is assumed that saturation in the q-axis is negligibly small. An induction machine, on the other hand, experiences equal saturation effects in both axes, hence, representation for saturation effects for the d and q-axis are available within the model in PSCAD.

The synchronous generator symbol used in PSCAD is shown Figure 4.1. With the option to model two damper windings in the q-axis, this component can be used to represent a round rotor machine or a salient pole machine by appropriate selection of its input data. The machine speed can be controlled by either inputting a positive value into the **w** input or by applying a mechanical torque to the **Tm** input.

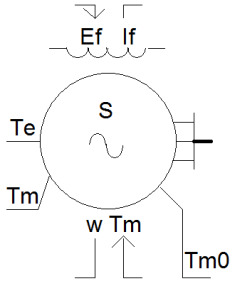

Figure 4.1 *A synchronous generator symbol in PSCAD.*

Several advanced options are included in this component for modeling a synchronous machine. It is recommended within PSCAD that all those parameters identified as *Advanced* are left as default values for general use, as this will not affect the performance of the machine within the simulation.

Using a power flow solution the desired steady-state condition may be established. The transient response can then be observed by applying a disturbance, such as a short-circuit fault or a step-change in load. Once the new steady-state is reached, the simulation is ended.

The input parameters entered for the synchronous generators of the test system, into the PSCAD environment correspond to a hydro generator, which are known to have a higher inertia than turbo-alternators. Hence the governor used in this work is a V2 Compatible Hydro Governor (HGOV18) which models an IEEE type 2 hydro governor and turbine. The PSCAD icon shown in Figure 4.2 and the transfer function given in Figure 4.3; it has three inputs:

- SP: The reference speed [pu]
- Tm0: Mechanical torque from the machine [pu]
- w: Machine rotor speed [rad/s]

and one output:

- Tm: Mechanical torque output [pu].

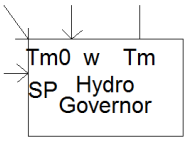

Figure 4.2 *Hydro Governor in PSCAD.*

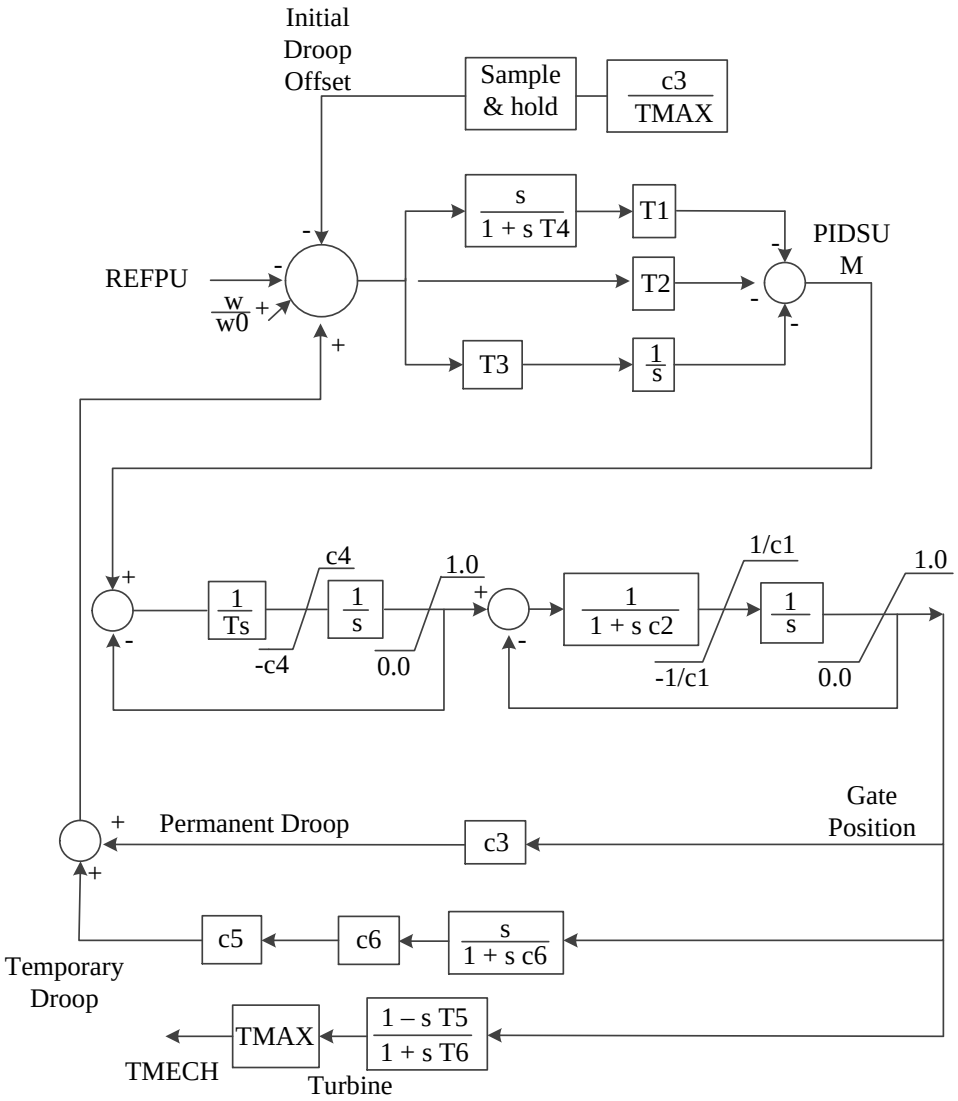

Figure 5.18 *HGOV18 governor block diagram in PSCAD.*

4.3 BESS model in PSCAD

The BESS basic structure is shown in Figure 4.4. The BESS model developed in this work comprises three major parts:

- Battery pack
- DC/DC boost converter: Active power control
- Voltage Source Converter: Reactive power control

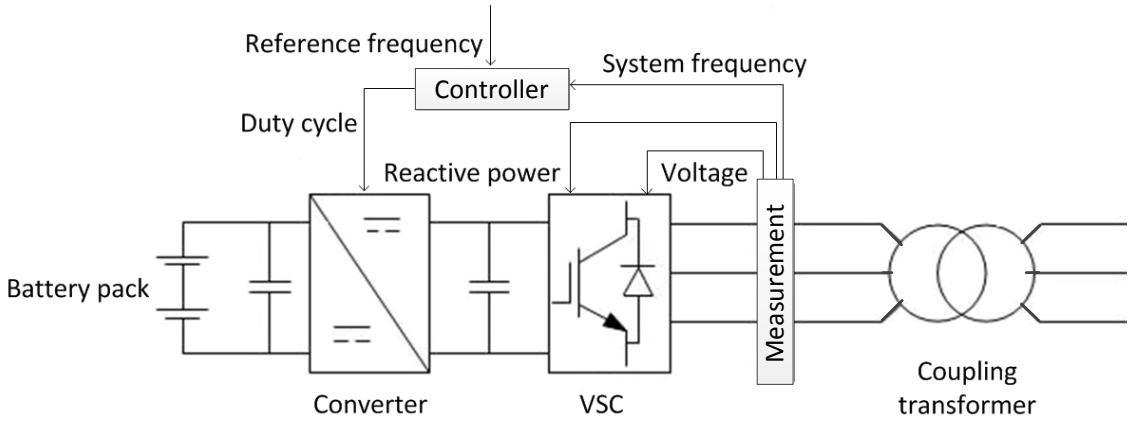

Figure 4.4 *battery energy storage system.*

4.3.1 Battery pack

The battery model used to carry out the simulations in PSCAD is a suitable model for simulating the battery dynamics. Although, it lacks some modelling capabilities such as battery ageing and temperature dependency, for the application pursued in this work, nor the temperature dependency neither the battery ageing are likely to have a significant impact on simulation times of less than one minute. The battery model is shown in Figure 4.5 and its parameters are given in Table 4.1.

It should be mentioned that this battery model is not available in the PSCAD library but that it can be obtained by contacting the software vendor.

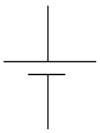

Figure 4.5 *Battery model in PSCAD.*

Table 4.1 *Parameters of the battery.*

Battery name	Bat1
Data entry	Shepherd model
Initial state of charge	80%
Nominal Discharge Current	20%
Nominal voltage	20 kv
Rated capacity	6.5 [kA*hr]
State of Charge [%]	80
Capacity at Exponential point	0.4 [pu]
Fullly Charged Voltage	1.15 [pu]
Nominal Capacity	0.95 [pu]
Resistive Drop	0.005 [pu]
Voltage at Exponential Point	1.03 [pu]

4.3.2 DC/DC boost converter

The converter developed in this simulation is a boost converter and shown in Figure 4.6.

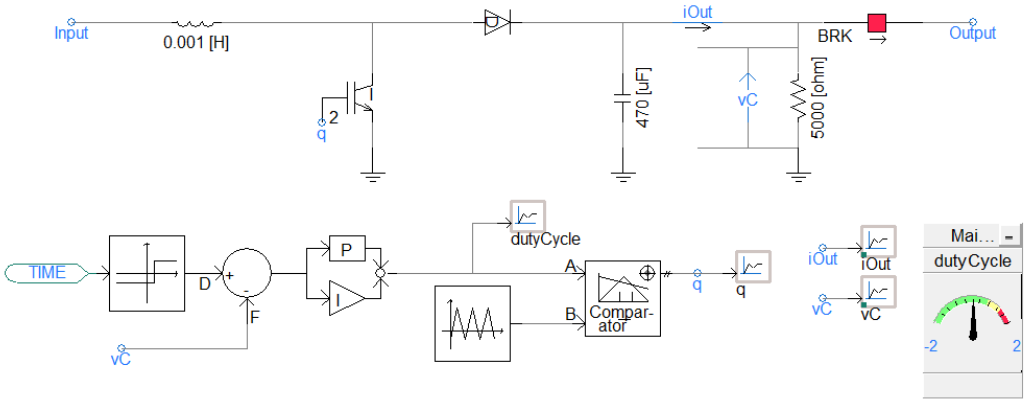

Figure 4.6 *DC/DC boost converter.*

The output voltage of the converter Vc is measured and compared against the desired value. Based on the deviation, the controller determines the duty cycle of the switch. The controller is a PI controller with the following parameters:

$$P = 0.02 \qquad I = 1.3$$

The controller parameters are obtained by trial and error. With these values the controller is able to set the converter output voltage at the desired value fast. When the frequency error is zero, the duty cycle is 0.29 which sets the converter output voltage at 40 kV. The maximum output voltage of the converter is 50 kV and that is when the duty cycle is 0.39.

4.3.3 VSC

The VSC used in this simulation is shown in Figure 4.7. It is a six-pulse PWM VSC with carrier frequency of 9 times the fundamental. A 25/230 kV transformer connects the inverter to bus 6. The capacitor (300 μF) voltage V_{DC} is 40 kV and the capacitor current I_{DC} is varying between +2.5 and -2.5 kA.

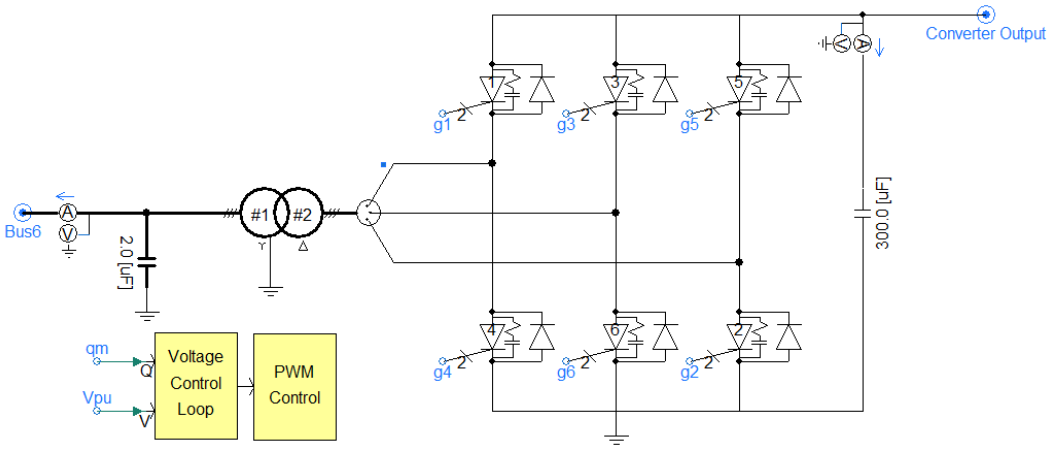

Figure 4.7 *Six-pulse PWM VSC.*

The voltage of bus 6 is measured, filtered and compared to the reference value (230 kV) to calculate the error. Based on the error, a PI controller in the *voltage loop control block* determines the angle order. The values for P and I are 1.4 and 0.1, respectively. The angle order, representing the required shift between the bus voltage and the voltage generated by the VSC, determines the direction and amount of reactive power flow. The *PWM block* generates the firing pulses for the switches based on the angle order. Please refer to Appendix A for more information on the *Voltage loop control* and *PWM control* blocks.

4.4 Power flow and the duty cycle

The storage system exchanges active power with the grid. The power flow is controlled by adjusting the VSC input voltage. The input of the VSC is the output of the DC/DC boost converter. The control system of the converter sets the output voltage of the converter at a certain level to control the amount of power that the BESS has to inject into the grid in case of a frequency drop. The duty cycle of the switch determines the converter output voltage. Thus, in order to control active power flow between the BESS and the grid, the duty cycle of the converter switch is adjusted.

The control system operation is split into the following three stages:

- Determination of the frequency error
- Calculation of the target output voltage

- Calculation of the duty cycle of the switch

(i) the angular frequency ω is measured "continuously" and compared to the reference value ω_{ref} to calculate the error. If the error is less than a pre-defined threshold, the BESS takes no action. This is to prevent the batteries from continually and unnecessarily charging and discharging at an unhealthy rate.

(ii) acting upon the deviation of the measured angular frequency from the reference value, the desired converter output voltage is calculated. In case of frequency changes in the system, the desired output voltage of the converter Vc will be adjusted according to the following relationship:

$$V_c = V_{init} + k_p\left(\omega_{ref} - \omega\right) + k_i \int \left(\omega_{ref} - \omega\right) dt \tag{4.18}$$

where

ω_{ref} is the reference angular frequency = 377 rad/s

ω is the actual frequency of the system

k_p is the proportional gain of the controller, set at 40

k_i is the integral gain of the controller, set at 0.13

V_{init} is set at 40 kV

(iii), based on the required output voltage of the converter, the value of the duty cycle is calculated, converted to a PWM signal and fed into the gate of the switch in the converter.

Figure 4.8 shows the power flow control system.

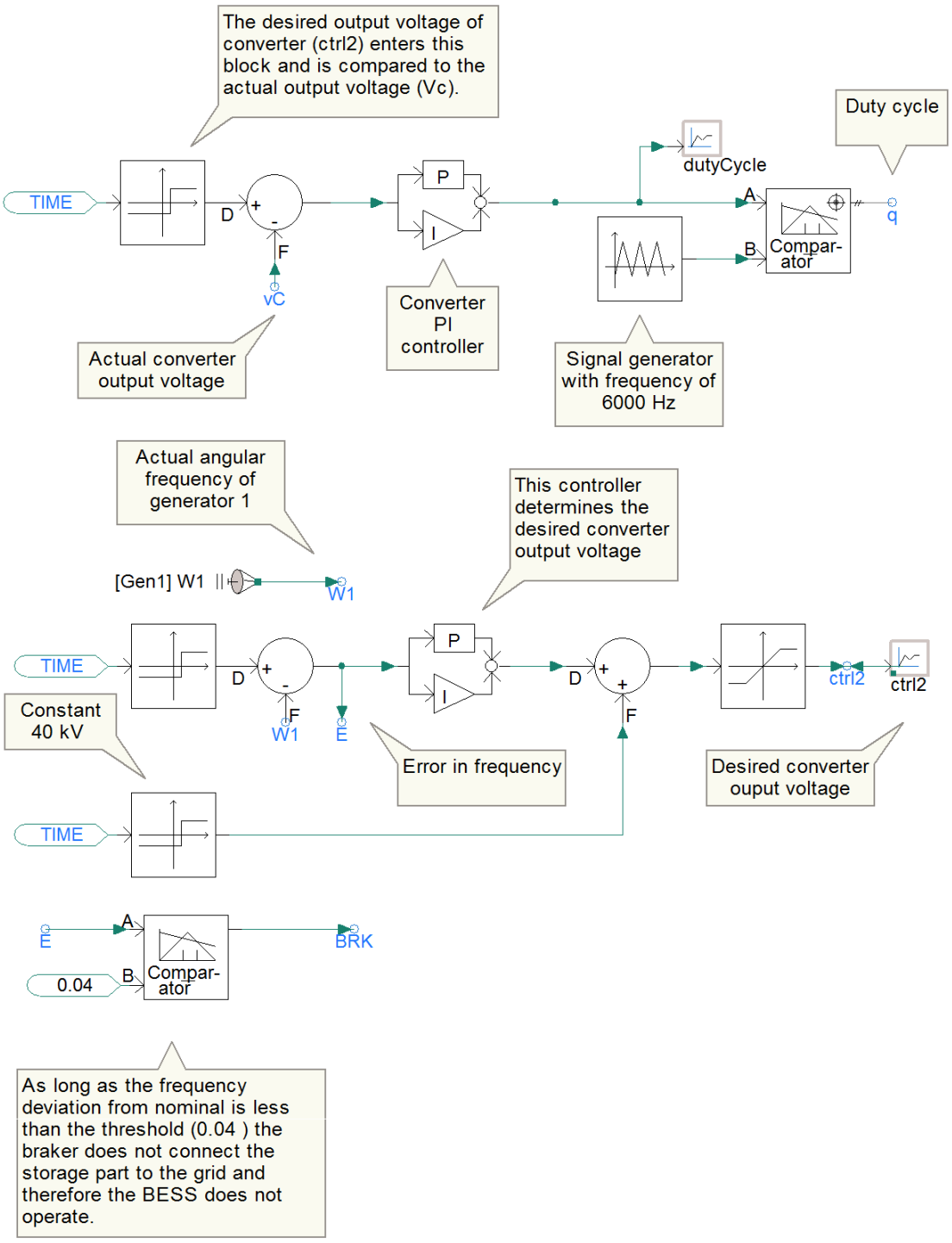

Figure 4.8 *Power flow control system.*

4.5 High Voltage Transmission System

Figure 4.9 shows the transmission power grid used to test the impact of the BESS. The original grid comprises eleven buses and, in this work, a 12th bus is added so that the BESS can be connected to the system. The system contains two loads, at buses 7 and 9, respectively, and two shunt capacitors. The shunt capacitors provide voltage support by

supplying reactive power. The system's fundamental frequency is 60 Hz. The grid is made up of two similar areas linked by a double circuit transmission line between buses 7 and 9. Each area consists of two synchronous generators, each one having a rating of 900 MVA and 20 kV. The left half of the grid is termed Area 1 and the right half is termed Area 2. The BESS injects power at bus 6 via a transformer connected between buses 6 and 12.

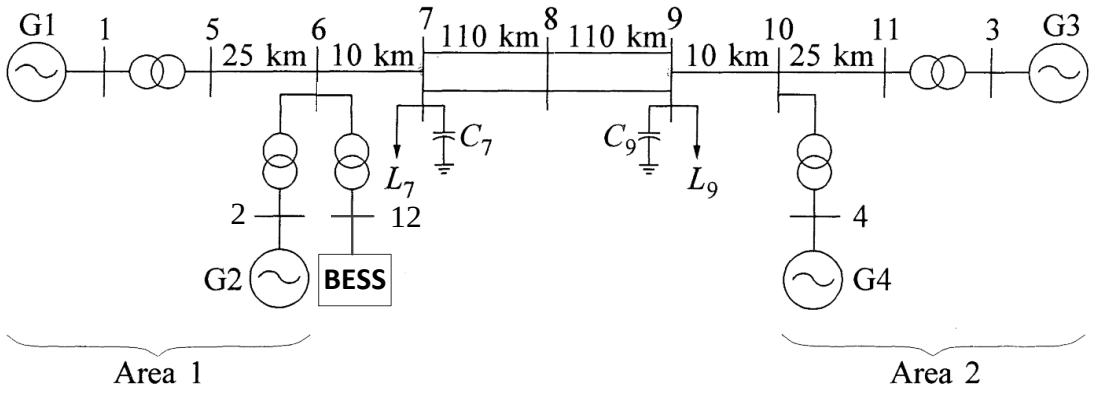

Figure 4.9 *Two area, four machine system.*

The parameters of the synchronous generators are given in Table 4.2. They are in per-unit on a 900 MVA base and a 20kV base.

Table 4.2 *Parameters of the synchronous generators.*

$T_a = 0.278\ s$	$X'_d = 0.314$	$T''_{d0} = 0.039$	$T''_{q0} = 0.071$
$X_p = 0.163$	$T'_{d0} = 6.55$	$X_q = 0.77$	$Air\ gap\ factor = 1$
$X_d = 1.014$	$X''_d = 0.28$	$X''_q = 0.28$	$R_a = 0.0025$
$H = 6.5(G_{1\&2}), H = 1.8(G_{3\&4})$			

The step-up transformers' impedance is 0 + 0.15 per unit on the 900 MVA and 20/230 kV base. The off-nominal tap ratio is 1. The parameters of the lines in per-unit on a 100 MVA and a 230 kV base are:

r = 0.0001 pu/km $\quad x_L = 0.001$ pu/km $\quad b_C = 0.00175$ pu/km

The loads at buses 7 and 9 are:

Bus 7: $\quad P_L = 967$ MW $\quad Q_L = 350$ MVAr
Bus 9: $\quad P_L = 1767$ MW $\quad Q_L = 100$ MVAr

The shunt capacitive compensation at the buses 7 and 9 are as follows:

Bus 7: Q_C = 200 MVAr
Bus 9: Q_C = 350 MVAr

The generators are loaded as:

G1:	P = 701 MW	Q = 159 MVAr
G2:	P = 500 MW	Q = 267 MVAr
G3:	P = 720 MW	Q =135 MVAr
G4:	P = 708 MW	Q = 201 MVAr

4.6 Load increment by 50 MW at bus 7

Frequency Regulation

In this section, the impact of the BESS on frequency regulation improvement is assessed. The load at bus 7 is increased by 50 MW after two seconds of simulation. The impact of the BESS on frequency improvement may be seen by comparing the frequency response of Figures 4.10 and 4.11. The frequency of Generator 1 is shown in these figures. Following the load increase, the frequency takes 13 seconds to start to rise after having reached its lowest value. With no BESS, the frequency drops to 59.73 Hz whereas when a 22 MW BESS is connected, it drops only to 59.83 Hz. The BESS reduces the frequency drop by

$$\frac{(60-59.73)-(60-59.83)}{60-59.73} * 100 = 37.04\ \% \tag{4.19}$$

As discussed in Chapter 2, further to the action of the BESS, the frequency is influenced by the speed of the governing system. With no BESS, after 43 seconds, following the load increase, the generator frequency regulator brings the frequency back up to 59.980 Hz by injecting additional active power to the grid. In contrast, with the 22 MW BESS, the frequency reaches a higher value, namely, 59.990 Hz.

The rated power of the BESS (22 MW) is similar to the state-of-the-art BESS installations in Chile and California. At this point, only for theoretical reasons, the contribution of a 40 MW BESS is explored. Figure 4.12 shows the Generator 1's frequency when the 40 MW BESS is connected. It is quite encouraging to observe that in this case the frequency drops to only 59.920 Hz and that it is almost restored to the reference value after 43 seconds of the load increase.

Voltage Regulation

The impact of the BESS on voltage regulation improvement can be assessed by comparing Figures 4.13 and 4.15. Figure 4.13.a shows the voltage at bus 6 when no

BESS is connected to the grid. To gain a closer view of the voltage variation, a voltage zoom is shown in Figure 4.13.b where it is appreciated that when the load change occurs, the voltage drops to its lowest value, 0.9675 p.u., whereas the lowest value of the voltage when the 22MW BESS is connected is 0.9725 p.u., as shown in Figure 4.14. The voltage profile at bus 6, when the 40 MW BESS is connected, is shown in Figure 4.15. As expected, the minimum voltage drop takes place when the 40 MW BESS is connected. The RMS voltage at bus 1 observes a similar voltage profile as those in Figures 4.16 to 4.18 but with higher magnitudes because the steady state value at bus 1 is higher than in bus 6.

4.7 BESS Operation

Figure 4.19 shows the frequency error when a 22 MW BESS is connected to the grid. The load is increased after two seconds of the simulation. The error starts to increase until it reaches a maximum of 1.05 rad/s at $t = 15\,s$. After that point, it starts to decrease and eventually reaches 0.03 rad/s at $t = 45\,s$. Figure 4.19 also shows at $t = 2.5\,s$ the error becomes greater than the threshold which stands at 0.04 rad/s.

The converter output voltage is shown in Figure 4.20. After detecting the error, the converter output voltage starts to increase. The converter output voltage is limited to a maximum of 50 kV since the nominal power of the BESS is 22 MW (voltages greater than 50 kV result in a BESS with nominal power of more than 22 MW). Once the converter output voltage V_c, reaches 50 kV, its upper limit, does not decrease as the error decreases. The reason can be understood by exploring Figure 4.12 (the 40 MW BESS). To completely remove the frequency error, a BESS with nominal power higher than 40 MW is required and a 22 MW BESS cannot restore the frequency back to 60 Hz. Hence, V_c remains 50 kV in order to keep injecting as much active power as possible.

The active and reactive powers injected to the grid by the BESS following the load change, are shown in Figures 4.21 and 4.22, respectively. When the frequency deviation from nominal is smaller than 0.04 rad/s, the BESS injects no power, to safeguard the battery. It is well known that excessive discharging of the battery reduces its lifespan.

Figure 4.23 shows the state of charge (SOC) of the battery. The SOC decreases as the BESS contributes active power to the grid. Before t= 2.5s, the SOC is constant as the frequency deviation is insignificant. When the BESS operates with its maximum power, the battery energy is linearly drained.

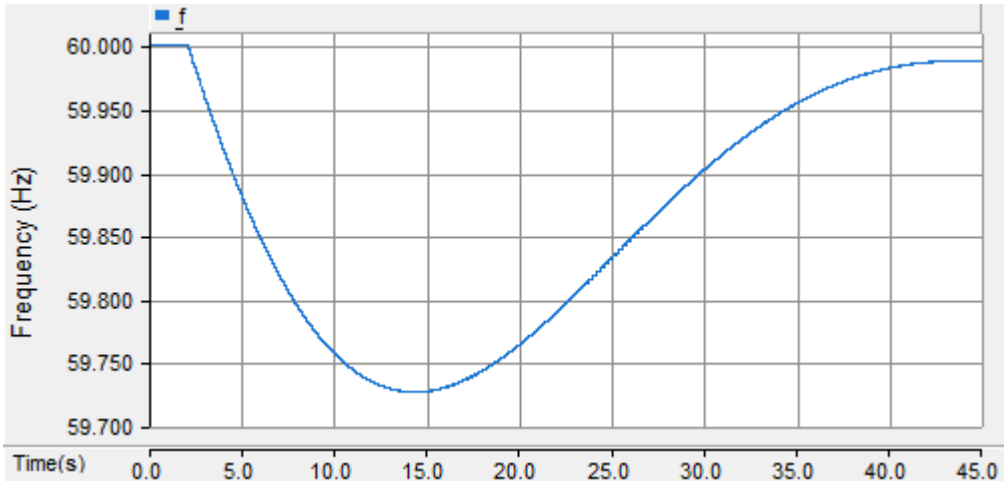

Figure 4.10 *Rotor speed when load is increased by 50 MW _ with no BESS.*

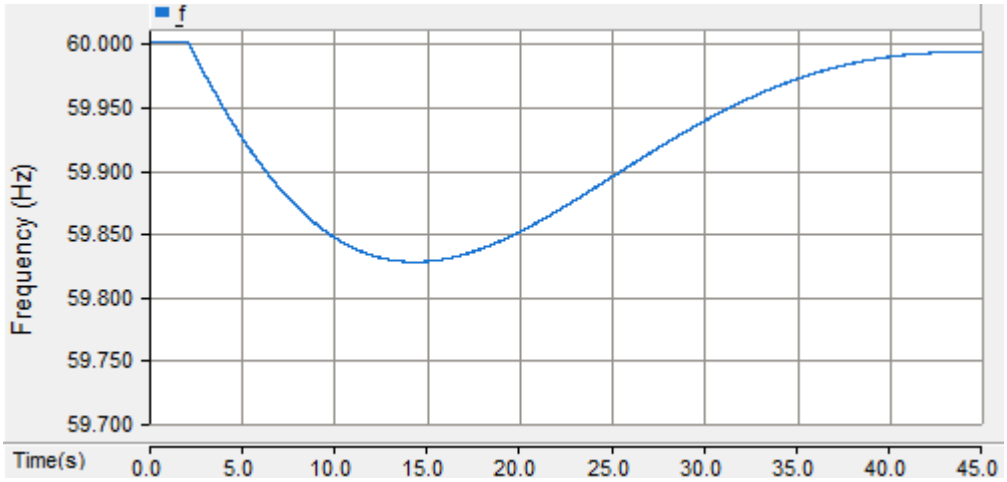

Figure 4.11 *Rotor speed when load is increased by 50 MW by 50 MW _ with a 22 MW BESS.*

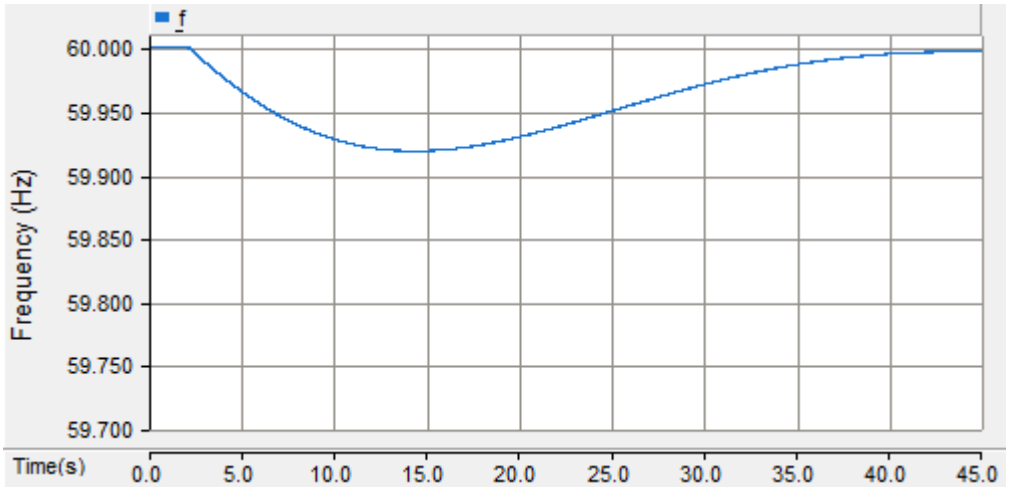

Figure 4.12 *Rotor speed when load is increased by 50 MW _ with a 40 MW BESS.*

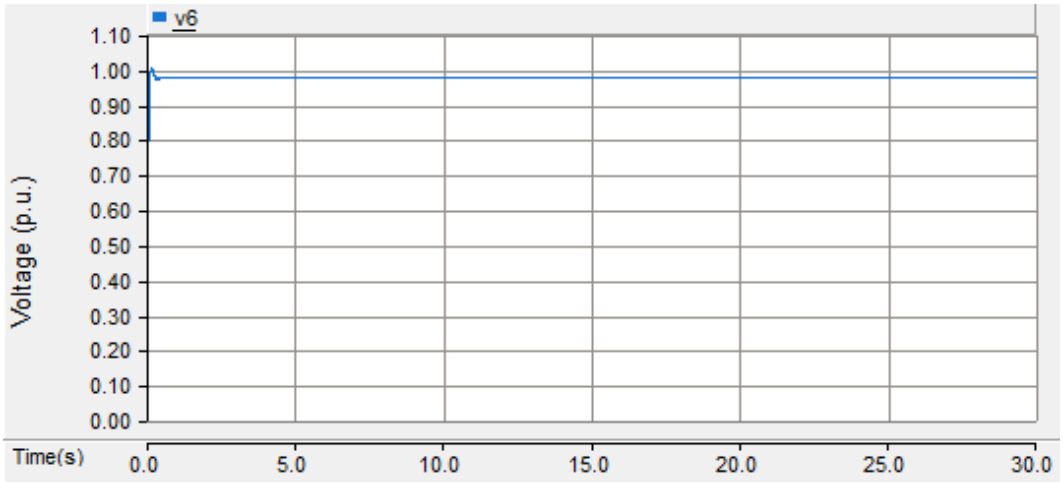

(a)

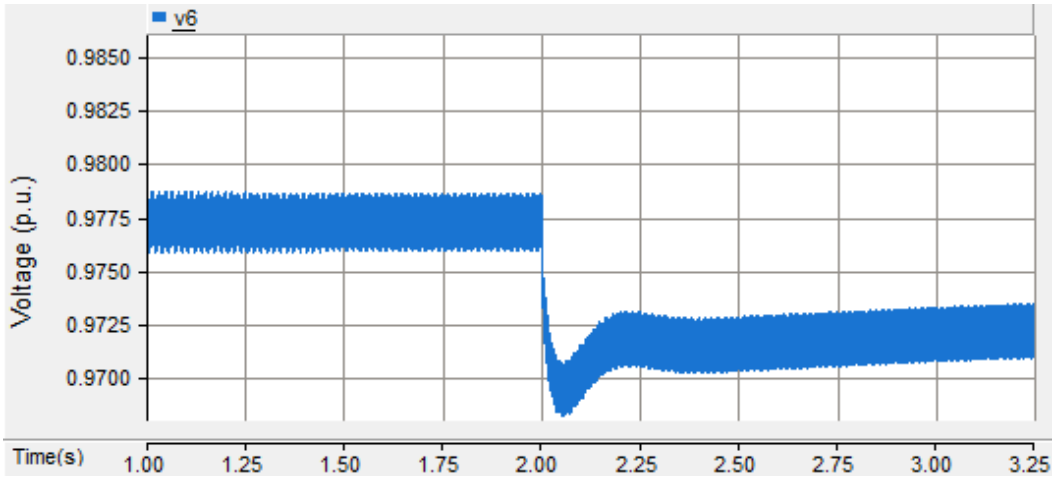

(b)

Figure 4.13 *Voltage at bus 6 when load is increased (no BESS), (a) full-range, (b) zoomed.*

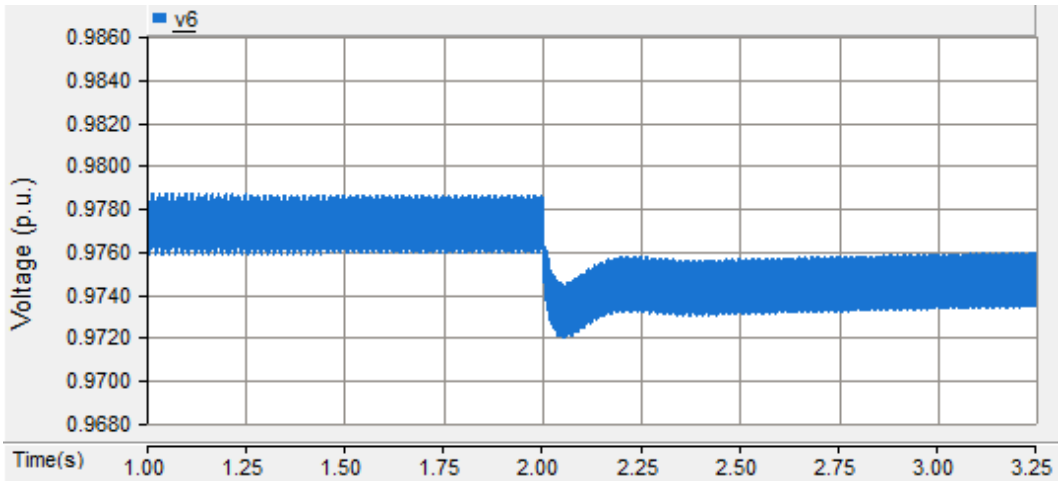

Figure 4.14 *Voltage at bus 6 when load is increased (with 22 MW BESS).*

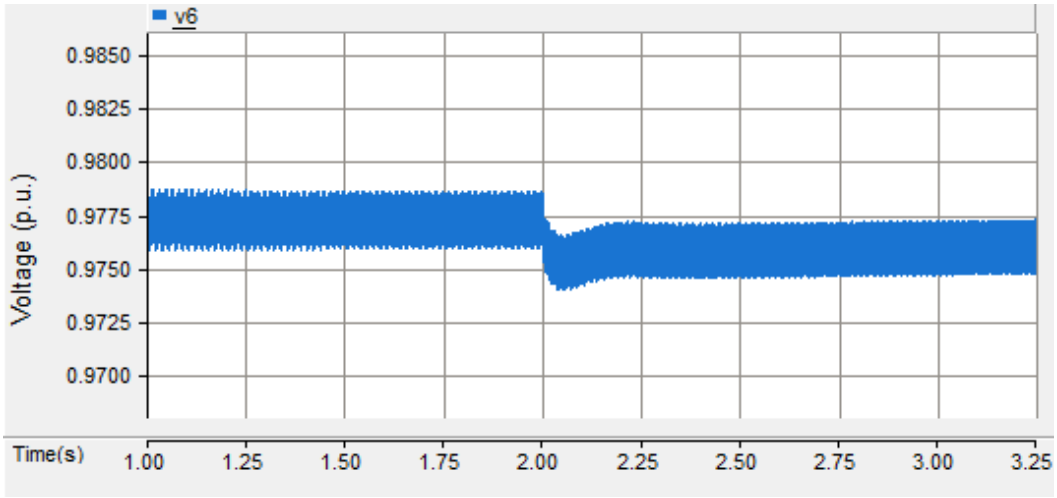

Figure 4.15 *Voltage at bus 6 when load is increased (with 40 MW BESS).*

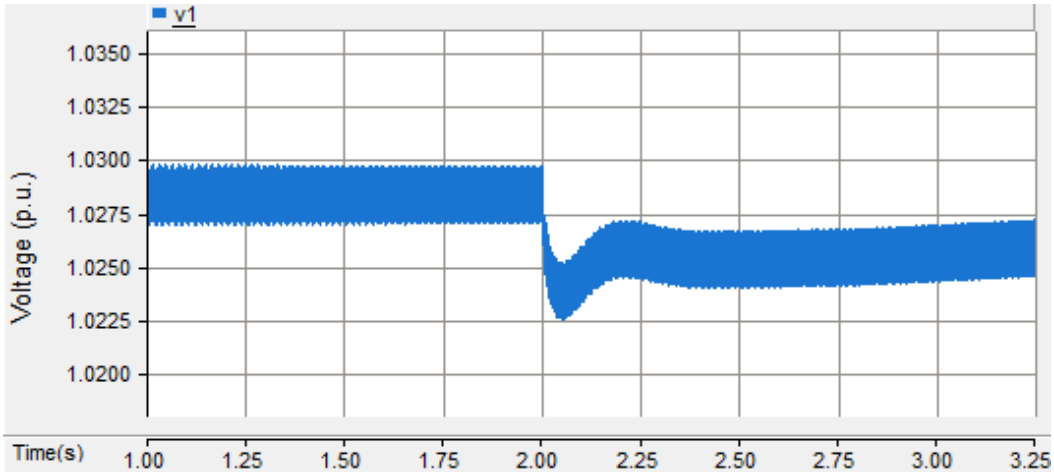

Figure 4.16 *Voltage at bus 1 when load is increased (no BESS).*

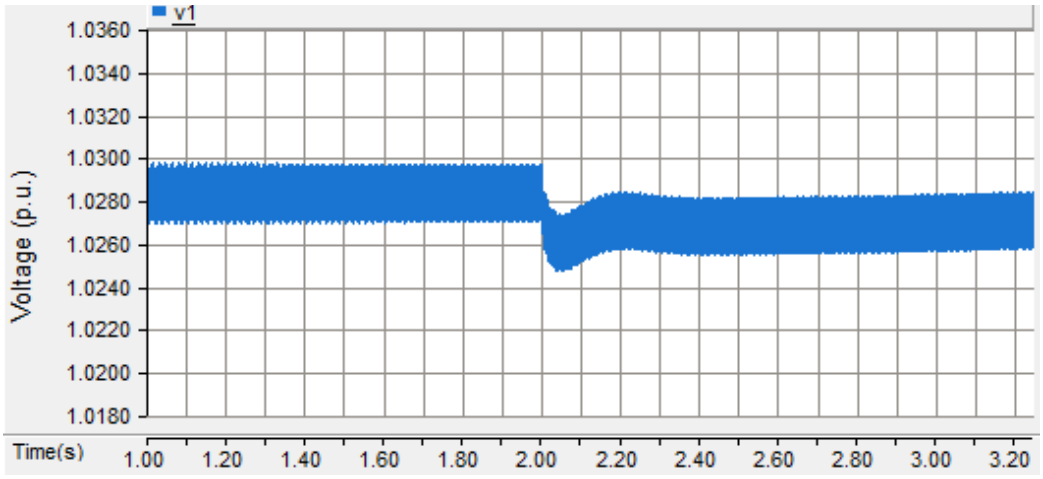

Figure 4.17 *Voltage at bus 1 when load is increased (with 22 MW BESS).*

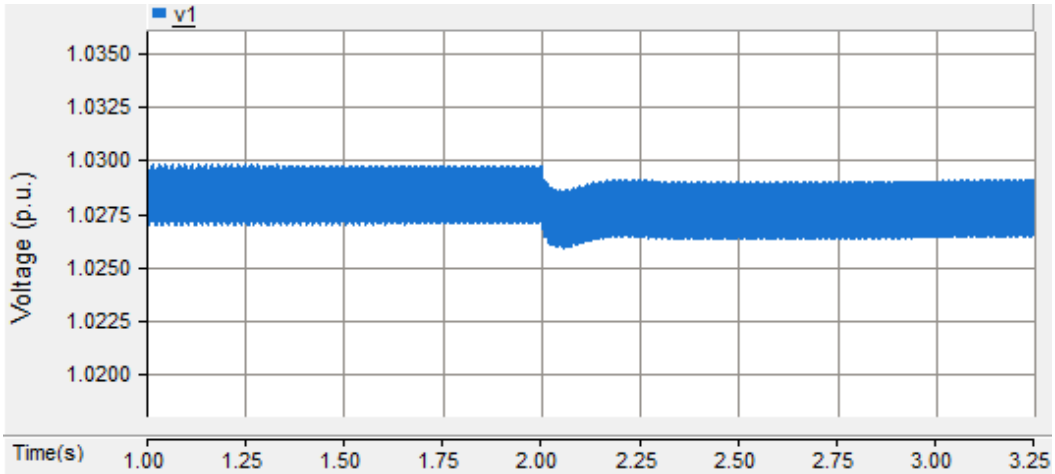

Figure 4.18 *Voltage at bus 1 when load is increased (with 40 MW BESS).*

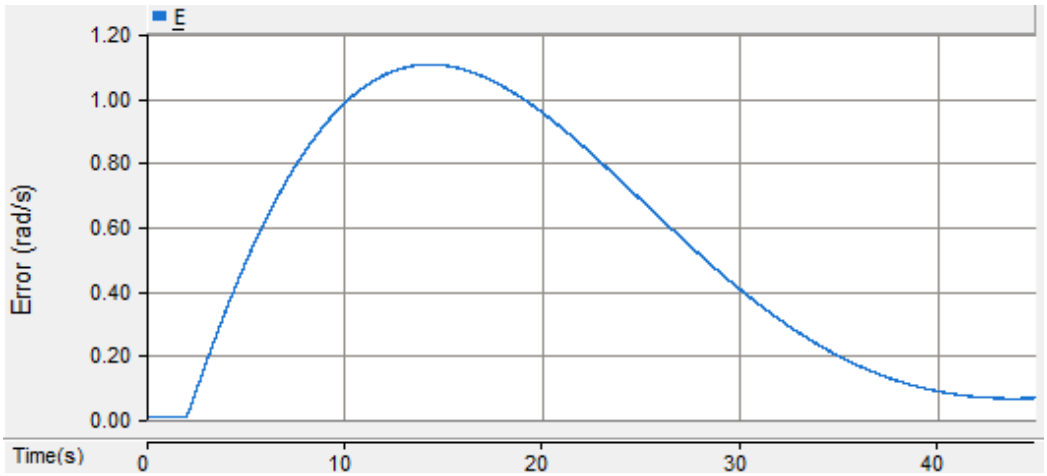

Figure 4.19 *Frequency error.*

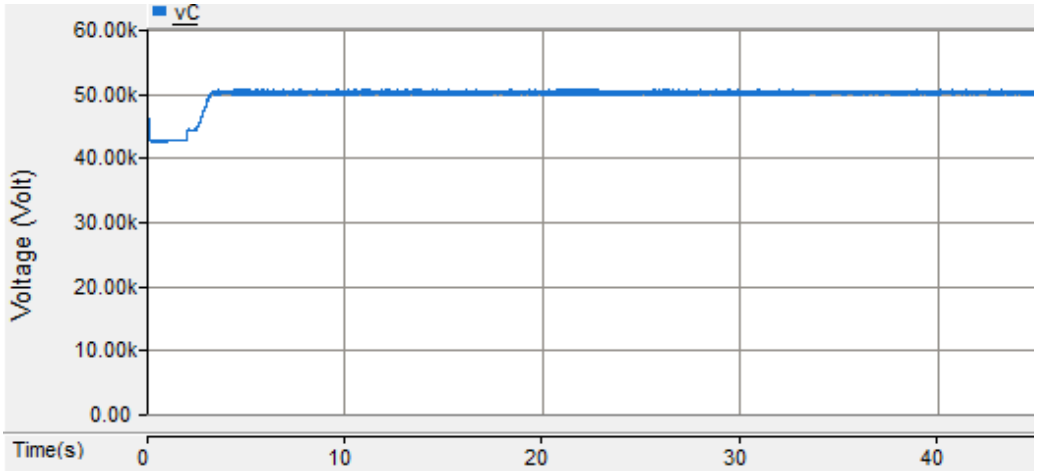

(a)

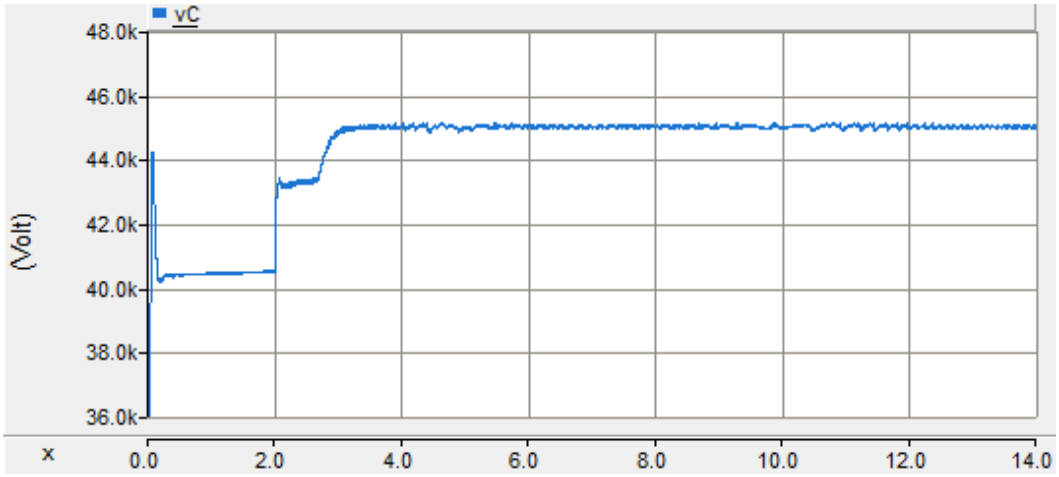

(b)

Figure 4.20 *Converter output voltage; (a) full-range , (b) zoomed.*

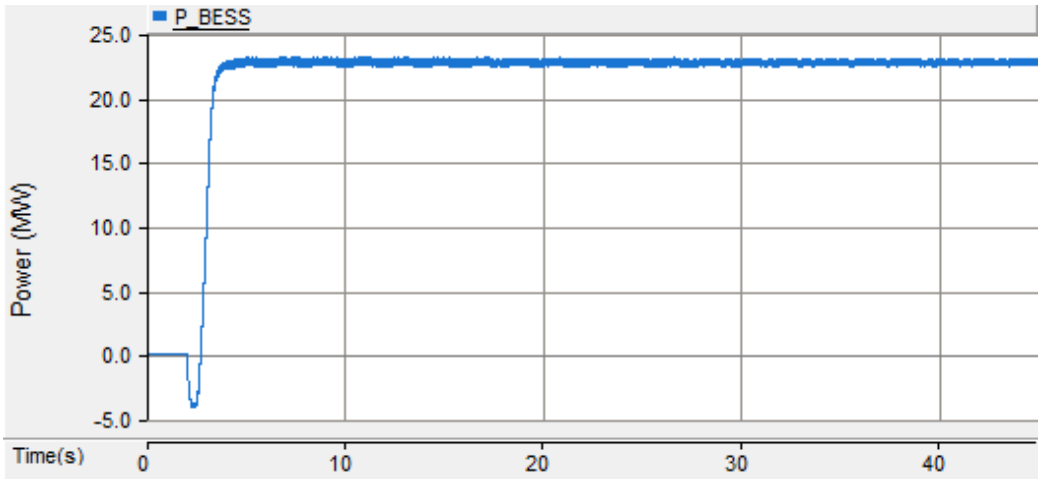

Figure 4.21 *Active power injected by the BESS.*

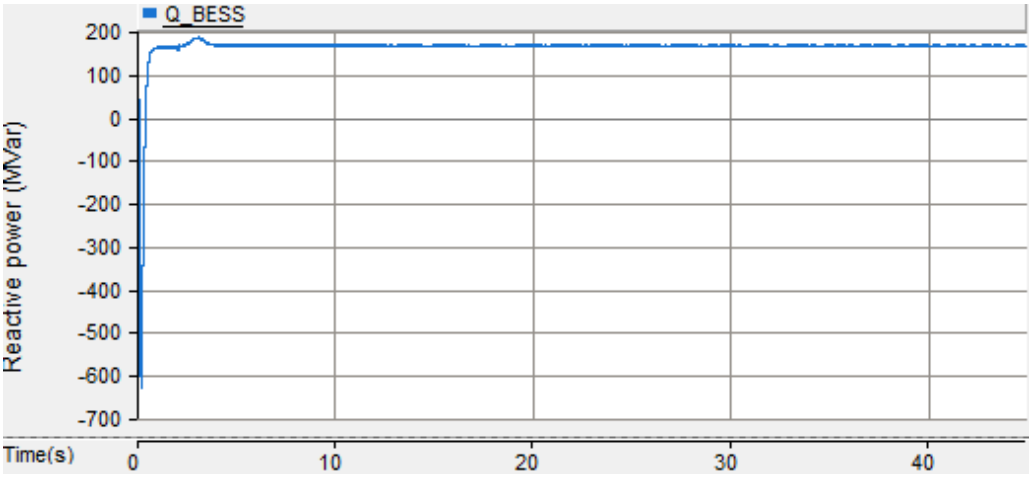

Figure 4.22 *Reactive power injected by the BESS.*

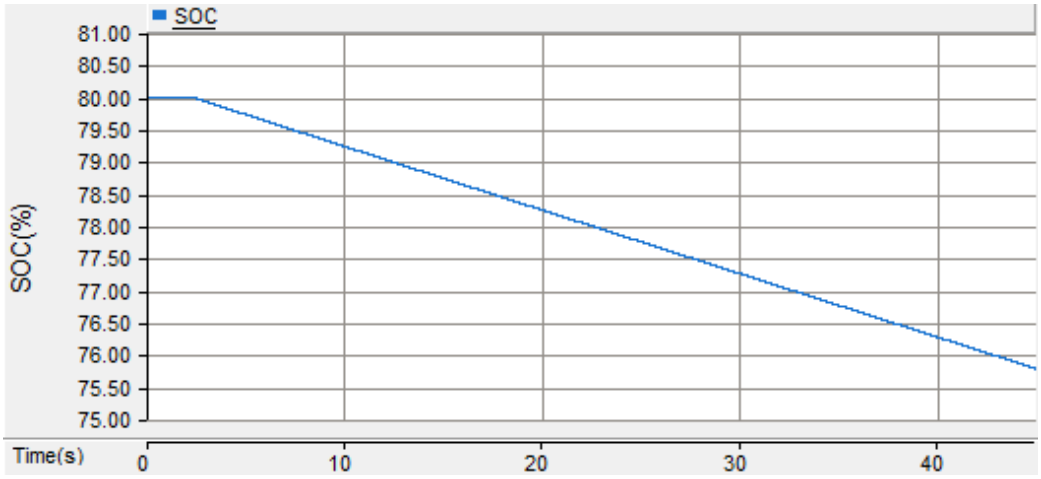

Figure 4.23 *State of charge of the battery.*

4.8 Summary

This section highlights the strengths and weaknesses found in PSCAD while modeling and simulating the BESS-upgraded power transmission system used in this work.

The implemented BESS model comprises a battery pack, a DC/DC boost converter and a DC-AC inverter. Despite lacking some modeling features, the battery model used is considered sufficiently accurate for the application pursued in this work. The main role of the DC-DC converter is to control the power flow exchange between the BESS and the grid. The VSC has the main duty of converting the DC voltage and current generated by the battery pack into three-phase AC voltages and currents enabling the connection of the storage system to the power grid as well as to regulate voltage magnitude at its AC side.

The implemened BESS model was assessed on an equivalent representation of a large high-voltage transmission system comparizing four equivalent hydro-generators. The assessment indicates that the BESS is very effective in reducing frequency drops, as well as in regulating voltage magnitude at its point of connection with the grid. From comparing the results from the 22MW BESS and the 40MW BESS, it is evident that frequency and voltage stability improvements are strongly linked to the capacity of the BESS.

4.8.1 Advantages and disadvantages of PSCAD

PSCAD is the *de facto* industry standard simulation tool for studying the transient behavior of power systems. Its comprehensive library of system models ranges from simple passive elements and control functions to electric machines and complex power electronic devices. Simplicity of use is an outstanding feature of PSCAD, where FACTS and HVDC systems can be modeled with high precision. Circuits are constructed schematically and users can create their own components.

One area for improvement within PSCAD is the representation of its battery model; at present it lacks ageing and temperature-dependency. Also, the full charging-discharging cycle is not possible, only the discharging operation seems to be available.

5 MODELING AND SIMULATION USING POWERWORLD

This chapter discusses modeling and simulations of the BESS in PowerWorld. PowerWorld is a power system simulation package aimed at the study of high-voltage power grid operation on a time-frame ranging from several minutes to several days. The simulator contains a highly effective power flow analysis package capable of solving large-scale power systems.

In this chapter, the model of a BESS available in PowerWorld is presented first. Then, the model is connected to the test transmission system model used in the previous chapter (Kundur system) in order to assess the effectiveness of the BESS model to provide frequency regulation. However, it should be noted that the characteristics of the generators used in the simulations of this chapter correspond to a turbo-alternator as opposed to a hydro-generator. The former types of synchronous generators have multi-pole rotors, rotate at relatively low speeds and are known to possess higher damping than the turbo-alternators which have two or four-pole rotors and rotate at very high speeds.

5.1 BESS model in PowerWorld

Unlike PSCAD, in PowerWorld, each component block has only one output port and no input port. Therefore, the components in PowerWorld cannot be series-connected. The BESS model available in PowerWorld can be found under the generators stability settings as “CBattery” model. The CBattery is a new model available in PowerWorld 18 (notice that this model is not available in older versions of PowerWorld). The model has four operating modes (mode 2 to mode 5), as explained in section 5.1.1. The main focus of this work is in mode 2 since this is the mode most suitable for this work. However, modes 3 to 5 will also be briefly explained.

Even though “CBattery” offers a good model for the simulation of the BESS dynamics for under-frequency emergencies, it still lacks some important modeling capabilities, such as temperature dependency, battery ageing and a state-of-charge indicator. Moreover, the default values of the control system are not well-tuned to be able to operate in every situation. In case of frequency drops caused by an increase in the load, the BESS control parameters determine the proper active power needed to be injected to the system to raise the frequency. The default control parameters operate properly for

very large disturbances (and consequently high frequency deviations). For less severe cases, such as load changes, when the frequency drop is small, the default control values in the BESS model do not warrant proper operation. This is expanded upon in section 5.1.2.

It should be stressed that this model is a very recent addition to the software package and documentation for the block diagrams, operation mechanism and the role of the parameters, has not yet officially been released by the vendor.

5.1.1 Operation modes

- Mode 2 relates to an under-frequency operating mode. The battery charges during normal operation and it is assumed to be fully charged and ready for releasing energy in the event of an adverse event in the power system.

- Modes 3 and 5 represent modes for which there is some other source of power sitting behind the battery, such as a PV array.

- Mode 4 represents a mode where the battery is providing a frequency regulation response.

5.1.2 Operation of BESS on mode 2

In mode 2, the actual frequency is continuously measured. Following a disturbance, such as an increase in load, the deviation of the actual frequency from the reference value (e.g. 60 Hz) is calculated. The BESS control system determines the required power to be injected into the grid to restore the frequency.

The “CBattery” model has several key parameters which characterize its performance, whith the fourteen parameters presented in Table 5.1 being the most significant as they provide the basis for the calculation of the required power to be injected by the BESS. Note that the values presented in Table 5.1 are the default values available in PowerWorld for the “CBattery” model.

Figure 5.1.a shows a graphical representation of the values in Tables 5.1. This characteristic guides the action of the BESS in cases of frequency deviation following a disturbance. Note that PREF (vertical axis) is the power in per-unit to be injected by the BESS and "FN" represents the total frequency deviation from nominal. Thus at nominal frequency, i.e. 60 Hz, FN = 0. If the frequency varies 1% above the nominal frequency, then FN = 1 and if it is 1% below the nominal frequency then FN = -1. The required power the BESS has to provide is generated according to the frequency deviation (FN) measured by the BESS and the corresponding PREF.

It has been found that the default settings of the BESS model available in PowerWorld do not operate well with the test transmission system used in this research. The reason can be understood by looking into Figure 5.1.a. The BESS starts injecting power once the frequency deviation exceeds -4.17%. In other words, the BESS does not operate as long as the frequency error is less than 2.5 Hz. Therefore, a suitable BESS characteristic needs to be determined, one that ensures the satisfactory operation of the BESS in cases of small frequency drops.

According to the discussion in Chapter 3 and Figure 3.1, it is observed that there is a linear relationship between the active power injected by a synchronous generator and the frequency increase. Therefore, a common-sense approach to construct the power-frequency characteristic of the BESS to ensure the satisfactory operation of the BESS model in this test system is to appeal to almost linear relationship observed by the power and the frequency drawing from the observations made in Chapter 3. The new values are shown in Table 5.2.

Table 5.1 *Power-frequency parameters of the BESS _ default values*

M2_DF_STOP = - 0.25	M2_P_STOP = 0.0
M2_DF_START = -4.17	M2_P_START = 0.0
M2_DF_STAGE_1 = -0.5	M2_P_STAGE_1= 0.06
M2_DF_STAGE_2= - 1.0	M2_P_STAGE_2 = 0.12
M2_DF_STAGE_3 = -1.5	M2_P_STAGE_3 = 0.329
M2_DF_EMERG_1 = -1.583	M2_DF_EMERG_1 = 0.675
M2_DF_EMERG_2 = -1.67	M2_P_SPIN_MAX = 0.625

Table 5.2 *Power-frequency parameters of the BESS _ tuned values*

M2_DF_STOP = - 0.047	M2_P_STOP = 0.0
M2_DF_START = -0.05	M2_P_START = 0.0
M2_DF_STAGE_1 = -0.07	M2_P_STAGE_1= 0.2
M2_DF_STAGE_2= - 0.09	M2_P_STAGE_2 = 0.4
M2_DF_STAGE_3 = -0.11	M2_P_STAGE_3 = 0.6
M2_DF_EMERG_1 = -0.13	M2_DF_EMERG_1 = 0.8
M2_DF_EMERG_2 = -0.15	M2_P_SPIN_MAX = 1

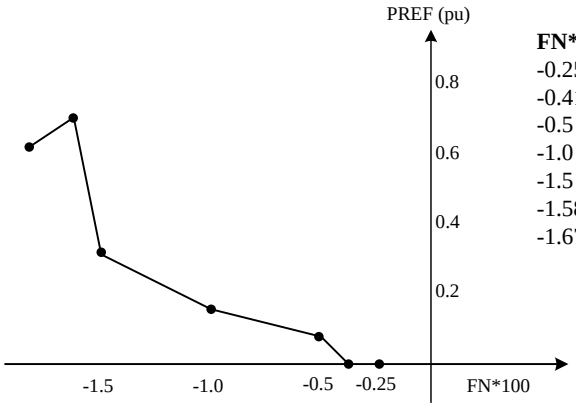

FN*100	PREF
-0.25	0.00
-0.417	0.00
-0.5	0.06
-1.0	0.12
-1.5	0.239
-1.583	0.675
-1.67	0.625

(a)

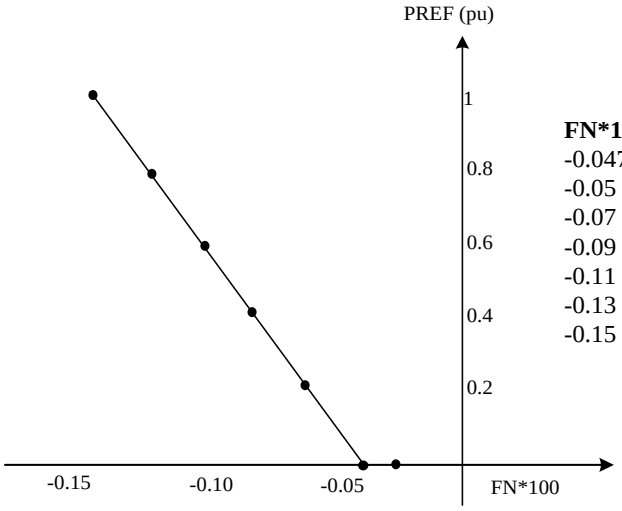

FN*100	PREF
-0.047	0.00
-0.05	0.00
-0.07	0.2
-0.09	0.4
-0.11	0.6
-0.13	0.8
-0.15	1

(b)

Figure 5.1 *Mode 2, power-frequency curve; (a) default characteristic, (b) tuned characteristic.*

Similar curves representing the operation of the BESS for modes 3 to 5 are shown in Figures 5.2 to 5.4. Since these modes are not used in this work, only the power-frequency curves are presented here without further explanation.

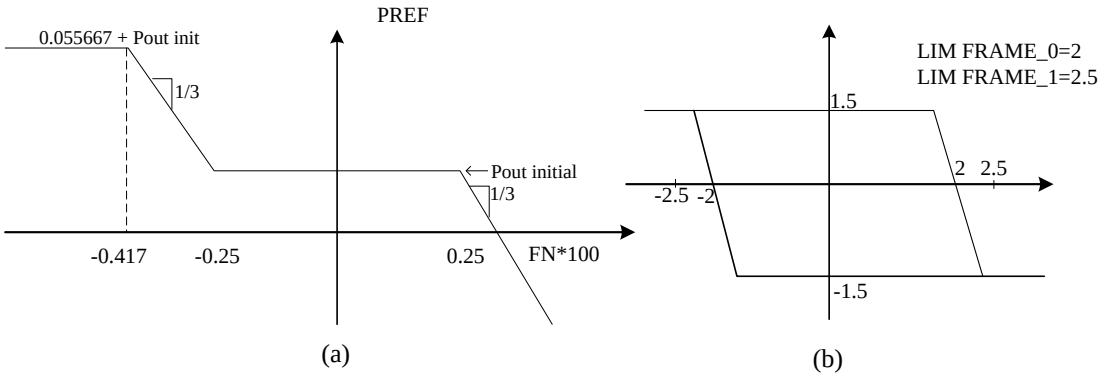

Figure 5.2 *Mode 3; (a) power-frequency curve, (b) frame limits.*

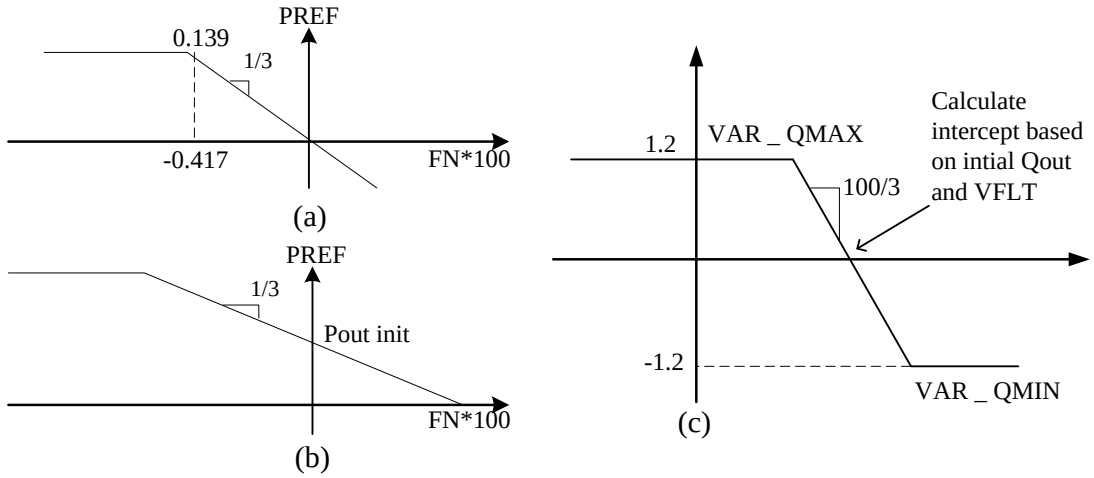

Figure 5.3 *Mode 4 and 5; (a) power-frequency characteristic of mode 4, (b) power-frequency characteristic of mode 5, (c) reactive power control characteristic of modes 4 and 5.*

5.2 High Voltage Transmission System

The test system used in this chapter is the same as the one used in the previous chapter. The system comprises 12 buses, with loads connected at buses 7 and 9 and with two shunt capacitors. The shunt capacitors provide voltage support by supplying reactive power. The system frequency is 60 Hz. The grid comprises two similar areas linked by a double circuit transmission line between buses 7 and 9. Each area consists of two synchronous generators, each having a rating of 900 MVA and 20 kV. The BESS injects power to bus 6 via a transformer connected between buses 6 and 12.

5.2.1 Synchronous generators

In PowerWorld, there are different models available for the synchronous generator. The classical model “GENCLS” represents the machine dynamics as a fixed voltage

magnitude behind a transient impedance R_a + j$X_{d'}$. The model is shown in Figure 5.4. This model is easy to use but it yields poor synchronous generators' dynamics.

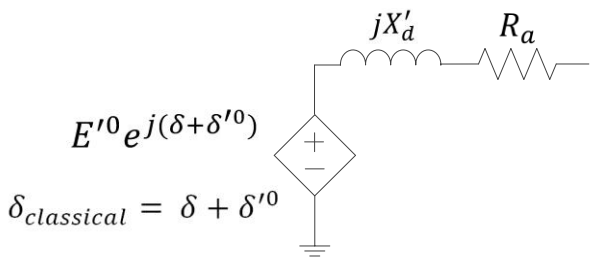

Figure 5.4 *Classical model GENCLS [2].*

Hence, the synchronous generators GENROU model is used. The model yields a good representation of the synchronous generator's dynamic over the range of interest in this work (up to about 10 Hz). This model is used to represent a solid rotor machine with three damper windings. More than 2/3 of the machines in the 2006 North American Eastern Interconnect study (MMWG) are represented by GENROU models [2]. The corresponding parameters of the generators are given in Table 5.3. The values are in per-unit on a 900 MVA base and a 20 KV base.

The exciter and the generator excitation system adjusts the generator field current to maintain the terminal voltage. The SCRX model and the HYPID model are used for the governor system and exciter system of the generators, respectively.

Table 5.3 *Synchronous generators' parameters in per-unit.*

$R_a = 0.0025$	$X_d = 1.014$	$X_L = 0.2$	$T''_{q0} = 0.071\ s$
$D = 0$	$X_q = 1.7$	$T'_{q0} = 0.4\ s$	$H = 1.8(G_{3\&4})$
$X'_d = 0.314$	$X''_d = 0.28$	$T''_{d0} = 0.039\ s$	$H = 6.5(G_{1\&2})$
$X'_q = 0.55$	$X''_q = 0.28$	$T'_{d0} = 6.55\ s$	

As discussed in the previous chapter, the step-up transformers have a reactance of j0.15 per-unit on a 20/230 KV base and a 900 MVA base. The parameters of the transmission lines in per-unit, on a 230 KV base and a 100 MVA base, are:

R = 0.0001 pu/km x_L = 0.001 pu/km b_C = 0.00175 pu/km.

The loads in buses 7 and 9 are:

Bus 7: P_L = 967 MW Q_L = 350 MVAr
Bus 9: P_L = 1767 MW Q_L = 100 MVAr

The shunt capacitive compensation at buses 7 and 9 are:

Bus 7: Q_C = 184.8 MVAr
Bus 9: Q_C = 330.4MVAr

After running the simulation in steady state mode, the generators are loaded as follows:

G1: P = 700 MW Q = 185 MVAr
G2: P = 700 MW Q = 234 MVAr
G3: P = 719 MW Q = 175 MVAr
G4: P = 700 MW Q = 202 MVAr

5.3 Load increment by 50 MW at bus 7

5.3.1 Frequency regulation

To assess the effectiveness of the BESS to provide frequency regulation improvement, the load at bus 7 is increased by 50 MW after two seconds of simulation. The frequency of the generator 1 is plotted with and with no BESS in Figures 5.5 and 5.6, respectively. The impact of the BESS on the frequency improvement can be seen by comparing these figures. Following the load increase, the frequency takes about 11 seconds to start to rise after reaching its lowest value (for both cases). With no BESS, the frequency drops to 59.557 Hz whereas when a 22 MW BESS is connected, it drops to 59.755 Hz. As expected, the BESS reduces the frequency drop by

$$\frac{(60 - 59.557) - (60 - 59.755)}{60 - 59.557} * 100 = 44.7\ \% \qquad (5.1)$$

It should be noted that the inertial response of the turbo-alternators used in the simulation of this chapter is slightly weaker than the inertial response of the hydro-generators used in the simulations of Chapter 4, owing to their intrinsically weaker dynamic characteristics.

It should also be remembered that further to the action of the BESS, the speed governing mechanism also influences the system frequency. With no BESS, after the frequency drops to its lowest value, the generator frequency regulator brings the frequency back to 59.956 Hz by enabling the injection of additional active power into the grid. The share of Generator 1 to meet the new power demand is 13 MW, as it can be seen from Figure 5.8. In this case, there will be a steady state error of 0.044 Hz in the system frequency. In contrast, the steady state error for the case where a 22 MW BESS

is connected to the grid is 0.042 Hz. The active power injected by Generator 1 when the BESS is connected, is shown in Figure 5.9. As it can be seen from this figure, the extra active power injected by the generator to provide the new demand power is substantially reduced.

Similarly to the case presented in Chapter 4 concerning the 40 MW BESS, results are presented in Figures 5.7 and 5.10. It is quite encouraging to observe that the frequency drops only to 59.859 Hz and almost returns to the reference value after 36 seconds.

5.3.2 Voltage regulation

The role of the BESS in voltage regulation improvement can be seen by looking at Figures 5.10 to 5.12, where the RMS voltage at bus 1 with and with no BESS connected to the grid, are presented. As expected, in all cases (with and with no BESS) the voltage at bus 1 drops after the disturbance occurs and returns to its initial value. For the study case with BESS (22 and 40 MW) this voltage drop is relatively smaller. The RMS voltage of bus 6 observes a similar behavior with a difference in the steady state value which is less than the initial value as presented in Figures 5.13 to 5.15.

Rotor speed

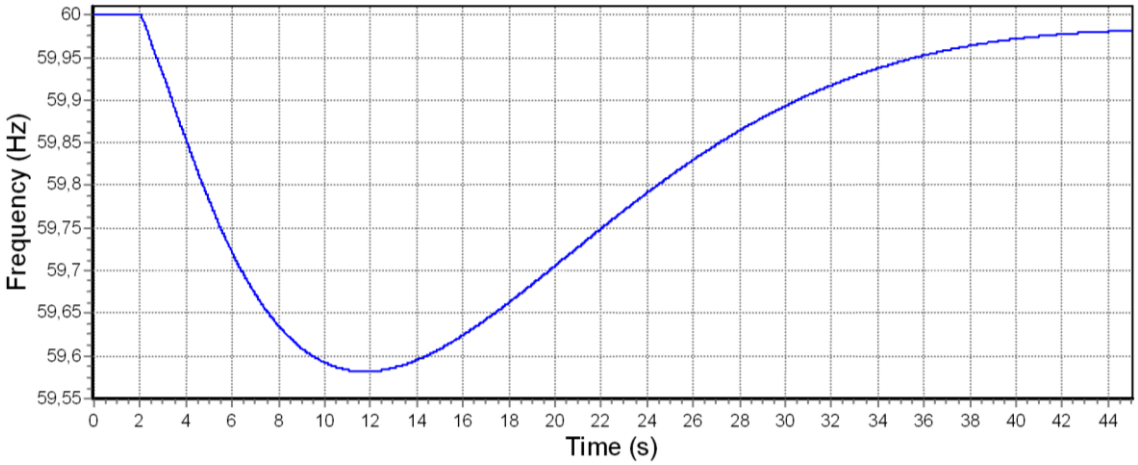

Figure 5.5 *Rotor speed when load is increased (no BESS).*

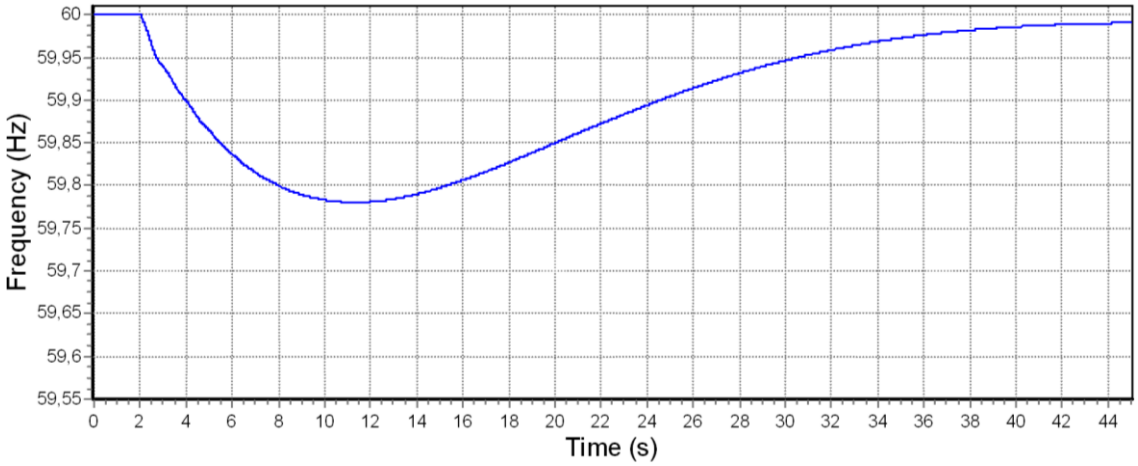

Figure 5.6 *Rotor speed when load is increased (with 22 MW BESS).*

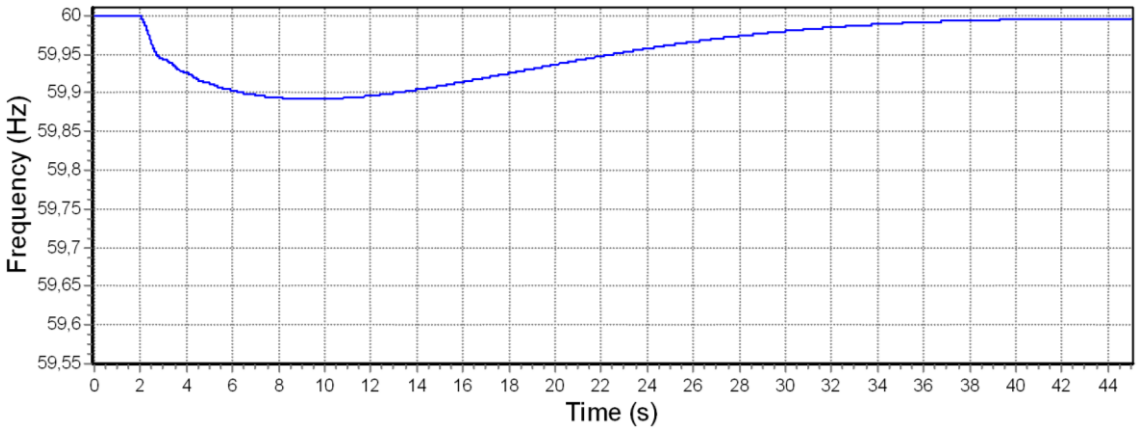

Figure 5.7 *Rotor speed when load is increased (with 40 MW BESS).*

Active power injected by generator 1

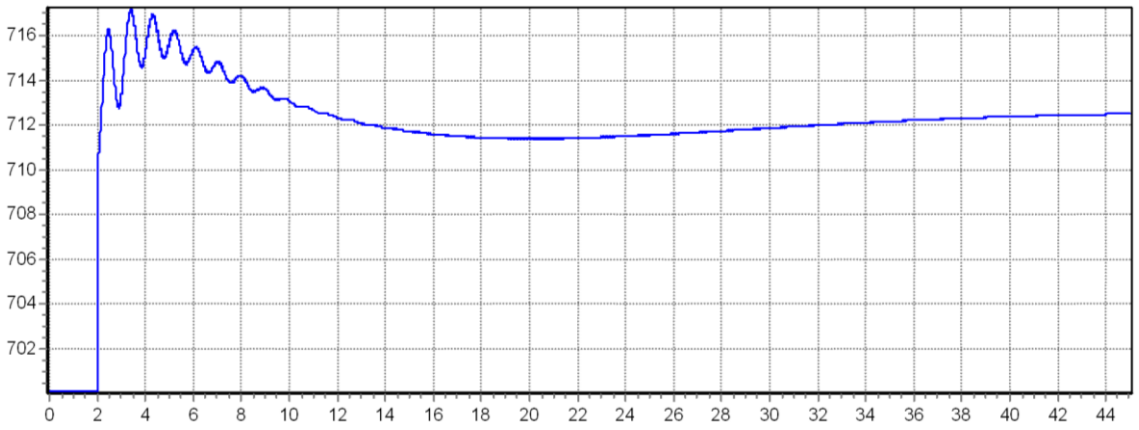

Figure 5.8 *Active power injected by generator 1 (no BESS).*

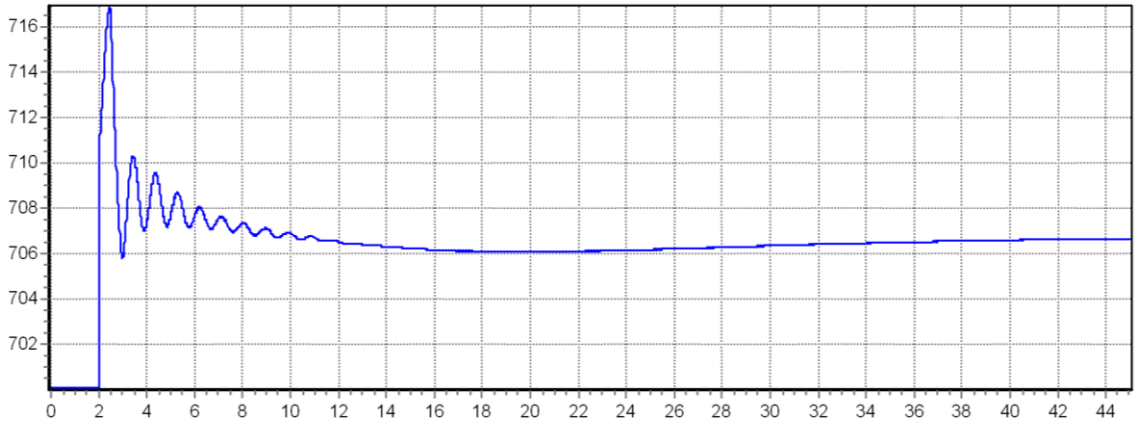

Figure 5.9 *Active power injected by generator 1 (with 22 MW BESS).*

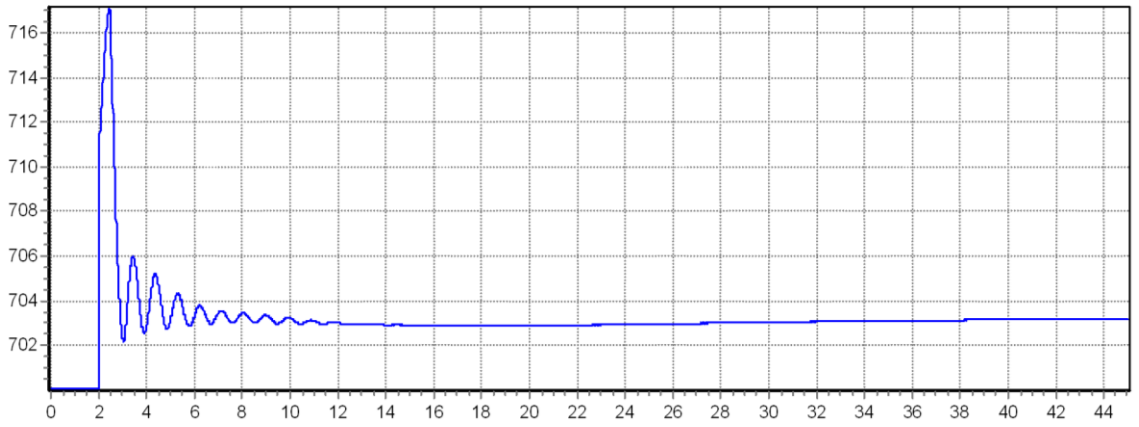

Figure 5.10 *Active power injected by generator 1 (with 40 BESS).*

Voltage at bus 1

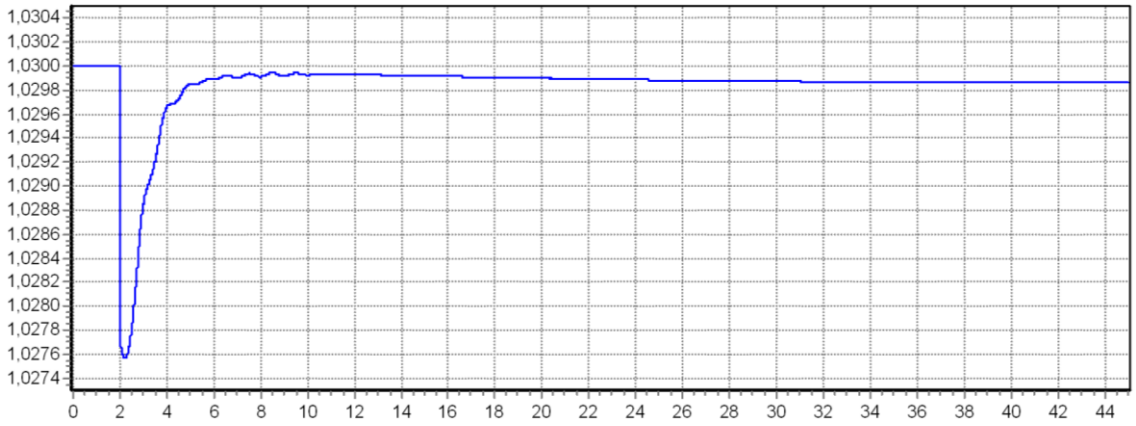

Figure 5.11 *Voltage at bus 1 when load is increased (no BESS).*

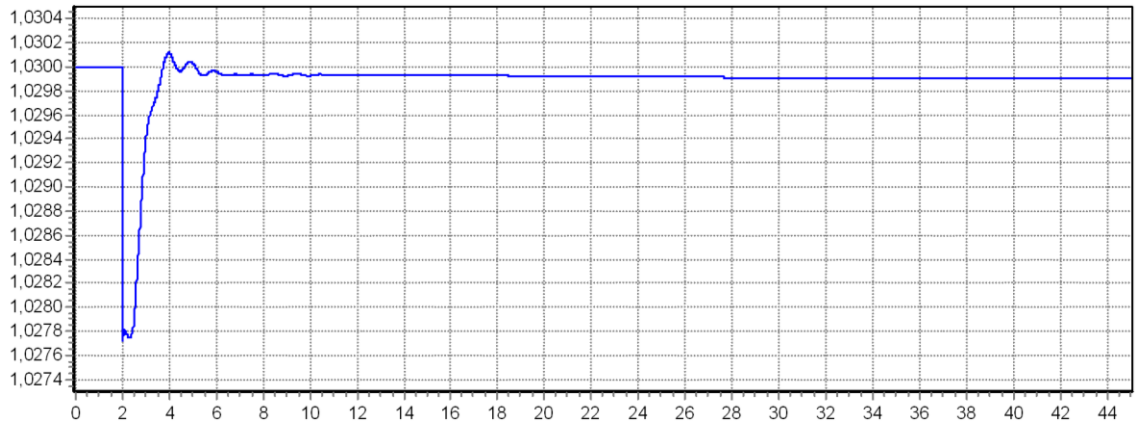

Figure 5.12 *Voltage at bus 1 when load is increased (with 22 MW BESS).*

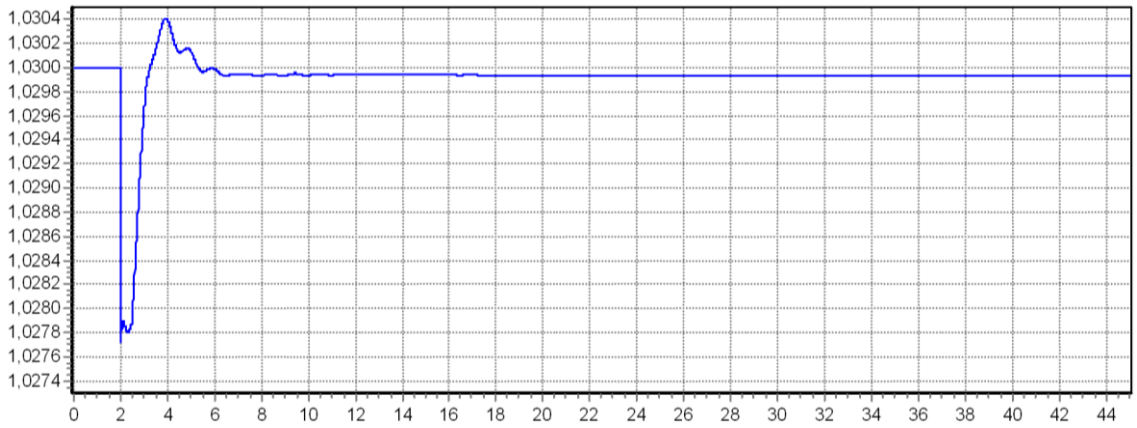

Figure 5.13 *Voltage at bus 1 when load is increased (with 40 MW BESS).*

Voltage at bus 6

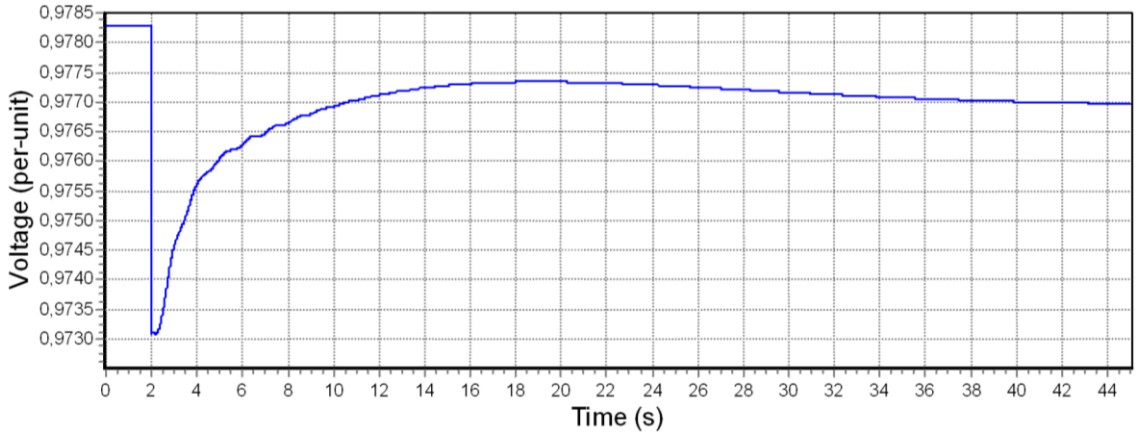

Figure 5.14 *Voltage at bus 6 when load is increased (no BESS).*

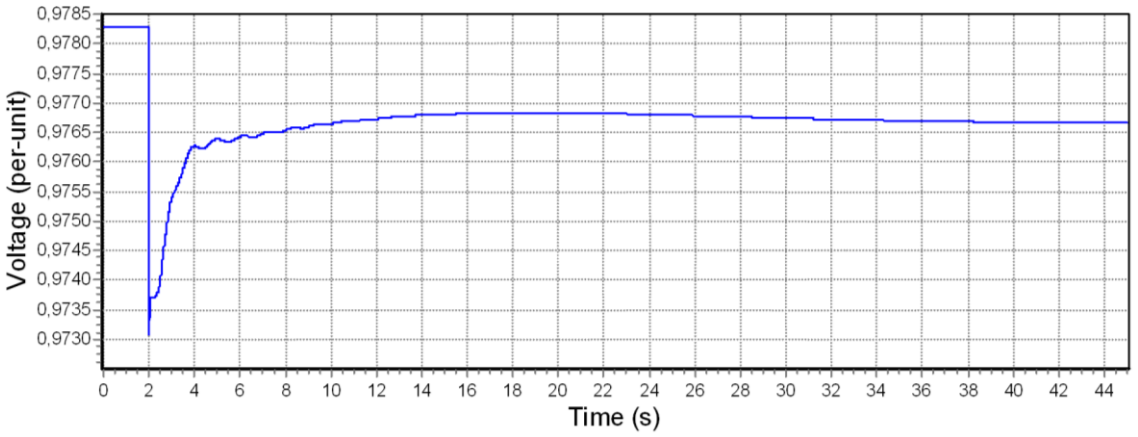

Figure 5.15 *Voltage at bus 6 when load is increased (with 22 MW BESS).*

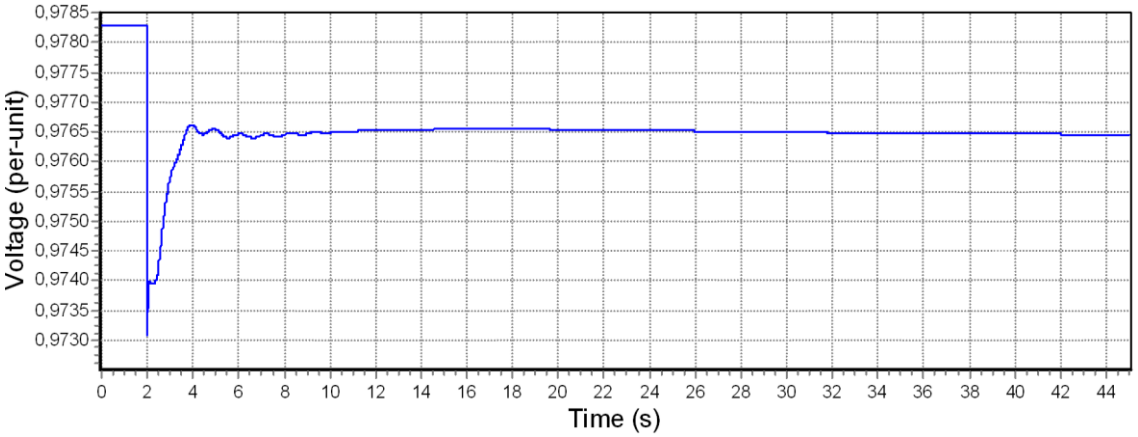

Figure 5.16 *Voltage at bus 6 when load is increased (with 40 MW BESS).*

5.4 Summary

The BESS model available in PowerWorld is presented as “CBattery” and can be found under the generators stability settings. In spite of its seemingly simple nature, it models the BESS dynamics with sufficient accuracy. However, it should be noted that the default values of the BESS available in PowerWorld designed to operate in every situation, they would require tunning to every specific test system and type of system perturbation. Moreover, “CBattery” lacks some importing capabilities, such as temperature dependency, battery aging, a state-of-charge indicator and a full charging-discharge cycle.

The “CBattery” model has four operating modes. Mode 2 is the mode suitable for under-frequency emergencies. The model has several key parameters characterizing its performance. Fourteen parameters are the most significant as they provide the basis for the calculation of the required power to be injected by the BESS. In order to ensure a satisfactory operation of the BESS model for the test system and power levels involved, the default values of the BESS need to be tuned. In this particular case, after tuning the parameters default values, the response of the BESS model was assessed. The simulation results indicate that the BESS is very effective in reducing frequency drops, as well as in regulating voltage magnitude at its point of connection with the grid. As expected from the light shed by the results provided by PSCAD in Chapter 4, it was reassuring to see that these results also show that the frequency and voltage stability improvements are strongly linked to the capacity of the BESS. This further corroborated the preliminary findings of Chapter 4, using a different commercial package with a completely different modeling philosophy and applied to two quite distinct types of synchronous generator, namely, a hydro-generator and a turbo-alternator.

6. COMPARISON OF SIMULATION RESULTS FURNISHED BY PSCAD AND POWERWORLD

The purpose of this chapter is to contrast the impacts of the BESS on frequency regulation using two very different kinds of simulation packages, namely, PSCAD and PowerWorld. To enable a meaningful comparison, it is necessary to have the two test systems, similar to one another, as much as possible. In other words, the generator, exciter and governor models and their parameters in both simulators need to be similar within the constraints of the proprietary nature of both commercial packages as well as the very distinct nature that the two packages take to model each element of the power system. This applies to transmission lines, compensating equipment, generators and their controls as well as to the battery and power electronics equipment. For a fundamental description of the approach taken by PSCAD to power systems modeling, refer to [56]. For a fundamental description of a tool such as PowerWorld refer to [55].

Two sets of frequency responses are obtained for the purpose of this comparison:

i. With no BESS
ii. With BESS

Further to comparing the impact of the BESS models on frequency improvement, the BESS model components, control mechanisms and their appearance are also contrasted. A note is taken of the computing time the simulators take to carry out their respective simulations.

6.1 With no BESS

In this chapter the hydro-generator model used for the comparisons is the one used for PSCAD simulations in Chapter 4. Hence, a different generator model should be used for the PowerWorld simulations, one that has the characteristics of a hydro-generator as opposed to a turbo-alternator which is the one that was used in Chapter 5. Such a generator within PowerWorld seems to be the GENTRA model. The parameters for the generators' models are presented in Table 6.1. As it can be seen, the two generator models have similar parameters, however, there are some parameters which are only available in PSCAD and *vice versa*. It should be remembered that the philosophy modeling of the two software tools used here are quite different. PSCAD is an electro-magnetic transient p-type package whereas PowerWorld is an electro-mechanical-type

package. Hence, they model the dynamics of the synchronous generator with a different degree of detail.

Table 6.1 *Generators' parameters in PSCAD and PowerWorld.*

PSCAD	PowerWorld
$H = 6.5$ [s]	$H = 6.5$ [s]
$X_d = 1.014$ [pu]	$X_d = 1.014$ [pu]
$X'_d = 0.314$ [pu]	$X'_d = 0.314$ [pu]
$T'_{do} = 6.55$ [s]	$T'_{do} = 6.55$ [s]
$R_a = 0.0025$ [pu]	$R_a = 0.0025$ [pu]
$T''_{do} = 0.039$ [s]	$A_f = 0.25$
$X_q = 0.77$ [pu]	$X_q = 0.77$ [pu]
$T''_{qo} = 0.071$ [pu]	$D = 0$
$X''_d = 0.28$ [pu]	
$X''_q = 0.28$ [pu]	

The block diagrams of the exciters used in the PSCAD and PowerWorld simulations are shown in Figures 6.1 and 6.2 and their parameters are presented in Tables 6.2 and 6.3, respectively. Although not identical, the block diagrams are similar.

The block diagrams (transfer functions) of the governors used in the PSCAD and PowerWorld simulations are shown in Figures 6.3 and 6.4 and their parameters are presented in Tables 6.4 and 6.5, respectively.

To facilitate the comparison, the rotor speeds of Generator 1 obtained with PSCAD and PowerWorld are plotted in the same figure (Figure 6.5). The two curves show a great deal of similarities; the two frequency responses reach the same lowest value (59.72 Hz) at almost the same time and reach 59.98 Hz at the end of the simulation.

6.2.1 With 22 MW BESS connected

The rotor speeds of Generator 1 with the 22 MW BESS connected are shown in Figure 6.6. The curves exhibit similar trends. The two frequency responses reach almost the same lowest value at almost the same time and reach 59.99 Hz at the end of the simulation.

6.2.2 With 40 MW BESS connected

The rotor speeds of Generator 1 with the 40 MW BESS connected are shown in Figure 6.7. As expected, the curves exhibit similar behavior, however, the figure indicates a slightly superior frequency response of the BESS model implemented in PSCAD.

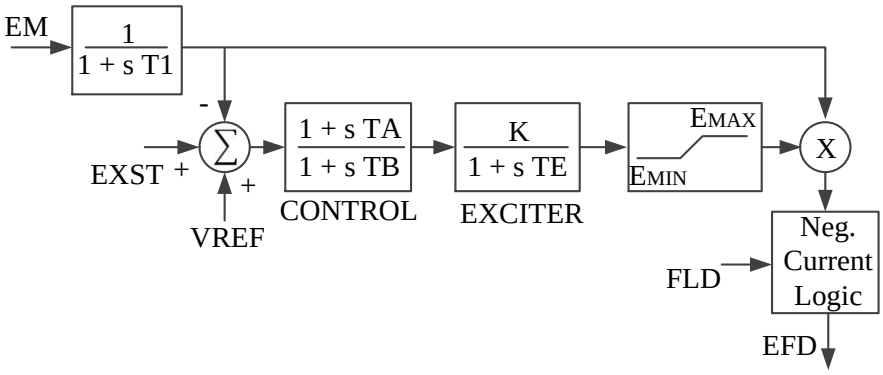

Figure 6.1 *SCRX exciter block diagram in PSCAD.*

Table 6.2 *SCRX exciter parameters in PSCAD.*

Rectifier Smoothing Time Constant	0.02 [s]
Controller Lead Time Constant	1.5 [s]
Controller Lag Time Constant	1.0 [s]
Exciter Time Constant	0.02 [s]
Exciter Gain 100	[pu]
Maximum Field Voltage	5 [pu]
Minimum Field Voltage	-5 [pu]
L-G Voltage Base	11.55 [kv]
Line Current Base	100.02 [kA]
Reverse Resistance	15000 [ohm]

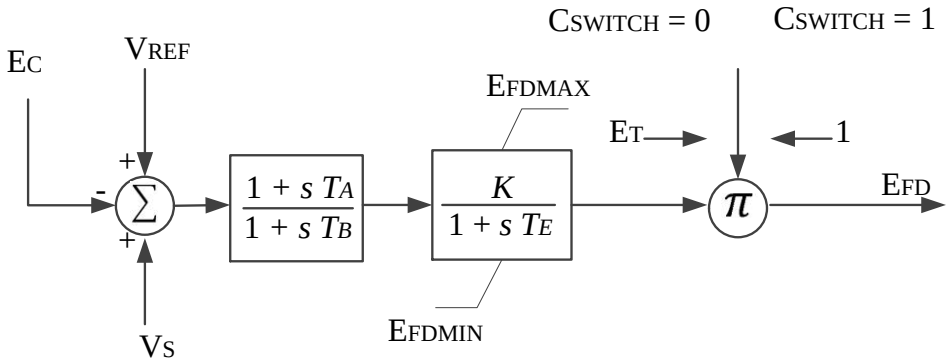

Figure 6.2 *SCRX19 exciter block diagram in PowerWorld.*

Table 6.3 *SCRX 19 exciter parameters in PowerWorld.*

Ta/Tb = 0.1	K = 200	Efdmin = 0	Cswitch = 0
Tb = 10	Te = 0.05	Efdmax = 5	Rc/Rfd = 0

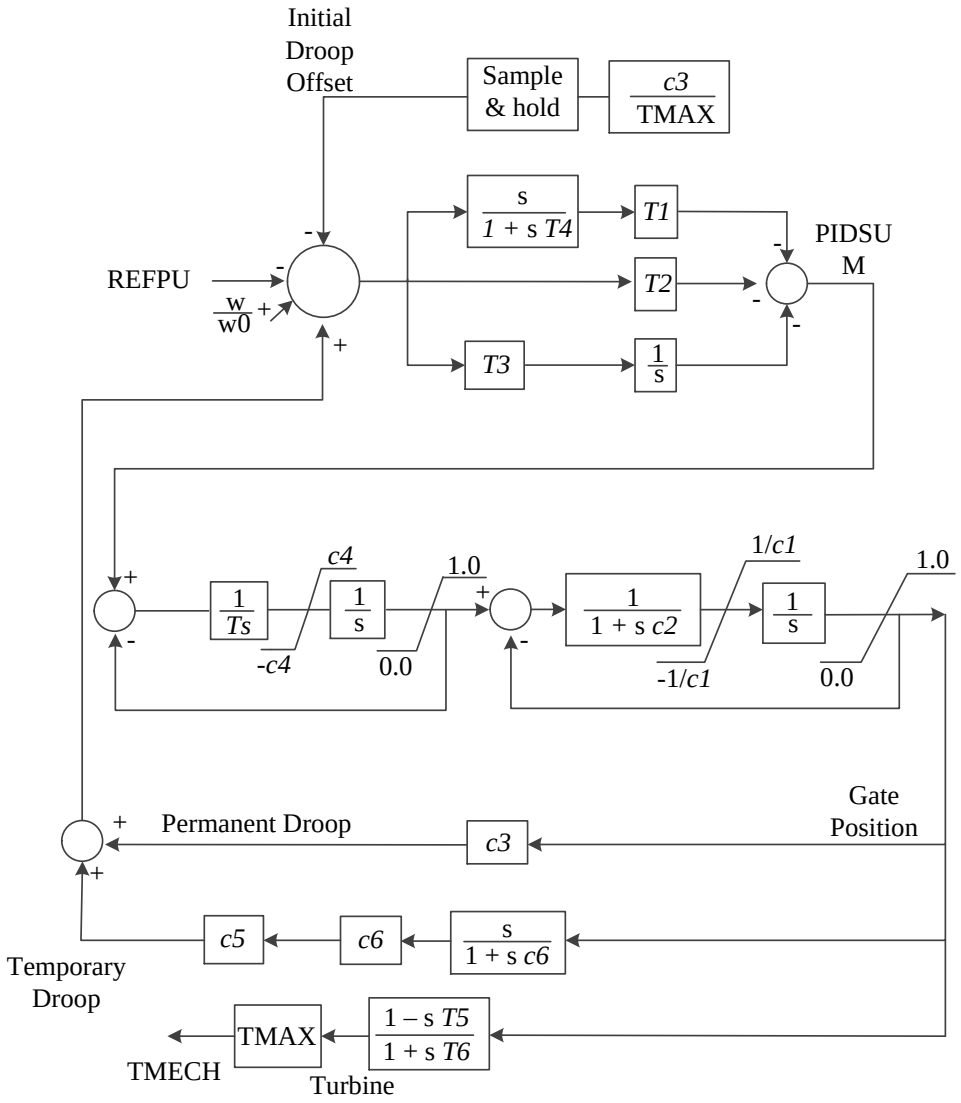

T_1 = Controller real pole gain
T_2 = Controller proportional gain
T_3 = Controller integral gain
T_4 = Controller real pole time constant [s]
T_5 = Turbine lead time constant [s]
T_6 = Turbine lag time constant [s]
T_s = Governor time constant [s]
C_1 = Inverse gate velocity limit [s/pu]
C_2 = Gate velocity time constant [s]
C_3 = Permanent droop gain
C_4 = Gate position control rate limit [pu/s]
C_5 = Temporary droop gain
C_6 = Temporary droop time constant [s]
T_{max} = Conversion constant

Figure 6.3 *HGOV18 governor block diagram in PSCAD.*

Table 6.4 *HGOV18 parameters in PSCAD.*

Controller Real Pole Gain	0.88
Controller Proportional Gain	3.7
Controller Integral Gain	0.44
Controller real Pole Time Constant	0.02 [s]
Turbine Lead Time Constant	0.01 [s]
Turbine Lag Time Constant	0.01 [s]
Governor Time Constant	0.05 [s]
Inverse Gate Velocity Limit	4.8 [s/pu]
Gate Velocity Time Constant	0.1 [s]
Permanent Droop Gain	0.08
Gate Position Control Rate Limit	0.22 [pu/s]
Temporary Droop Gain	0.0
Temporary Droop Time Constant	0.01 [s]
Conversion Constant	0.895
Time Constant for Smoothing Tm0	0.02 [s]
Initialization Switch	ENAB

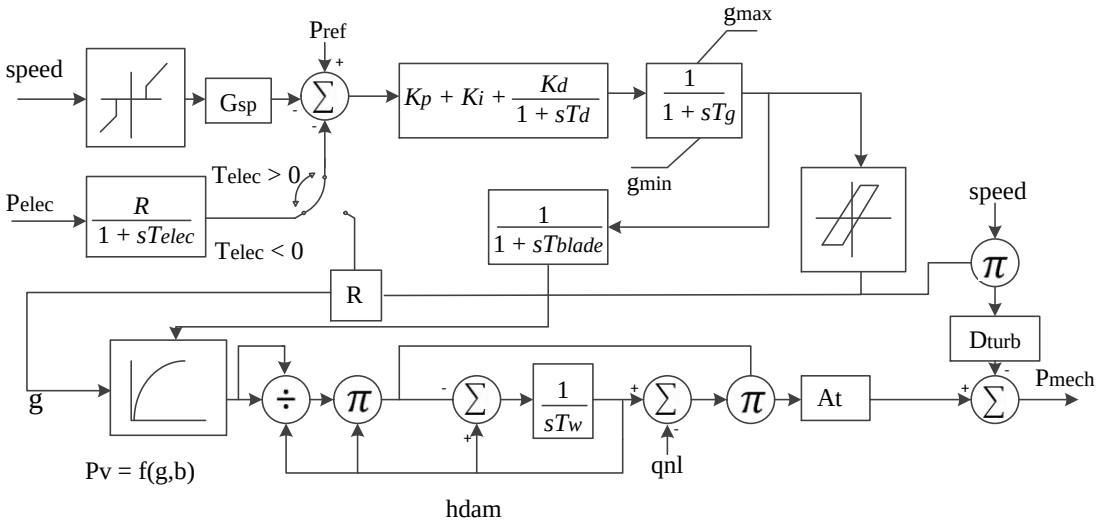

Figure 6.4 *HYPID governor block diagrams in PowerWorld.*

Table 6.5 *HYPID governor parameters in PowerWorld.*

$Relec = 0.04$	$Gmin = 0.0$	$Gv0 = 0.0$	$Td = 1.0$
$Tpelec = 1.0$	$Tw = 1.0$	$Pgv0 = 0.0$	$Gsp = 1.0$
$Kp = 1.9$	$At = 1.2$	$Gv1 = 0.0$	$Tg = 0.5$
$Ki = 0.2$	$Dturb = 0.5$	$Hdam = 1.0$	$Db1 = 0.0$
$Kd = 7$	$Qnl = 0.08$	$Tblade = 100$	$Eps = 0.0$
$Velm = 0.2$	$Gmax$ 1.0	$Db2 = 0.0$	

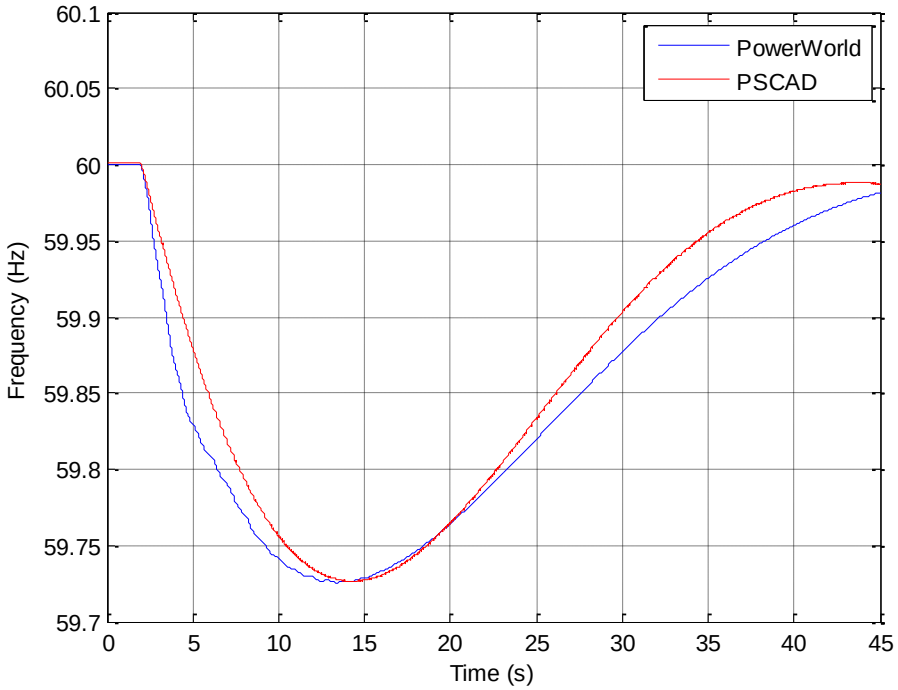

Figure 6.5 *Rotor speed in PSCAD and PowerWorld when no BESS is connected.*

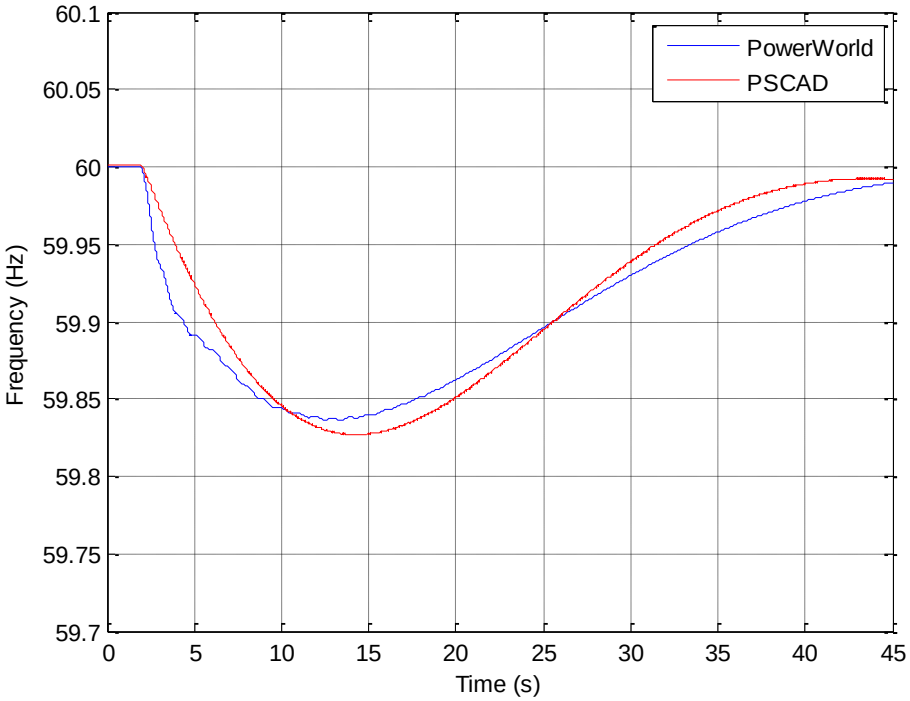

Figure 6.6 *Rotor speed in PSCAD and PowerWorld when a 22 MW BESS is connected.*

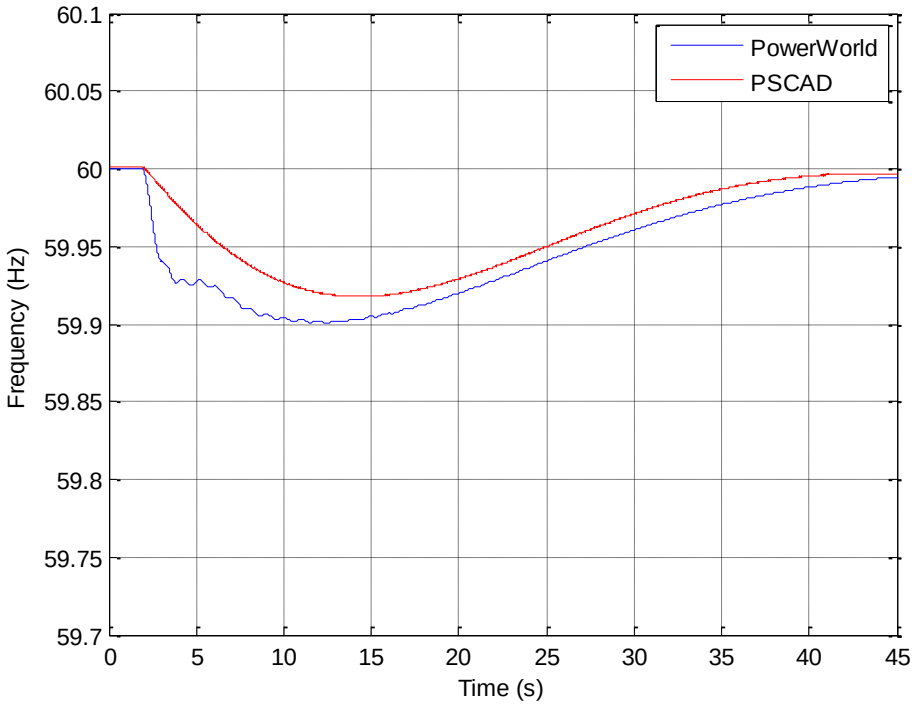

Figure 6.7 *Rotor speed in PSCAD and PowerWorld when a 40 MW BESS is connected.*

6.3 BESS model in PSCAD and PowerWorld

In PSCAD, the rate of discharge of the battery is controlled by adjusting the output voltage of the DC/DC converter (equation (4.18)), whereas in PowerWorld the power exchange between the battery pack and the grid is done by using the characteristic shown in Figure 5.1.b.

One of the shortcomings of PowerWorld is that the SOC of the battery is missing from the model.

A key issue when comparing the performance of PSCAD and PowerWorld, is computing time. For a 45 seconds of simulation time, using a time-step of 20 μs, PSCAD takes 20 minutes to carry out the simulation whereas PowerWorld takes 56 seconds.

It should be noted that the inverter used in the PSCAD simulations does not operate properly for time-steps greater than 20 μs, whereas the simulation results in PowerWorld are valid for time-steps much greater than 20 μs, due to the absence of proper power electronics in the model.

Clearly, the two BESS models are very different in nature. The BESS model in PowerWorld is an input-output characteristic which facilitates its ease of use within the

modeling philosophy of PowerWorld. On the other hand, the BESS model implemented in PSCAD takes the approach of representing each individual element in detail and although it may appear complex, it does provide a wide variety of modeling options.

6.4 Conclusion

The current BESS model available in PowerWorld seems to be very basic and there is clearly ample scope for carrying out research and development work in this area of BESS-upgraded power systems from the vantage of transient stability and frequency control. One big advantage of the simulations in PowerWorld is that they are much faster than the simulations in PSCAD, hence, for large power systems it is clearly advantageous to use a simulation tool such as PowerWorld. In contrast, the BESS model implemented in PSCAD is a more accurate and with a wider range of capabilities. It may be argued that this model is closer to an actual BESS.

It may be concluded that until a more flexible and accurate BESS model is available in PowerWorld, the best way forward to carry out the kind of studies conducted in this research, would be to start the simulations with PSCAD and use these results to fine tune the battery model available in PowerWorld to carry out the large volume of simulations that a given case study would normally require.

7. CONCLUSIONS

This chapter draws on the salient points and main conclusions furnished by this piece of research on the effectiveness of a BESS model to provide frequency control and stability in a high-voltage transmission system. From the outset, a key objective of this thesis was to investigate the effectiveness or otherwise of the new generation of BESS technology on the voltage and frequency stability of a high-voltage transmission system – a modern BESS comprises the battery pack, a DC-DC converter and a DC-AC inverter. So far, there is very little work reported on the impact that a modern BESS exerts on a high-voltage transmission system and it was deemed appropriate to carry out a preliminary investigation using computer-based simulations. Aiming at being as comprehensive as possible and within the time constraints of this research project, two different simulation packages were used to carry out the dynamic simulations involved in this research, namely, PSCAD and PowerWorld.

It should be remarked that both types of simulations tools enable dynamic assessments of electrical power networks but they take a fundamentally different approach to the modeling of the electrical power system components making up the power grid. PSCAD takes the approach of representing the voltage and currents waveforms that exist in every component of the power grid by means of differential equations, which require discretization at rather small time steps, in the order of micro-seconds, to ensure a stable numerical solution of the differential set of algebraic equations. On the other hand, the solution of the algebraic-differential set within PowerWorld is carried out only for the positive-sequence (one phase) network, as opposed to the three-phases as it is done in PSCAD. In PowerWorld, the BESS is modeled by a simple linear relationship between the power and the frequency, which seems to yield remarkably good results given its simplicity. One further key point in the differing approach to the modeling and solution of the two software packages to a common dynamic problem is that PowerWorld uses fundamental-frequency phasors of voltages and currents whereas PSCAD uses instantaneous waveforms of voltages and currents. Hence, the maximum resolution that a tool like PowerWorld can offer is that of one full cycle (50 Hz or 60 Hz) compared to PSCAD which may afford very detailed resolutions which each cycle. Nevertheless, in this particular application such a degree of detail would be rarely required. Needless to say that such great level of information calculation comes with an onerous price-tag to pay in terms of a very considerable computational time compared to the more modest computing times incurred by the PowerWorld's dynamic simulations.

An equivalent transmission system corresponding to a bulk-power power system widely used in academic circles, namely, the two-area Kundur system, was modeled in both PSCAD and PowerWorld for the purpose of carrying out the relevant dynamic

simulations of this work. A battery model available in PSCAD was used to make up the BESS model implemented in Kundur's system. The ensuing BESS model was put through its paces and it is concluded that the model showed to possess very realistic voltage and frequency regulating characteristics. The four equivalent generators in Kundur's system were taken to be hydro-generators which are known to possess high inertia and damping capabilities.

A similar development exercise was carried out for PowerWorld where the experience gained in implementing Kundur's system in PSCAD, proved to be very useful. Certainly the dynamic simulations carried out in PSCAD furnished key information which was used to set up a modified input-output characteristic for the BESS model in PowerWorld. It was concluded that the default information contained in input-output table of values did not yield meaningful answers for the problem being researched and that, in contrast, the modified input-output table based on the PSCAD result provided results that made good engineering sense. The four equivalent generators used in Kundur's system in this case are assumed to be turbo-alternators and these are known to exhibit lower inertia and posses lower damping than hydro-generators. The frequency responses afforded by the PowerWorld simulations showed a more pronounced drop than the frequency responses provided by the PSCAD simulations, which is a manifestation of a generator with a lower inertia and damping.

It may be concluded from the simulation results obtained with PSCAD and PowerWorld and applied to cases with hydro-generators and turbo-alternators that the BESS is very effective in providing frequency stabilization in cases when a load increase induces a deceleration of the rotors of the synchronous generators, resulting in frequency drops. The simulation results also showed that the BESS yields very effective voltage magnitude regulation at its point of connection with the grid – this was an expected outcome owing to the use of a voltage source converter in the BESS as the interface with the power grid. It is also concluded that the frequency and voltage stability improvements achieved by the BESS, are strongly linked to its capacity.

Since the two selected commercial packages to carry out this investigation on the effectiveness of a BESS to provide frequency stabilization in a high-voltage transmission system, yielded good results; it seemed appropriate to compare the closeness or otherwise of the results provided by the PowerWorld simulator with those of the PSCAD simulator. At the same time, this provided a good opportunity to benchmark the computing time taken by the two simulators to carry out one of such dynamic simulations, since the modeling approach taken by the two simulators is fundamentally different; PSCAD is an electro-magnetic transient program (EMTP) whereas the dynamic application tool within PowerWorld is an electro-mechanical transient computer program. Their power systems application strengths lies within quite different time spans, the former is used to simulate quite naturally very fast transient phenomena within the range of a few hundreds of milliseconds whereas the latter is

used to simulate slower transient phenomena, those that occur above one hundred milliseconds. It is clear that EMTP-type packages can perform very accurate simulations of electrical phenomena that are very far away from their natural zone of computational domain, such as the application pursued in this research work but this is at the expense of exceedingly long computing times. It is perhaps less obvious to understand the fact that electro-mechanical transient-type tools are fundamentally prevented from simulating any electrical phenomena that takes place within a time span of less than 20 milliseconds, in a system that operates at 50 Hz.

Following on this argument it is not difficult to forecast that the PSCAD simulations would be in great disadvantage when conducting frequency stability studies, compared to equivalent simulations carried out with PowerWorld. On the other hand and in spite of its shortcomings, it is concluded that the BESS model in PSCAD is a very close representation of an actual BESS whereas the BESS representation available in PowerWorld is only a gross representation of an actual BESS. To enable a more punctual comparison of the strengths and weaknesses of the two different approaches, the Kundur test system with hydro-generators –the one used for the PSCAD simulations – was also solved with PowerWorld and the simulation results compare reasonably well with those of PSCAD for cases of no BESS, with a 22 MW BESS and with a 40 MW BESS. It should be noted that an exact match is not achieved even for the basic case of no BESS because of the two quite different approaches to the modeling adopted by the two packages as well as their proprietary nature. It is concluded that the results furnished by the PowerWorld simulator represent a close approximation to the more accurate results produced by the PSCAD simulator. However, when it comes to execution times, for the test system used in this research, the ratio is more than 20 to 1 in favor of the simulations carried out with PowerWorld. It should be noted that the Kundur system is not a large power system by any means and that in a power system of a realistic size, this type of studies may not be very practical to be carried out with PSCAD and yet the BESS characteristic used in PowerWorld seem to yield realistic results when built on the strength of the results achieved by PSCAD. Hence, it may be concluded that the use of PSCAD in this power systems application area will be required until a self-standing procedure or model is developed for the BESS in electro-mechanical transient stability-type packages. In the present time the following is recommended: to carry out sufficient studies with PSCAD to build an input-output BESS characteristic with which to conduct the bulk of studies using PowerWorld.

The overriding conclusion emanating from this piece of research is that the BESS is well placed to improve on the frequency and voltage stability in a high-voltage transmission system and that further research is required to develop more accurate and quicker BESS models.

REFERENCES

[1] J. Klimsta and M. Hotakainen, *Smart Power Generation*, Avain Publishers, 2011.

[2] J. Klimstra, *Power Supply Challenges*, Avain Publisher, 2011.

[3] M. Yoshio, R. Brodd and A. Kozawa, *Lithium-Ion Batteries, Science and Technolies*, Springer.

[4] R. Huggins, *Energy Storage*, Springer, 2010.

[5] C. Spitzer, U. Ferrrell and T. Ferrell, *Digital Avionics Handbook*, Third Edition, CRC Press, 2014.

[6] C. Mikolajczak, M. Kahn, K. White and R. Long, *Lithium-Ion Batteries Hazard and Use Assessment*, Springer, 2012.

[7] A. Balakrishnan and K. Subramanian, *Nanostructured Ceramic Oxides for Supercapacitor Applications*, CRC Press, 2014.

[8] M. Patel, *Spacecraft Power Systems*, CRC Press, 2004.

[9] A. Emadi, *Handbook of Automotive Power Electronics and Motor Drives*, CRC Press, 2005.

[10] A. Chakraborty, S. K. Musunuri, A. K. Srivastava and A. K. Kondabathini, "Integrating STATCOM and Battery Energy Storage System for Power System Transient Stability: A Review and Application," Advances in Power Electronics, vol. 2012, Art. ID 676010, 12 pages.

[11] L. O. Vasquez, *Fuel Cell Research Trends*, Academic Press, Nova Publishers, Science, 2007.

[12] B.K. Bose, “Introduction to Power Electronics, Modern Power Electronics”, IEEE Press, Piscataway, NJ, USA, 1991.

[13] B.K. Bose, “Evaluation of modern power semiconductor devices and future trends of converters”, IEEE Transactions on Industry Applications, Vol.28, 1992, pp. 403 – 413.

[14] S. Atcitty, S. Ranade, A. Gray-Fenne, “Summary of State-of-the-Art Power Conversion Systems for Energy Storage Applications”, SAND98-2019, 1998, Sandia National Laboratories, Albuquerque, NM, USA.

[15] P. Moseley, J. Garche, C. Parker and D. Rand, *Valve-Regulated Lead-Acid Batteries*, Elsevier, 2004.

[16] http://www.aesenergystorage.com/news/aes-combines-advanced-battery-based-energy-storage-traditional-power-plant.html. May 6 2013.

[17] N.W. Miller, R.S. Zrebiec, G. Hunt and R.W. Deimerico, “Design and Commissioning of a 5 MVA, 2.5 MW-h Battery Energy Storage System”, in Proceedings of IEEE Transmission and Distribution Conference, 1996 , pp. 339 – 345.

[18] N. Chaudhuri, B. Chaudhuri and A. Yazdani, *Multi-terminal Direct-Current Grids: Modeling, Analysis, and Control*, John Wiley & Sons, 2014.

[19] A. Baggini, *Handbook of Power Quality*, John Wiley & Sons, 2008.

[20] H. Bevrani, M. Watanabe and Y. Mitani, *Power System Monitoring and Control*, John Wiley & Sons, 2014.

[21] N. W. Miller, R. S. Zrebiec, R. W. Delmerico and G. Hunt, “Battery Energy Storage Systems for Electric Utility, Industrial and Commercial Applications”, Battery Conference on Applications and Advances, Eleventh Annual, 1996, pp. 235 – 240.

[22] M.W. Tsang and D. Sutanto, “Damping Inter-area Oscillation Using a Battery Energy Storage System”, Advances in Power System Control, Operation and Management. APSCOM-97. Fourth International Conference, vol. 2, 1997, pp. 409 – 414.

[23] S.K. Aditya and D. Das, “Battery Energy Storage for Load Frequency Control of an Interconnected Power System”, Journal of Electric Power Systems Research, vol. 58, 2001, pp. 179 – 185.

[24] A. Oudalov, D. Chartouni, C. Ohler and G. Linhofer, “Value Analysis of Battery Energy Storage Applications in Power Systems”, Power Systems Conference and Exposition, 2006, pp. 2206 – 2211.

[25] P. Mercier, R. Cherkaoui and A. Oudalov, “Optimizing a Battery Energy Storage System for Frequency Control Application in an Isolated Power System”, IEEE Transaction on Power Systems, vol. 24, 2009, pp. 1469 – 1477.

[26] S. V. Giannoutsos and S. N. Manias, “A Cascade Control Scheme for a Grid Connected Battery Energy Storage System (BESS)”, IEEE International Energy Conference and Exhibition (ENERGYCON), 2012, pp. 469 – 474.

[27] Z. Kun, M. Chengxoing, X. Junwen and L. Jiming, “Determination of Characteristic Parameters of Battery Energy Storage System for Wind Farm”, Renewable Power Generation, IET, vol.8, 2014, pp. 22 – 32.

[28] J. Kyung-Hee, K. Hoyong and R. Daeseok, “Determination of the installation site and optimal capacity of the battery energy storage system for load leveling”, , IEEE Transactions on Energy Conversion, vol. 11, 1996, pp. 162 – 167.

[29] L. Tsung-Ying and C. Nanming, “Determination of Optimal Contract Capacities and Optimal Sizes of Battery Energy Storage Systems for Time-of-use Rates Industrial Customers”, IEEE Transactions on Energy Conversion, vol. 10, 2002, pp. 562 – 568.

[30] Bagen and R. Billinton, “Incorporating well-being Considerations in Generating Systems Using Energy Storage”, IEEE Transactions on Energy Conversion, vol. 20, 2005, pp. 225 – 230.

[31] D. Kottick, M. Blau and D. Edelstein, Battery Energy Storage for Frequency Regulation in an Island Power System, IEEE Transactions on Energy Conversion, vol. 8, 1993, pp.455 – 459.

[32] P. J. Grbovic´, *Ultra-capacitors in Power Conversion Systems Applications, Analysis and Design from Theory to Practice,* John Wiley & Sons, 2012.

[33] K.C. Divya and J. Østergaard, “Battery energy storage technology for power systems—An overview”, Electric Power Systems Research, 2009, pp. 511–520.

[34] M. Rashid, *Power Electronics Handbook,* Elsevier Science, 2011.

[35] K. R. Padiyar, *FACTS Controllers in Power Transmission and Distribution*, Technology & Engineering, 2009.

[36] F. Blaabjerg, *Power Electronics for Renewable and Distributed Energy Systems*, Springer, 2012.

[37] A. Emadi, A. Nasiri, Stoyan and B. Bekiarov, *Uninterruptible Power Supplies and Active Filters*, CRC Press, 2004.

[38] P Weicker , *A Systems Approach to Lithium-Ion Battery Management*, Artech House, 2012.

[39] D. Pavlov, *Lead-Acid Batteries: Science and Technology*, Elsevier Science, 2011.

[40] J, Szymborski, G. Hunt and R. Jungst, "Examination of VRLA Battery Cells Sampled from the Metlakatla Battery Energy Storage System" The Sixteenth Annual Battery Conference on Applications and Advances, 2001, pp. 131 – 138,

[41] http://www.aesenergystorage.com/2012/05/03/aes-combines-advanced-battery-based-energy-storage-with-a-traditional-power-plant/

[42] http://www.desertsun.com/story/tech/2014/10/17/affordable-solar-battery-storage/17465467/

[43] http://variablegen.org/wp-content/uploads/2013/04/ConnectedJan2014.pdf

[44] http://variablegen.org/wp-content/uploads/2013/04/ConnectedJan2014.pdf

[45] http://www.alstom.com/press-centre/2013/12/alstom-launches-a-battery-storage-solution-maxsine-estorage/

[46] H. Bevrani, *Robust Power System Frequency Control*. Springer, 2009.

[47] P. Kundur, J. Paserba, V. Ajjarapu, G. Andersson, A. Bose, C. Canizares, N. Hatziargyriou, D. Hill, A. Stankovic, C. Taylor, T. Van Cutsem and V. Vittal, "Definition and classification of power system stability IEEE/CIGRE joint task force on stability terms and definitions", IEEE Transaction on Power Systems, vol. 19, 2004, pp. 1387–1401.

[48] F. Riehle, *Frequency Standards: Basics and Applications*, John Wiley & Sons, 2006.

[49] A. Exposito, A. Conejo and C. Canizares, *Electric Energy Systems: Analysis and Operation*, CRC Press, 2008.

[50] http://www.centrel.org/ucte.html

[51] European Network of Transmission System Operators for Electricity, available at: https://www.entsoe.eu/fileadmin/user_upload/_library/publications/ce/oh/policy1_v23.pdf

[52] P. M. Anderson and A. A. Fouad, *Power System Control and Stability*, USA: IEEE Press, 2nd Edition, 2003.

[53] J. Machowski, J. Bialek and J. Bumby, *Power System Dynamics: Stability and control*, second edition, John Wiley & Sons, 2008.

[54] NEMMCO, *Frequency and Time Deviation Monitoring in NEM*, vol. 2007, NEMMCO, 2007, Available on-line at: http://www.nemmco.com.au/powersystemops/250–0069.pdf.

[55] P. Kundur, *Power System Stability and Control*, McGraw-Hill, 1994.

[56] N. Watson and J. Arrillaga, *Power Systems Electromagnetic Transients Simulations*, Newnes, 2002.

APPENDIX A: VOLTAGE LOOP CONTROL AND PWM CONTROL BLOCKS

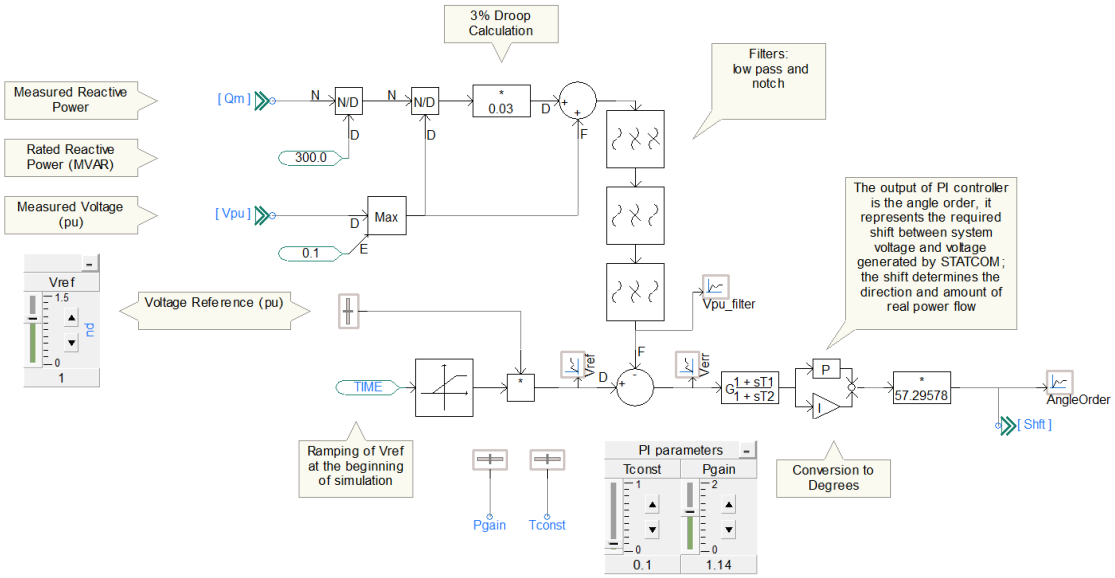

Figure A.1 *Voltage control loop; the generation of angle order based on the voltage error.*

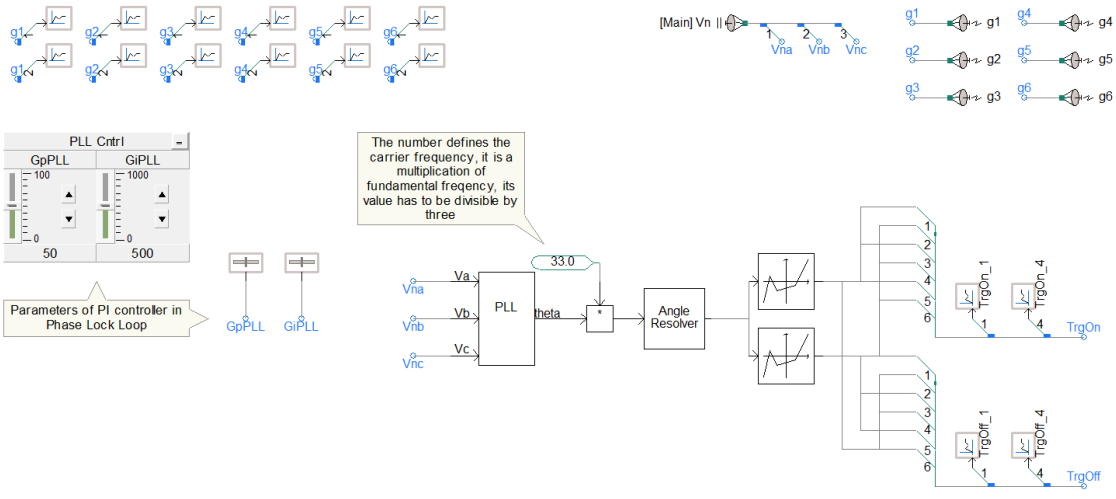

Figure A.2 *PWM control –part 1; the generation of triangular waveforms.*

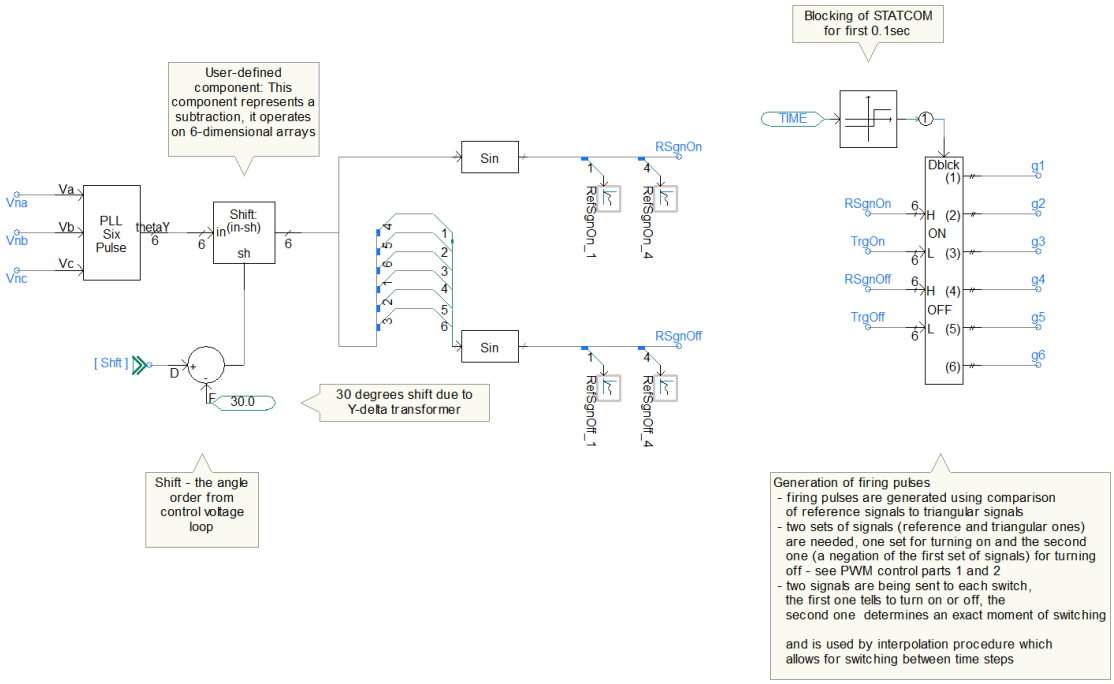

Figure A.3 *PWM control - part 2; the generation of reference waveforms.*